A COMPARATIVE STUDY FOR VARIOUS COIL GEOMETRIES IN ELECTRIC VEHICLE WIRELESS CHARGING SYSTEMS

by

Hanin Hassan Kabalan

A Thesis presented to the Faculty of the
American University of Sharjah
College of Engineering
In Partial Fulfillment
of the Requirements
for the Degree of

Master of Science in
Electrical Engineering

Sharjah, United Arab Emirates

November 2020

Declaration of Authorship

I declare that this thesis is my own work and, to the best of my belief and knowledge, it does not contain material published or written by a third party, except where permission has been obtained and/or appropriately cited through full and accurate referencing.

Hanin Hassan Kabalan

Signed…….

26/11/2020

Date……

Approval Signatures

We, the undersigned, approve the Master's Thesis of Hanin Hassan Kabalan

Thesis Title: A Comparative Study for Various Coil Geometries in Electric Vehicle Wireless Charging System.

Date of Defense: 29/11/2020

Name, Title and Affiliation	**Signature**
Dr. Mohamed Hassan Professor, Department of Electrical Engineering Thesis Advisor	
Dr. Ahmed Osman-Ahmed Professor, Department of Electrical Engineering Thesis Advisor	
Dr. Taha Landolsi Professor, Department of Computer Engineering Thesis Committee Member	
Dr. Shayok Mukhopadhyay Professor, Department of Electrical Engineering Thesis Committee Member	
Dr. Nasser Qaddoumi Head Department of Electrical Engineering	
Dr. Lotfi Romdhane Associate Dean for Graduate Studies and Research College of Engineering	
Dr. Sirin Tekinay Dean College of Engineering	
Dr. Mohamed El-Tarhuni Vice Provost for Graduate Studies Office of Graduate Studies	

Acknowledgement

I would like to thank my advisors Dr. Mohamed Hassan and Dr. Ahmed Osman for providing knowledge, guidance, support, and motivation throughout my research stages.

I would like to thank the Electrical Engineering department professors who taught me the master level courses with mighty teaching methods and skills. I really appreciate their honourable advices and motivation. I would like to express my sincere gratitude to the American University of Sharjah for awarding me a graduate teaching assistantship.

Abstract

Inductive coupling wireless power transfer technology is gaining interest in recent years, especially in the field of wireless charging. Range limitations and charging of electric vehicles are major concerns in the modern intelligent transportation systems. A systematic approach to design the inductive link power pads is presented in detail and the Society of Automotive Engineers (SAE) recommended practice J2954 is followed for designing the physical dimension of these power pads. In this thesis, a comparative study for the design of different coil geometries considered for EV's wireless charging systems is carried out. In particular, a comparative performance analysis is conducted for rectangular, Double-D (DD), Double-D Quadrature (DDQ), and Bipolar (BP) power pads. This study also aims at showing how design aspects, height and vertical displacement affect the coupling behavior and misalignment tolerance while investigating the effect of the different parameters on the magnetic null phenomenon. Based on the simulation results, the geometries in which DD and DDQ coils are considered for primary and secondary coils respectively provide the highest coupling factor and the highest inductive link efficiency at various alignment conditions over a range of horizontal displacement from -800 mm to +800 mm lateral misalignment, while having the minimum charging pads weight, when compared to DD coils. A commercial electromagnetic simulation software called (ANSYS Maxwell) was adopted to simulate different coil structures and evaluate the performance of the inductive link. It is concluded that turn-to-turn spacing has the most dominant effect on the coupling performance at a fixed wire diameter. The power pad combinations such as DD_DD, and DD_DDQ are considered the best combinations that gives the best coupling performance for misalignment conditions. Rectangular power pad combined with non-polarized geometries is the proper geometry combination for static charging in perfect alignment conditions. The conducted analysis reveals that the existence of ferrite core is necessary to enhance the inductive link overall performance.

Keywords: ***Electric Vehicles (EVs); inductive Power Transfer (IPT); inductive link efficiency; power pads; coupling factor; mutual inductance; misalignment tolerance.***

Table of Contents

List of Figures

List of Tables

List of Abbreviations

BP	Bi-Polar
CPT	Capacitive Power Transfer
D	Rectangular
DD	Double D
DDQ	Double D Quadrature
EMF	Electromotive Force
EV	Electric Vehicle
FEM	Finite Element Method
IPT	Inductive Power Transfer
SAE	The Society of Automotive Engineers
WPT	Wireless Power Transfer

Chapter 1. Introduction

Plug-in EVs are suffering due to two major barriers: cost and range. In order to increase the EV travelling range, EVs are required to charge either quite frequently or to install a larger battery pack (which results in additional problems such as cost and weight). In addition, it is not economical to charge a vehicle very often. The dynamic wireless EV charging systems) is a promising technology, which can reduce the problems associated with range and cost of EVs. It is the only solution for future mass adoption of EVs. It is also known as a ‘‘roadway powered” [1], ‘‘on-line” or ‘‘in motion” wireless EV charging system. Wireless power transfer systems consist of primary and secondary coil systems that made up of Litz wires varying greatly in dimensions, shape and in material for confining and guiding the magnetic flux. A large number of geometric degrees of freedom and variables must be defined and optimized in designing the power pad system. In this chapter, thesis overview, problem statement, and the contributions will be highlighted.

The global interest in developing efficient and environment friendly transportation systems is growing rapidly, electric vehicles (EVs) are gaining a rising momentum, especially with the expected considerable reduction in carbon footprint as a result of utilizing the zero-emission vehicles in contrast to their fuel-operated counterparts. State-of-the-art researches presently focusing on EV charging techniques, in particular wireless charging through resonant inductive power transfer, in which concepts of Faraday’s and Ampere’s laws of induction are utilized to allow an alternating magnetic field in one coil, namely transmitter or primary coil, to induce an electromotive force (EMF) in a receiver or secondary coil without the use of conductive chargers. This ensures no direct electrical connection between both coils. The basic theory of wireless power transfer (WPT) was introduced by Tesla. The wireless charging system for EVs is the extended configuration of the WPT technology. Various limitations of plug-in charging systems expanded the research on EV wireless charging system development. Using wireless charging systems, an EV can be charged either in stationary mode or when the vehicle is in motion and the overall battery capacity of the vehicle [2]. State-of-the-art research is currently on-going worldwide in order to develop highly efficient EV wireless charging systems, that maximize the efficiency of power transfer from the grid to the vehicle’s battery.

For dynamic charging, the major challenge is to keep the EV aligned with the road-embedded charger. The electric vehicle is subject to travel on the road which makes the coupling varies in a wide range. To make this technology more practical, the system characteristics under coupling variation caused by the lateral misalignment, vehicle forward movement and vehicle types shall be investigated further. The EV motion with a lateral displacement along reduces the power transferred to the EV on account of the lower value of the mutual inductances between the transmitter track and pickup coils. Effects of the lateral displacement in coil have been evaluated by a FEM analysis, executing a parametric analysis of the mutual inductance between primary and secondary coils for lateral displacements increasing from 0 up to the lateral dimension of the EV pickup coil. Several solutions have been proposed to reduce the sensitivity of the dynamic wireless charging system to the lateral displacement, by either designing suitable compensation networks or modifying the coil shape [3].

The primary coils and secondary coil together form the magnetic coupler. To improve the dynamic performance of the magnetic couplers in the Dynamic Wireless Power Transfer (DWPT) system for electric vehicles (EVs), the primary coils should be well designed and optimized to achieve high output power, high efficiency, and low EMF. Depending on the coil structure types, the magnetic coupler for the DWPT system can be classified into two categories. The first type is the long rail, and the other is coils array. Long rail suffers from the large EMI and low efficiency issues. Hence the coils array is more effective. Circular coils and Double-D (DD) coils are the two commonly coil types used in (segmented rails). Compared to the Circular coils, the DD coils have higher coupling coefficients and a higher offset tolerance. However, it still has such a problem that the mutual inductance drops dramatically when EV moves into the switching area, making EVs fail to achieve sufficient power [4].

Inductive Power Transfer (IPT) is the technology that permits efficient and real-time energy exchange where vehicles can play an important role in the energy exchange process. In stationary WPT system, it is recommended to perfectly align the charging pad to the receiving pad placed in the car. The perfect alignment between transmitting and receiving pads ensures the maximum power transfer. In dynamic charging systems, the misalignment challenges the power transfer efficiency. Hence, a reduction of system power transfer efficiency is expected. However, stationary WPT does not extend the

vehicle's driving range and hence, does not solve problems of range anxiety reported in [2] associated with the use of EVs. With dynamic EV charging, the driving range can be expanded while the vehicle is in motion. Furthermore, the weight of the EV battery pack can be reduced as the required energy storage is lower when the vehicle is powered wirelessly while driving. However, the deployment of such a system relies on the charging infrastructure development, which in turn is limited by its cost and design complexity [5].

Generally, a set of power pads (consisting of one power pad on the transmitting side and another power pad on the receiving side) is used for the stationary wireless charging, while multiple power pads are combined in a single system for EV's dynamic wireless charging. Power pads play a fundamental role to transfer power efficiently to the vehicle. The appropriate design of power pads guarantees efficient power transfer to the vehicle as well as reducing system complexity. As the modern EV wireless charging system is mainly based on the Inductive Power Transfer (IPT), it is expected that power pads should exhibit a higher value of coupling coefficient. The performance of power pads in different misaligned positions highly influences the power transfer efficiency of the entire charging system [6] [7]. Different types of power pads have been introduced in research, including the circular power pad, Double D power pad and Double D Quadrature (DDQ) power pad [8]. This study is focusing on investigating different power pads shapes and structures to compare their performance in misaligned positions, especially under lateral and vertical misalignment. In addition, these two major types of power pad, bipolar/tripolar power pads are also developed to improve the overall power transfer efficiency for various misalignment positions [9]. In this thesis, the main focus is to design and develop the most effective coil design to achieve efficient power transfer to EVs. The fundamental challenge with the design of the power pad is to maximize the coupling/quality factors and the geometrical arrangement. However, the efficiency of the WPT directly depends on the coupling coefficient and the quality of the transmitting and receiving coils

1.1. Problem Statement

In case of dynamic wireless charging, it is required that power pads should exhibit a high coupling coefficient (k) and high efficiency power transfer in different misalignment displacements [10]. Based on the charging system configuration and the

misalignment distance between the power pads, the k value varies. For a typical 85 kHz system, the k value can range between 0.1 to 0.6, and a lower k value due to large misalignment distances can be improved by using ferrite bars to enclose the magnetic flux. Power pads are important parts of the EV wireless charging system, as the link between power grids and vehicles is established through transmitter and secondary power pads. Power rails are used for roadway powered vehicles, and these power pads are only energized when an EV is passing over it. However, the system configuration complexity and maintenance cost is still an unsolved issue when deployed in dynamic wireless charging systems. Stable output is a critical issue for the EV dynamic wireless charging system. However, the output of a practical dynamic WPT system is highly influenced by factors, such as mutual inductance, resonant compensation network topology, and load resistance. Hence, there is a great potential in the selection of proper coil design for the transmitter and the receiver sides to ensure the highest inductive link efficiency. The variation of mutual inductance between primary and secondary coils due to the misalignment issue is the major challenge of dynamic wireless charging system [11]. As the vehicle travels along the charging lane, the alignment between the transmitter and receiver pads varies as the vehicle is moving along the lane. A transformer is the best example to explain how mutual induction works in which the direct contact between the primary and secondary coils does not exist. The coupling coefficient of a transformer is an essential parameter influencing the performance of the wireless power transmission system. Based on the magnetic reluctance model under perfectly aligned condition, as well as a practical and precise model for finding the coupling coefficient under coil misalignment and varying air gap.

The main goal is to design and build the inductive link power pads with a developed coil geometry to reduce the mutual inductance fluctuation, in order to guarantee the stability in output power delivered to EV battery. Furthermore, maintaining high wireless charging efficiency with the use of polarized coil geometries such as DD, DDQ, and Bipolar technology developments. Enhancements shall be conducted to the existing coil geometries including Double-D, DD-Quadrature and Bipolar coil topologies to significantly increase power transfer through providing better positioning tolerance and less mass while requiring lower-rated power electronics, which also reduces the materials cost. In addition, the analysis of the WPT systems can

be achieved by analyzing the coupling and quality factors that are one of the key parameters of the inductive link. Furthermore, improvements shall be done to the design various coil geometries to tolerate the changes in other parameters such as the relative position between the transmitter (grid side) and receiver (vehicle side) coils. These parameters are vertical, lateral, and longitudinal displacements, coil size and coil shape. This study aims at the design and FEM simulations of the inductive link to maximize Figure-of-merit (kQ) and improve misalignment tolerance. The simulation results shall be validated against analytical estimations as well as hardware implementations and measurements. The main contributions of this research study can be summarized as follow:

- Designing and modeling of different coil geometries that can fit both static and dynamic IPT systems
- Providing detailed comparative analysis between state-of-the-art designs of the charging coils based on both FEM simulations and analytical estimations. This is done by:
    - Introducing a change in different coil parameters such as coils turns/ Litz wire diameter/ turn-to-turn spacing.
    - Investigating the impact of inner to outer coil dimensions ratio on the coupling performance.
    - Evaluating different types of coil designs embedded with ferrite core and aluminum shielding to improve the coupling coefficient by shaping the magnetic field and comparing their power transfer efficiency.
- Evaluation of the inductive link performance at resonance frequency.
- Choosing the optimum coil design to enhance the misalignment tolerance of the IPT system designed for charging of moving EV.
- Modeling the overall WPT systems to evaluate the power transfer efficiency.

1.2. Thesis Outline

The remaining parts of the report are organized as follows: Chapter 2 introduces EV charging techniques, inductive power transfer technology, types of wireless charging, and wireless power transfer system components. It discusses existing WPT methods and examines how the existing IPT methods in EVs can be improve the

performance of the overall system by using resonant systems. Furthermore, it presents an overview of the available literature on the selection of a proper wireless power pads for WPT system by explaining the design approach followed in this thesis for an inductive link power pad. Chapter 3 describes the design process of the power pads and the system model. In addition, the analysis of the power transfer efficiency jointly with the calculation of coupling and quality factor, Figure-of-Merit, and inductive link efficiency as well as the simulation design of the inductive link will be studied. Chapter 4 includes simulations and preliminary results are compared for various coil geometries and structures. It reviews the output results for the Finite Element Method tool performed at different distances between the transmitter and receiver and alignment options. Finally, Chapter 5 concludes by illustrating how the designed coil geometry can be verified for practical applications. The report is finally concluded.

Chapter 2. Background and Literature Review

This chapter covers the inductive power transfer phenomenon and the electric vehicle charging techniques. It starts with an explanation of EV Charging system techniques and classification to understand the difference between static and dynamic WPT systems. A brief description of power transfer history and related work follows, with emphasis on inductive link and magnetic coupling characteristics. Then, the issues behind the shape and structure of wireless charging coils in static and dynamic WPT system will be described. After that, the usual method used to analytically calculate the coupling factor will be explained. The purpose of this chapter is to provide a summary of the state-of-art technologies for EV wireless charging systems with a particular focus on achieving high power transfer efficiency. In this thesis, a performance analysis of various power pad structures is carried out and several enhancements are proposed to improve power transfer efficiency. The literature review is mainly focusing on different power pads and their applications in the EV wireless charging system.

2.1. EV Charging System Classifications

The fundamental principle of EV wireless charging is presented; topologies used for charging the vehicle with a short air gap distance between transmitting and receiving ends (Near-Field), topologies available to transfer power through a long air gap distance namely (Far-Field), comparative discussion between different power pad topologies. EV wireless chargers generally apply coupling plates known as a transmitting end (at roadside) and a receiving end (at vehicle side). Wireless power transfer (WPT) categorized into radiative and non-radiative power transfer. Radiative power transfer is transmitting high power density, which is unsafe for humans when it is been implemented for EVs charging [63]. The power transfer efficiency of microwave power transfer is very low due to the inevitable free space path loss. Hence, nonradiative power transfer technologies have been chosen to charge the batteries [12]. Non-radiative power transfer includes inductive power transfer (IPT) and capacitive power transfer (CPT). Inductive charging technology is based on the concept of transformers. Based on the reviewed literature, A general classification of EV wireless charging system is presented in Figure 2.1. The charging process of the EV can take place either statically (stationary charging), while the EV is parked over a charging pad, or dynamically while the vehicle is in motion (dynamic charging). The dynamic

wireless charging technology enables a vehicle to be charged while cruising; a vehicle must be parked when using the stationary wireless charging technology.

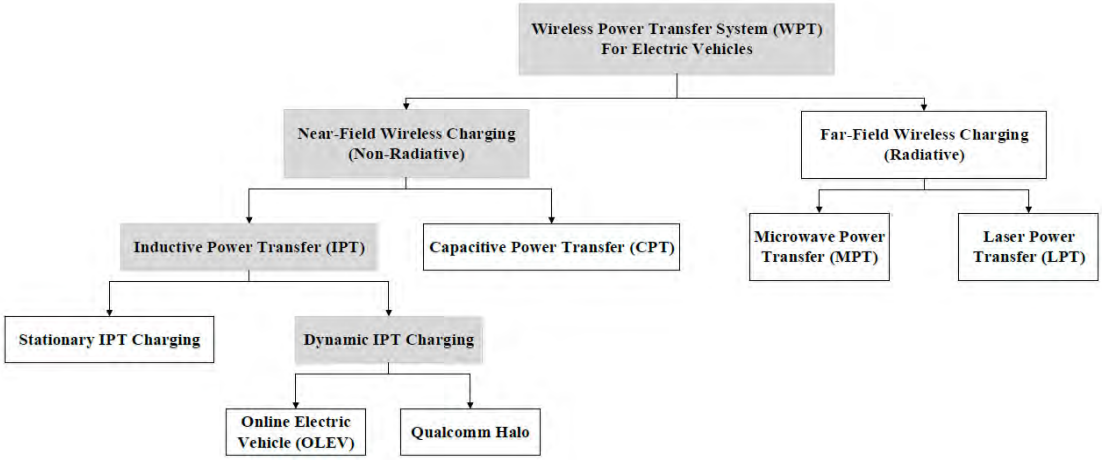

Figure 2.1: EV wireless charging system classification.

Qualcomm Technologies designed and built a WPT system that is capable of charging an electric vehicle (EV) dynamically at up to 20 kilowatts at highway speeds. Qualcomm Technologies also demonstrated real-time and simultaneous charging, in which many vehicles on the same transmitter track can charge dynamically at the same time. The vehicles can be charged in both directions along the track, and in reverse. To reduce the drivers' range anxiety from the EVs, charging while the vehicle is moving is a promising solution. On-line Electric Vehicle (OLEV) is one type of dynamic IPT systems, it was developed by the Korean Advanced Institute of Science and Technology (KAIST). Initially, IPT was introduced in order to transfer large amount of power to vehicles [10]. Energy storage of the OLEV system can be recharged whether the vehicle is moving or stopped.

2.2. Wireless Power Transfer

Wireless power transfer systems consist of two independent electrical systems with mutual coupling. The current in the primary coil generates an oscillating magnetic field, which transfers through the coil of the receiving tool. Thus, an electric voltage is induced in the secondary coil. Then, the voltage is converted and used to power the vehicle. In WPT systems, power is transferred from the transmitter coil to the receiver coil, and the two coils need to be perfectly overlapped and aligned to make sure the system work successfully. However, in practical applications, the misalignment

between the coils can easily occur when the objects are moving or cannot be placed very precisely. Furthermore, in Figure 2.2. coil misalignment significantly decreases the power transfer efficiency and leads to system instability, which are not practically tolerable. Consequently, we need to improve the misalignment tolerance of the coil for the WPT systems. In order to improve the misalignment tolerance, a number of design variations for the WPT coil geometry have been proposed [9] [10]. In [13], an investigation into the use of the transmitter electrical information to estimate the mutual inductance and regulate the power consumption of the receiver side has been proposed. However, it does not highlight the stability and the reliability of signal transfer in dynamic power transfer conditions.

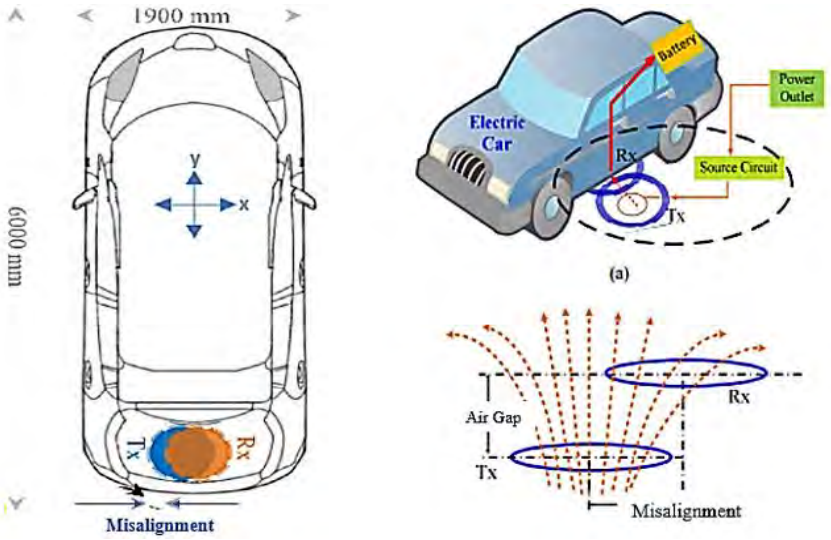

Figure 2.2: (a) Wireless EV charging system basic components and typical misalignment of wireless charging system for EV application [69].

2.2.1. Stationary wireless charging. The wireless charging systems can be either dynamic or stationary. Stationary IPT system is generally employed for transferring power up to 50 kW. Figure 2.3 shows the system configuration and equivalent circuit of a stationary IPT system. A rectifier is connected with utility grids to generate DC power, the DC input voltage and current, further feeds into a full bridge inverter and generate high frequency AC power (85 kHz in this system), the high frequency AC input voltage and current, are fed into the primary coil. A rectifier is also applied on the secondary side to store the transferred energy. C1 and C2 are the primary and secondary resonant capacitors. The review indicates that the IPT technology has

merits for stationary charging (when the vehicle is parked), opportunity charging (when the vehicle is stopped for a short period of time, for example, at a bus stop).

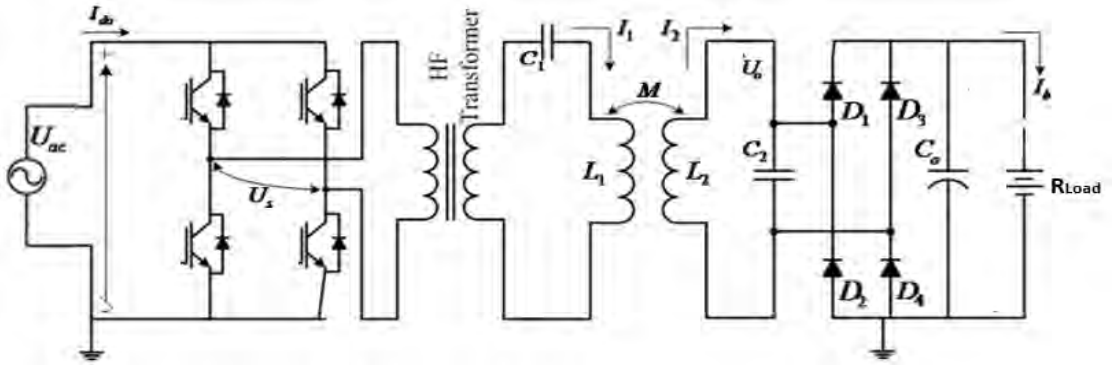

Figure 2.3: A stationary IPT system circuit configuration [14].

The stationary IPT circuit is shown in Figure 2.3. Where L_1 and L_2 are the self-inductance of road and vehicle side coil, respectively; M is the mutual-inductance between the two coils; ω is the operating frequency; U_{ac} is the input high frequency AC current fed into the primary coil; and I_{ac} is the current on the secondary coil [14]. Stationary wireless charging system for electric vehicles can simply replace the plug-in charger with minimal driver involvement, and it solves associated safety issues such as trip hazards and electric shock. Figure 2.4 shows the basic arrangement of static WPT system. The primary coil is installed underneath in the road or ground with additional power converters and circuitry.

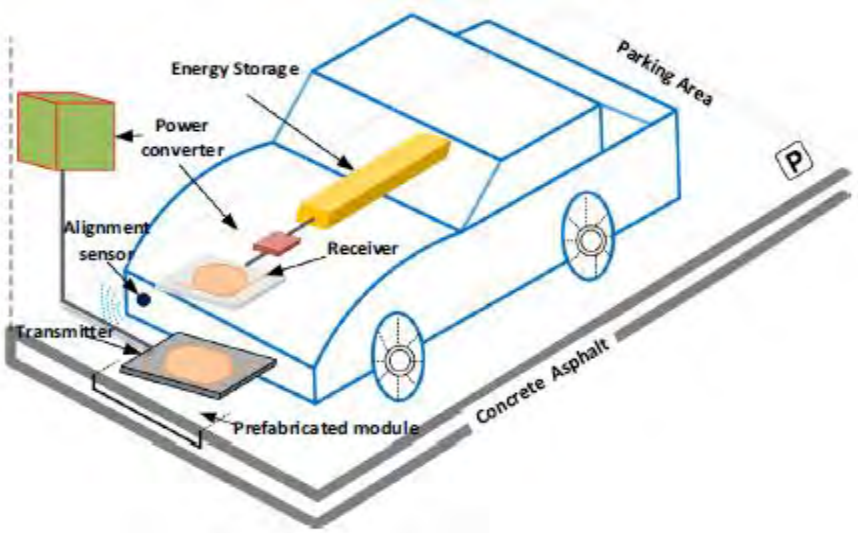

Figure 2.4: Basic diagram of stationary wireless EV charging system [15].

The receiver coil, or secondary coil, is normally installed beneath the EVs front, back, or center. The receiving energy is converted from AC to DC using the power

converter (rectifier) and is transferred to the battery pack to power the vehicle. In order to avoid any safety issues, power control and battery management systems are fitted with a wireless communication network to receive feedbacks from the primary side [16]. The charging time depends on the level of power source, charging pad sizes, and air-gap distance between the two windings. The average distance between lightweight duty vehicles is approximately 100–300 mm. Static wireless EV charging system can be installed in parking areas. Many prototypes have been developed by universities at research and commercial levels, as presented in [2] [17]. Their power levels meet with the recently announced international SAE standards (J2954) power class for levels 1 (3.3 kW) and 2 (7.7 kW), including frequency ranges 81.9–90 kHz.

Currently, the SAE organization is working on the standards, which are related to acceptable misalignment and the installation location of the receiver pads in the car. A number of prototypes have been implemented with various mounting locations, such as front, rear, and center of the receiver pads on the underneath of the car. The Oak Ridge National Laboratory (ORNL) is mostly focusing on improving the power transfer efficiency by coil designing while the University of Auckland has proposed some hardware and software (including charging pad development) to improve plug-in charging efficiency. In general, prototypes or lab experiments of stationary wireless charging system for EVs have been developed from power ranges 1–20 kW, air-gap distance 100–300 mm with efficiency from 71 to 95% [18].

2.2.2. Dynamic wireless charging. Dynamic charging is defined to be the process to charge the electric vehicle when it is moving along a dedicated lane equipped with an IPT system. Dynamic wireless charging holds promises to partially or eliminate the overnight charging through a compact network of dynamic chargers installed on the roads that would keep the vehicle batteries charged at all times, Consequently, reducing the range anxiety and increasing the reliability of EVs. Dynamic wireless power transfer (DWPT) can help lower the price of EVs by reducing the size of the battery pack. Indeed, if the recharging energy is readily available, the batteries do not have to supply the EV with power the whole driving range but only supply power when the IPT system is not available in streets. The dynamic wireless charging technology enables a vehicle to be charged while cruising. EV dynamic wireless charging system development research is led by the Korean Advanced Institute of Science and Technology (KAIST),

but the concept of highway charging was first reported in [19]. For dynamic charging, the EV runs on the road which results in coupling variations in a wide range. To make this method more practical, the system characteristics under coupling variation caused by lateral misalignment, vehicle forward movement and vehicle types should be investigated further.

Compared to the stationary charging, Dynamic charging can deliver power to EVs when the vehicles are moving so that the available time for charging is significantly increased. Dynamic charging has several advantages of reducing the weight and cost of the vehicles with less batteries while extending the EV's range. The dynamic charging scenarios can be divided into low-speed scenarios and high-speed scenarios. In low speed applications, the vehicles will slow down when approaching the bus stop or traffic light and then speed up when leaving. Once the vehicles enter the charging segment in which transmitters are buried, they can be charged, even without stopping.

In highspeed application scenarios, such as highways, vehicles pass one transmitter quickly, in fractions of seconds, and the time to power the receiver using one transmitter is limited. Besides, the fast variation coupling and loading conditions is a huge challenge for the control strategy of dynamic charging. Therefore, only the dynamic charging for low speed applications is considered. One of the most important problems to be solved for the dynamic charging is how to provide a relatively stable power to the vehicles in motion. Compensation network design has been studied to overcome this limitation [20].

Figure 2.5: Qualcomm Halo's power pad [21].

The charging pad area is around a meter square, while the car's receiving pad is enclosed in a smaller-sized device under the car. Once the two are aligned, charging can take place at 3.3kW, 6.6kW or 20kW speeds. In Figure 2.5, Qualcomm halo launched multi-coil technology that delivers magnetic interoperability across single coil, solenoid, and multi-coil vehicle pads. Qualcomm Halo proposed the multi-coil as primary pad for the base. On the other hand, single circular and square coils were proposed for the secondary vehicle pad in stationary charging. Halo uses high power, resonant magnetic inductive wireless energy transfer and holds a relatively wide air gap between transmitter charging unit and vehicle charging unit. The charging pad's multi-coil design ("Double "D" Quadrature") delivers high energy transfer efficiency and high power up to 3.3 kW, 6.6 kW or 20 kW, even if the pads are in misaligned positions. Halo multi-coil technology delivers magnetic interoperability across single coil, solenoid & multi-coil vehicle pads and supports various air gaps. The high degree of tolerance in both the vertical and lateral/longitudinal axes means drivers do not have to park accurately or need complex and expensive on-board alignment systems. This multi-coil technology delivers magnetic interoperability across single coil, solenoid & multi-coil vehicle pads and supports various air gaps.

Figure 2.6: Dynamic wireless charging topology [22].

As shown in Figure 2.6, A road equipped with a dynamic WPT system can be implemented at the roadside, sub-stations receive electric current from the grid, and they adjust it in order to supply the primary circuits embedded in the road. For dynamic WPT systems, transmitter pads and power supply segments need to be installed on

particular locations and pre-defined routes [23]. A large coil (around 5–10 m) is installed on the road surface, where multiple small sub-coils are utilized. In comparison with the segmented scheme, the centralized scheme has higher losses, lower efficiency including high installation, and higher maintenance costs. The installation of the infrastructure for this technology would be highly expensive. With the assistance of a self-driving car in future, it will help to create the perfect alignment between the transmitter and receiver coils which can significantly improve the power transfer efficiency. Dynamic WPT systems can be easily integrated in many EV transportation applications, such as light duty vehicles, bus, rail, and rapid transport.

2.3. Inductive Power Transfer

An IPT technology for the EVs applications transmits power with very high frequency, which causes a huge electromagnetic interference (EMI) [24]. Furthermore, human safety shall be carefully considered during inductive charging. The International Commission on Non-Ionizing Radiation Protection (ICNIRP) set a standard specifies that 200 mA/m^2 is the current density allowed to be exposed to the public. In the near field transmission, there are two primarily used techniques that are being applied in the current practical applications which can be categorized based on the coupling technology used in them. These coupling techniques are listed below.

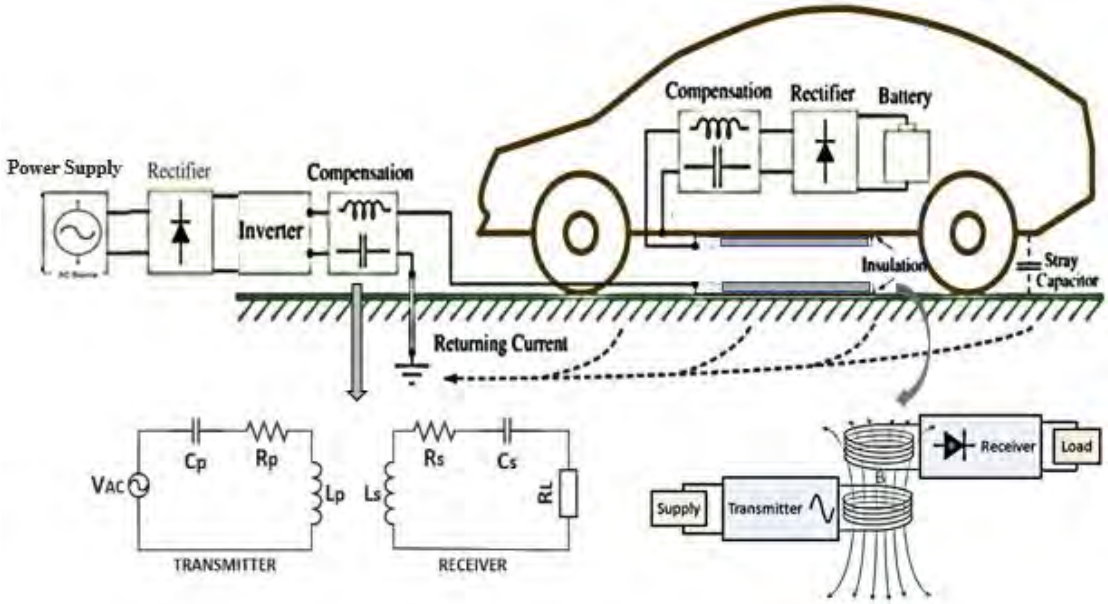

Figure 2.7: Inductive power transfer system for EV charging [1].

Inductive coupling is one of the near field transmission techniques, in which the energy transfer is done between two coils separated by small air gap through magnetic

fields. The coils will be located in close proximity for transmission from the transmitter to the receiver. The mutual induction principle is used to transfer the energy between the two coils without using any physical medium.

When a current is passing through the transmitter coil, it will produce a magnetic field in a short range ranged from 5 cm up to few centimeters. When the receiver coil is placed in this field, the voltage will be induced in the receiver coil. The induced voltage is utilized for charging the EV which is wireless or a storage system like a battery. In mutual induction, the energy will be transferred between the coils in inductive coupling using the magnetic field. A basic description of IPT system block diagram is shown in Figure 2.7.

Inductive power transfer can handle many types of power loads without major problems and with higher efficiency, and it is being utilized in a wide range of near field applications as it can provide better efficiency within a meter square. The mutual position and the distance of the transmitter and receiver plays an important role in measuring the capability of transmission. However, this technique works well only for limited, short distances. When the distance is increased between the coils, or the secondary coil is placed apart from the primary coil, the amount of power transfer will be decreased. The application of inductive coupling for power transmission through longer distances is still under development [13]. In the case of inductive coupling, capacitive coupling is also primarily used for shorter distances, but the transfer of power is done through electric fields.

2.4. WPT History and Related Work

In this section, prior studies focusing on comparative analysis and performance evaluation of the inductive link design will be presented. In literature, research institutions and commercial organizations are interested in the implementation of the overall WPT system. Researchers utilized were interested in the mathematical models and heuristic/empirical optimization to obtain and optimized design for the inductive link. Many authors and researchers used the mathematical toolboxes built-in MATLAB/Simulink and Finite Element Analysis simulation such as ANSYS Maxwell/Simplorer, COMSOL, JMAG, HFSS, and Advanced Design System (ADS) to simulate different coil geometries and evaluate their coupling performance to estimate the power transfer efficiency.

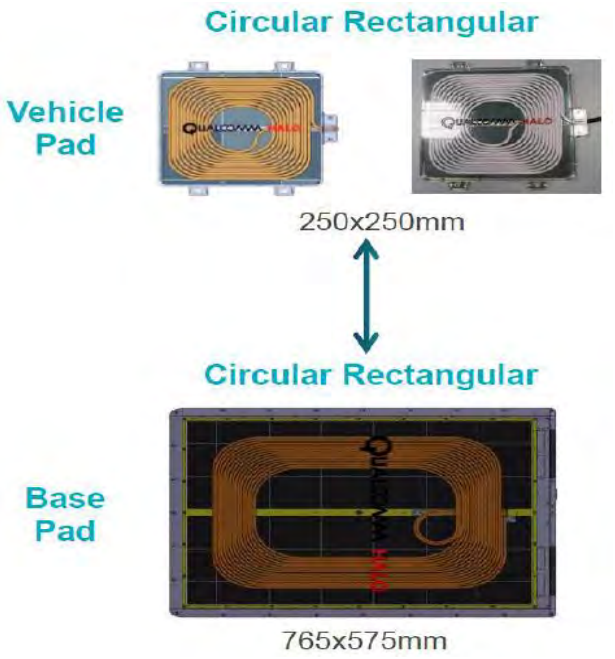

Figure 2.8: Qualcomm Halo power pads: circular rectangular coils for transmitter and receiver sides [25].

The major companies working on stationary WPT are WiTricity and Qualcomm [26] [27]. WiTricity is a spin-off from the MIT. They have developed transmitter and receiver that operate on strongly coupled magnetic resonance [28]. WiTricity has reported system efficiency of around 90% for 3.3-kW power rating operating at 145 kHz with lateral misalignment of ±20 cm and ±10 cm bumper to bumper [28]. Qualcomm's Halo collaborated with the University of Auckland to patent "Double D" polarized magnetic pads capable of delivering twice the power rating with a higher efficiency as compared to circular pads operating at 20-kHz frequency [27]. As shown in Figure 2.8, Qualcomm used circular rectangular shapes for both primary and secondary side of the WPT system. In other applications, they intended to use bipolar pads for the base (transmitter) and Double D for the vehicle (receiver) as shown is Figure 2.9. This indicates that based on the application, system infrastructure and vehicle specifications, the appropriate design of the power pads shall be chosen to satisfy the system requirements. The technical characteristics and benefits of DD and Bipolar coil topologies translate directly into product performance and economic advantages over circular coil implementations. Qualcomm has quantified superior performance in extensive hardware testing. The knowledge obtained from the on-line electric vehicle (OLEV) project conducted at the Korea Advanced Institute of Science and Technology (KAIST) also contributes to the WPT design.

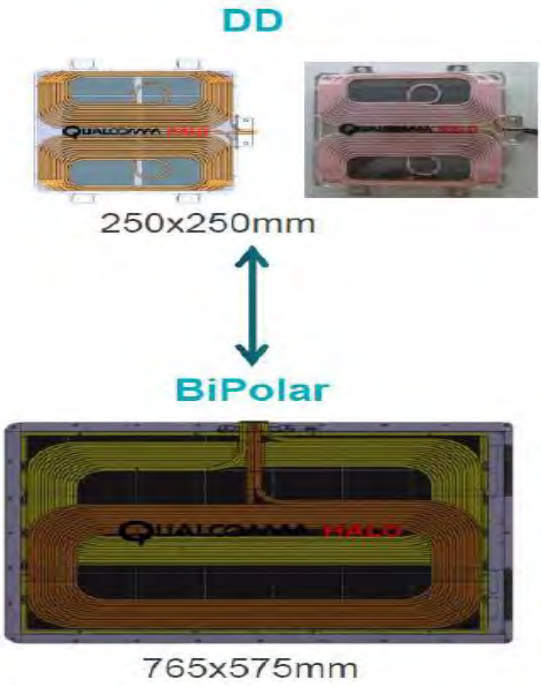

Figure 2.9: Qualcomm Halo power pads: Double-D coil (vehicle side) and bipolar for (transmitter side) [25].

Three generations of OLEV systems have been built: the first generation is a light golf car, a bus, and an SUV. The performance of the second and the third is noteworthy: 60 kW power is being transferred for the buses and 20 kW for the SUVs with an efficiency of 70% and 83%, respectively; acceptable vertical distance and lateral misalignment up to 160 mm and up to 200 mm, respectively [29], [30]. Utah State University startup wireless advanced vehicle electrification developed a 50 kW WPT system for an electric bus. Their system was capable of transferring 50 kW of power over an air gap of 15–30 cm at 20-kHz operating frequency with a reported system efficiency of 90%. The magnetic resonance technology was originally developed by Auckland University. Halo IPT was purchased by Qualcomm in 2011 to found Qualcomm Halo, it is currently working on a static charging system with ongoing research into dynamic charging. Researchers at Auckland University have focused on the inductive power transfer of mobile objects. Their recent achievement in designing power pads of 766 mm × 578 mm for the stationary charging of EV that delivers 5 kW with over 90% power transfer efficiency for about 200 mm was reported [21]. The achieved lateral and longitudinal misalignment tolerance is 250 and 150 mm, respectively.

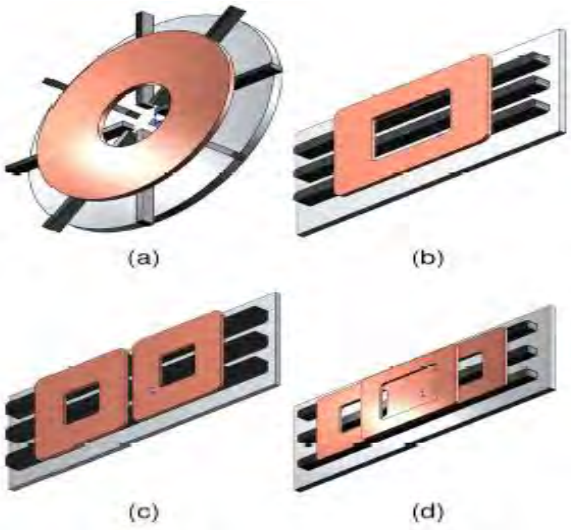

Figure 2.10: Selection of coil geometry: (a) Circular, (b) Rectangular, (c) Double D, (d) Double D Quadrature [31].

The design of the magnetic coupler is the most important part of WPT system. It consists of transmitter and receiver coils separated by an air gap. The desired characteristics for coupling pads are the high coefficient of coupling k quality factor Q and high misalignment tolerance [66]. Many researchers have proposed different coil structures to improve the coupling factor and to maintain a relatively high-quality factor. The influence of the different IPT coupler geometries on the performance factors such as efficiency, power density, misalignment tolerance, and stray field has been investigated in the literature. Many coupler topologies for IPT based EV charging is reported in literature [21], [32]. Based on the coil winding strategy, there can be two types of lumped IPT charge pads a solenoid (double-sided flux) couplers and planar or (single-sided) flux couplers. In Figure 2.10, different planar coupler topologies are categorized into two families based on the fundamental flux path. The polarized (multi-coil) and non-polarized (single) power pads. Non-polarized power pads such as the circular, rectangular and square shaped coils. While on the hand, polarized power pads like double-D (DD) [65] [33], bipolar pad (BP) [34], and double-D quadrature (DDQ) [67] [68], were discussed and evaluated to operate in the WPT system. Polarized couplers exhibit better tolerance toward horizontal and vertical misalignments between transmitter and receiver coils compared to circular and rectangular couplers. In addition, many researchers extended the above studies to include all major topologies and performance parameters.

In [35], the authors compared the following primary and secondary combinations of coil geometries: Circular (Transmitter and Receiver), Rectangular (Transmitter and Receiver), DD (Transmitter and Receiver), DD (Transmitter) and DDQ (Receiver). They concluded that IPT applications without misalignment, circular coupler provides the best performance. The optimized circular couplers are more efficient, lighter, and smaller compared to all other topologies. Likewise, they have lower leakage flux in both vertical and lateral direction. However, in IPT applications requiring misalignment operation, DD-DDQ provides better performance compared to other topologies.

This work shall be compared to other work presented in the literature [36], [37], [38] a benchmark for this study. In [36], the authors mentioned that to make it suitable to install in EV applications, a reasonable size of the pads is chosen as 0.48 m^2. Authors in [36] named the Double D geometry as rectangular bipolar. Furthermore, 3D FEM simulations were used to model the power pads and observe the coupling factor variations under misalignments in (x,y,z) directions [36]. Another benchmark from the literature utilized a 3D finite element method (FEA), due to the unconventional distribution of the flux [38].

Three coil geometries, D, DD, and DDQ, were taken to analyze the effect of magnetic coupling with and without ferrite core. At the end, [37] stated that asymmetrical coils with unequal outer dimensions and fixed self-inductance exhibit better tolerance to misalignment with the limitation of smaller averaged coupling coefficient. Authors in [37] considered the analytical model of asymmetrical coils to investigate the dependency of the coil system dimensions on mutual inductance and coupling coefficient with equal outer diameter. Simulations were performed through finite element method approach using ANSYS MAXWELL. Outcome of their investigations has been used for the design consideration of coil system, which is less sensitive to the misalignment [37]. The magnetic null phenomena define the limit of misalignment tolerance as power transfer in the vicinity of magnetic null is negligible. From the literature that most of the magnetic pads design for static charging is symmetrical pads, i.e., two identical pads to reduce complexity of optimization in design [39-42]. Asymmetrical pads with larger outer and inner diameter of transmitting coil, when compared to receiving coil, give larger tolerance to misalignment and gap

variation [43] [62]. The limitation with this type of structure is having less averaged coupling coefficient. As efficiency in WPT systems depends on the coupling coefficient, it is not advantageous to use the structure with larger outer diameter of transmitting coil when compare to receiving coil. The existence of magnetic null is due to flux cancelation in the pad. In [44] the limitations with DD pad are non-interoperable pad, as it generates only parallel component of flux and gives less misalignment tolerance in lateral direction due to the existence of magnetic null, when lateral offset is 35% of pad length [44].

To overcome the above limitations, DDQ pad is developed which is interoperable and having high misalignment tolerance in lateral and horizontal direction. The main limitation of DDQ pad is requirement of high amount of copper. To solve the above problem, BPP is developed which is having same advantages of DDQ pad with less requirement of copper. Moreover, magnetic null depends on magnetic characteristics of the coil and not on the pad which consists of ferrite and aluminum shielding [37] which is going to be the benchmark for this thesis as their results will be compared to the results of this case study.

Chapter 3. Methodology

This chapter covers the steps and procedures that are followed to achieve the target of this research. Different types of coil design will be presented and compared in terms of vertical and horizontal misalignment. The usage of ANSYS Maxwell is then elaborated together with the case studies conducted in this research. ANSYS Simplorer usage is also discussed in conjunction with the electric circuit used for simulation and how resonance is achieved. Furthermore, preliminary mathematical analysis on the inductive link efficiency and highlights the need for enhancements in the self and mutual inductances of the primary and secondary coils in order to maximize the power transfer efficiency.

3.1. Performance Evaluation Procedure

In this work, rectangular and DD power pads are designed and simulated using Finite Element Analysis (FEA) simulation software, ANSYS 3D Maxwell, based on physical dimensions recommended in SAE J2954 [45]. Different stages of the rectangular and DD power pad design using the software are presented. Figure 3.1 shows the rectangular power pad modeled in ANSYS Maxwell. Three coil arrangements are used for the analysis conducted in this work. Figure 3.1 (a) shows the rectangular power pad that consists of copper coil, ferrite bars placed on the top of the copper, and aluminum sheet on the top of the ferrite. Figure 3.1 (b) the power pad without aluminum shielding is presented. The third design in Figure 3.1 (c) shows the power pad with copper wires only.

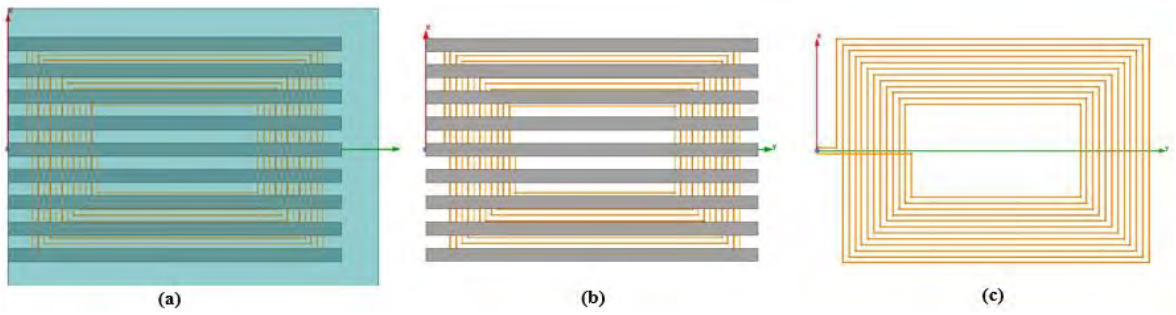

Figure 3.1: Rectangular Power pad (a) copper coil with ferrite bars and aluminum sheet, (b) copper coil with ferrite bars only (c) copper coil only.

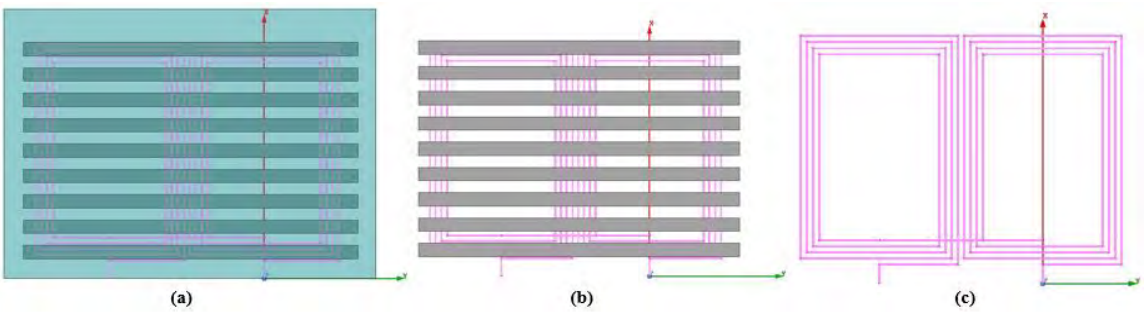

Figure 3.2: Double-D power pad (a) copper coil with ferrite bars and aluminum sheet, (b) copper coil with ferrite bars only (c) copper coil only.

Similarly, Figure 3.2 (a), (b), and (c) shows the power pad arrangements for DD structure. Thee three different power pad arrangements were presented in Figure 3.1 and Figure 3.2 to describe the components of the inductive link power pads used in this study. Furthermore, each arrangement was simulated to investigate the effect of ferrite and aluminum on the inductive coupling. Since the power pad arrangement (a) showed better results, all further simulations will be conducted for the power pad that consists of copper, ferrite and aluminum.

3.1.1. Coupling factor. The ability of a primary pad to transfer power to the secondary pad is an important performance index. In order to compare the magnetic properties of two different primary pad topologies another factor shall be considered in addition to its power transfer capability and that is the primary to secondary coupling coefficient (k). The coupling coefficient k varies between 0 and 1, a higher value indicates good coupling and transfer efficiency of the wireless charging system [46]. For loosely coupled coils, the values of k depend on the distance between the pads and must be in the range of 0.15–0.5 to ensure the overall feasibility, cost effectiveness, and the efficiency of the overall system. Commonly, pad designs with higher coupling coefficient are considered desirable. However, selecting a design with higher k while accepting a minor decrease in the uncompensated power is a good tradeoff [47]. This thesis focuses on studying the change of coupling coefficient for DD pads and rectangular pads with coil misalignment and air gap variations.

3.1.2. Quality factor. For a higher efficiency, it is necessary to have high coupling factor k and quality factor Q. Generally, for a given coil structure, the larger the size to gap ratio of the power pad is, the higher the k is. Moreover, the thicker the

wire and the larger the ferrite section area is, the higher the Q is. By increasing the dimensions and materials, higher efficiency can be achieved. However, It is preferred to have higher k and Q with the minimum dimensions and cost. Since Q equals ωL/R, high operating frequency is assumed to increase the value of Q [2]. To attain a high Q, inductors must be designed to have high self-inductance and low series resistance at high operating frequency. However, the maximum operating frequency is limited to approximately 85 ± 3.7 kHz considering SAE J2594/1 [45]. Therefore, in Chapter 4, simulations will ensure that to increase the Q, resistance of the coil must be decreased. Hence, the overall Q of the coil increases with increase in the number of turns. Thus, a balance must be found between wire diameter and number of turns to achieve an optimum self-inductance. Another way to increase the self-inductance is to add ferrite bars on the coil. The purpose of ferrite bars is to guide the flux so that leakage flux can be reduced, and high coefficient of coupling can be realized.

3.1.3. Mutual inductance. In dynamic WPT systems, researchers concentrate on analyzing the dynamic mutual inductance between the coils due to the misalignment as it has significant influence on the EV charging process, particularly, over the output power and the system efficiency. One of the reasons causing undesirable fluctuation and pulsation in dynamic wireless charging systems is the dynamic mutual inductance when the vehicle is in motion. This inductance comes through the shape of the coils as well as the horizontal arrangement and spacing between the transmitter and the receiver coils. A simulation study is carried out to explore the variations in the mutual inductance profile between the transmitter and receiver coils. With the development of Finite Element Analysis tools, the calculation of mutual inductance became simpler and more convenient. Hence, comparison of electromagnetic parameters of rectangular and Double D coils was performed. In addition, shielding of transmitter and receiver coils must be considered while designing a dynamic WPT system. The effects of the ferrite on mutual inductance should be considered, as this can minimize the leakage flux, and increase mutual coupling between transmitter and receiver coils.

3.1.4. Figure-of-merit. In the WPT system, the coupling coefficient and the quality factor of the winding were both related to the power losses and thus related to the efficiency of the system. For the WPT system with two coils,

$$\eta \propto k\sqrt{Q_1 Q_2} = \frac{\omega}{\sqrt{R_1 R_2}} M. \quad (1)$$

Where η is the efficiency, k is the coupling coefficient, M is the mutual inductance, and the Q is the quality factor of the winding. It was found that a power loss is inversely proportional to the product of kQ, indicating that the efficiency is proportional to the kQ product. When both transmitter and receiver coils are identical, the power transfer efficiency is only related to k. The operating frequency ω of the inverter is a determinant parameter for the efficiency of wireless charging. the power transfer efficiency is only related to the coupling coefficient It is involved in the "figure of merit" (FOM) of the inductive coupler [48] indicated by the product of two dimensionless coefficients: coupling coefficient k and the equivalent quality factor of the two coils Q.

$$\mathrm{FOM} = \mathrm{k}\,.\,\mathrm{Q} = \frac{\omega\,.M}{R}, \quad (2)$$

where k is determined by M of the two coils which decreases with the increasing vertical distance (air gap) and is the geometric average of the quality factors of the two coils. The relation (1) explains the influence of the operating frequency, the influence of air gap and the influence of the geometric average of AC resistance of the two coils. FOM product also determines the power transfer efficiency as will be shown better.

3.2. Modelling and Simulation of Power Pads

A comparative characteristic analysis is carried out between rectangular and double D (DD) power pads for EV wireless charging systems. The Society of Automotive Engineers (SAE) recommended practice J2954 is followed for designing physical dimension of these power pads. Finite Element Analysis (FEA) tool ANSYS Maxwell 3D is used for simulation. Parameters such as coupling factor and mutual inductance are evaluated for each type of power pads by applying vertical and horizontal misalignment. Based on the literature study, it is expected that DD power pads exhibit promising characteristics for EV wireless charging systems.

3.2.1. Design process. The procedure for a comprehensive evaluation for the designed power pad is presented. Figure 3.3 represents the design procedure followed to evaluate the performance of different coil geometries. The first stage is to design a

standardized power pad geometry using ANSYS Maxwell. Afterward, eddy current simulation will be used to calculate the coupling coefficient (k), mutual inductance (M), self-inductance for the primary and secondary coils (L_p and L_s), magnetic flux density (B), magnetic field intensity (H), magnetic flux lines etc.

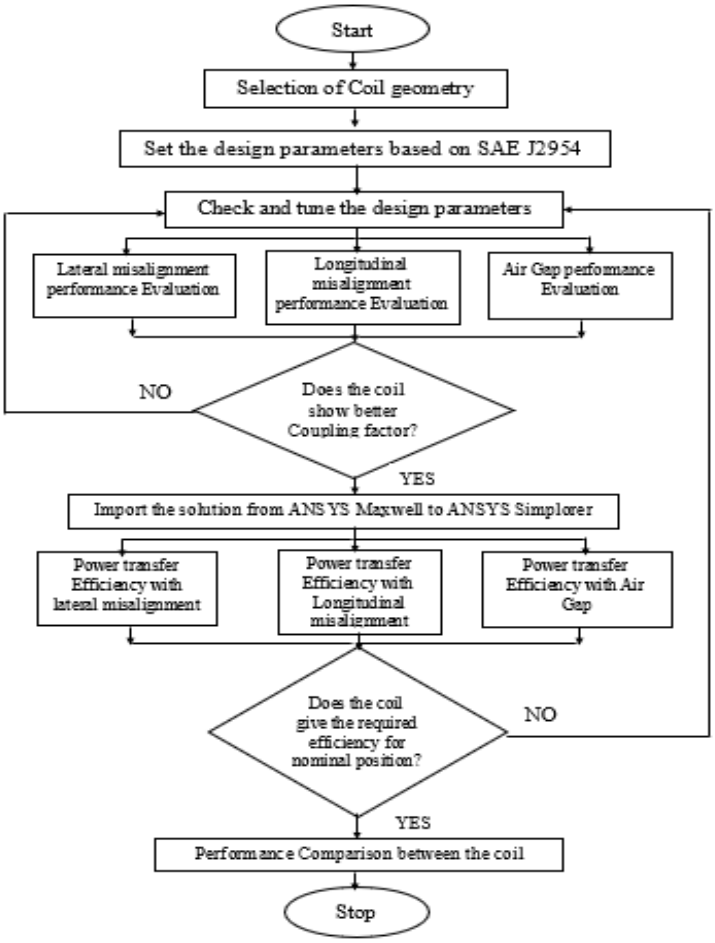

Figure 3.3: Flow chart of performance evaluation procedure for the design of power pads.

A simulation model is prepared using ANSYS Simplorer to simulate and analyze the power transfer efficiency of power pads. The power transfer efficiency is evaluated considering three different cases: parametric simulation for air gap variations from 10-30 cm with a step of 5 cm, lateral misalignment variations from -800 to 800 mm, and longitudinal misalignment variations from -900 to 900 mm. Then the efficiency calculation for this specific power pad is finished, otherwise, go back to Step 1 to fine tune the design parameters. If the calculated efficiency reaches the required value, 85% based on SAE J2954's recommendation. The simulation results are then verified by comparing the design criteria that is used in the literature.

3.2.2. Coil design. The transformer is the key component of WPT system and the coupling factor (k) is an essential parameter influencing the performance of the IPT system. Hence, an effective model for defining the coupling of the coils under predicted misalignment and air gap variation would be very helpful. In a static charging system, the loosely coupled coil resonators of the transformer are usually designed in a form of pad. All the pads are designed to generate a single-sided magnetic flux pattern. Therefore, all of these pad designs have a coil structure (consisting of single or multiple coils) placed under a ferrite bars and an aluminum sheet on the transmitter and the receiver sides to facilitate a low reluctance flux path while reducing the leakage flux on the back of the pad, with the other side facing the second pad in the system. Planar spiral winding design techniques are gaining attention due to their reproducibility and manufacturability.

The major design goal for windings in WPT systems is a high-quality factor (Q) for a given inductance. The resulting dimensional system provides an accurate geometrical description of the windings to obtain high Q and a simple set of manufacturing specifications. A comprehensive set of simulations shall confirm the validity of the dimensional system and the improvements in Q for wireless powered applications.

The system parameters considered for design are coil dimensions, winding and turn values, operating frequency and the user requirements are regarded as the amount of power to be transferred, voltage rating, space available for the system and cost etc. There can many combinations of IPT system parameters to meet the user requirement, however, this design process includes iterations to limit the use of a minimum cross section of coils and find the optimal number of turns of coils. Mutual inductance is the most sensitive and influencing parameter for IPT system.

It characterizes the coupling between the primary and secondary coil and varies rapidly with the movement of coils. It determines the capability of the system to transfer the power [49]. Figure 3.4 shows a detailed representation for the design of a 7-turn rectangular D coil with detailed design specifications using ANSYS Maxwell. The length and the width of the rectangular coil shown in Figure 3.4 are 80 cm and 60 cm respectively. The wire diameter is 4 mm and the spacing between the turns is 8 mm.

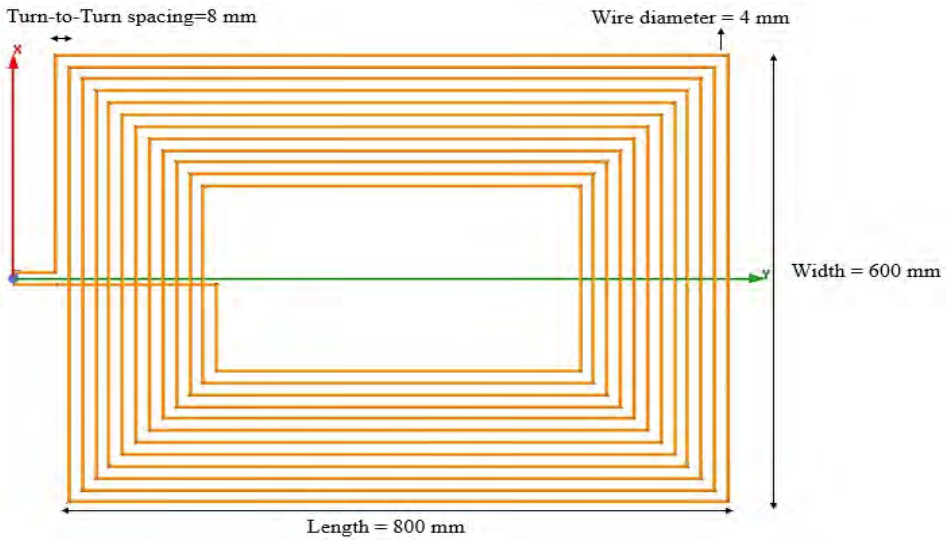

Figure 3.4: Detailed dimensions of rectangular coil.

Figure 3.5, Double-D coil designed using litz wire made up from copper of a diameter of 4 mm, and 4 turns. Furthermore, applying the same outer dimensions of the rectangular coil as well as 12 mm edge-to-edge spacing. All designed coils considered in this study are 60 X 80 cm^2 (i.e. The coil area is 0.48 m^2). A coil should be thin, compact, and light to be fixed onboard battery EVs as well as to be fitted in the ground. Moreover, the magnetic coupler formed by a track coil and the pickup should have both a sufficient coupling to operate with the ground clearance of a vehicle (it indicatively goes from 15 to 20 cm) and an acceptable tolerance to the misalignment [50].

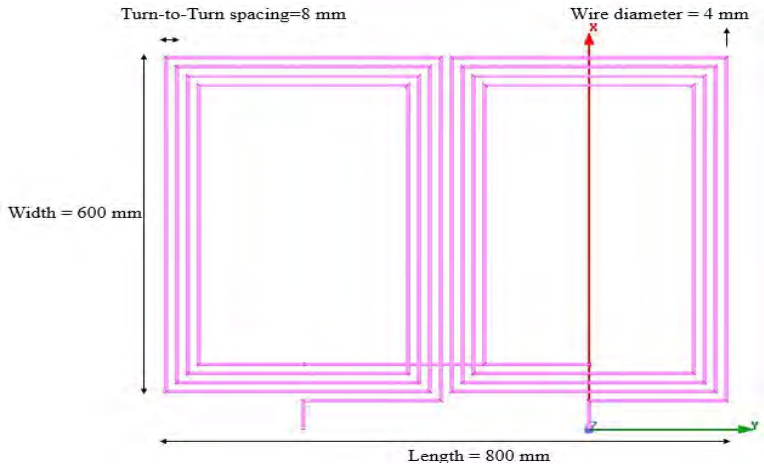

Figure 3.5: Detailed dimensions of Double-D coil.

3.2.3. ANSYS maxwell. ANSYS Maxwell is a powerful electromagnetic simulator which uses the accurate finite element method to solve electromagnetic fields. The analysis and design of the coils inductive coupling is being made with ANSYS

Maxwell software. One objective is to achieve more realistic and accurate coils models than the analytical equivalent coil circuits using lumped parameters. The approach is to generate and extract the coil parameters using the Magnetostatics and Eddy Current solvers available in ANSYS Maxwell 3D software. The coil models are created here by using the software's own geometry utilities. Air-core loosely coupled coils shall couple at a factor of ($k<0.5$). The primary (transmitter) coil is placed on the ground surface level, while the secondary (receiver) is mounted underneath the vehicle on its chassis, and the gap between them (e.g., the car ground clearance) is 200 mm. Simulation is a very important step in this research, due to the large number of degrees of freedom presented in this topic. The main source of importance generates from the fact that simulation will double check the values achieved from experiments and optimization, will help us better estimate the behavior and performance of the wireless power transfer system, as well as that it might help us reduce the cost or improve the full system efficiency.

3.3. Coil Geometry

Commonly, the problems associated with the conventional magnetic couplers of the inductive link are mainly large size for higher power rating and lower efficiency during misalignment. Different power pad structures considered for EV wireless charging are presented in Figure 3.6. Circular power pads are widely used for stationary wireless charging system design, due to their reduced leakage flux and compact design [4]. Due to design flexibility, circular power pads can be easily deployed for both grid side and vehicle sides. However, their performance fluctuates with the increment of the air gap. Double D power pads combine the advantage of both circular power pad and flux pipe topology, and thus result in a higher value of coupling coefficient than circular power pads [2] [51]. Due to the width of a DD power pad, it exhibits higher tolerance in misalignment conditions.

As DD power pads result in very low leakage flux, the overall power transfer efficiency does not fluctuate much by adding shielding [2]. For the same size of power pads, the flux path height of DD power pads is almost double compared to circular power pads, which significantly improves the overall power transfer efficiency of the system [10]. Bipolar power pads are being developed by combining two or three coils together, which results in better performance in misaligned positions [51]. These coils

can be energized by supplying current to each coil individually, and the independent control technique can be applied.

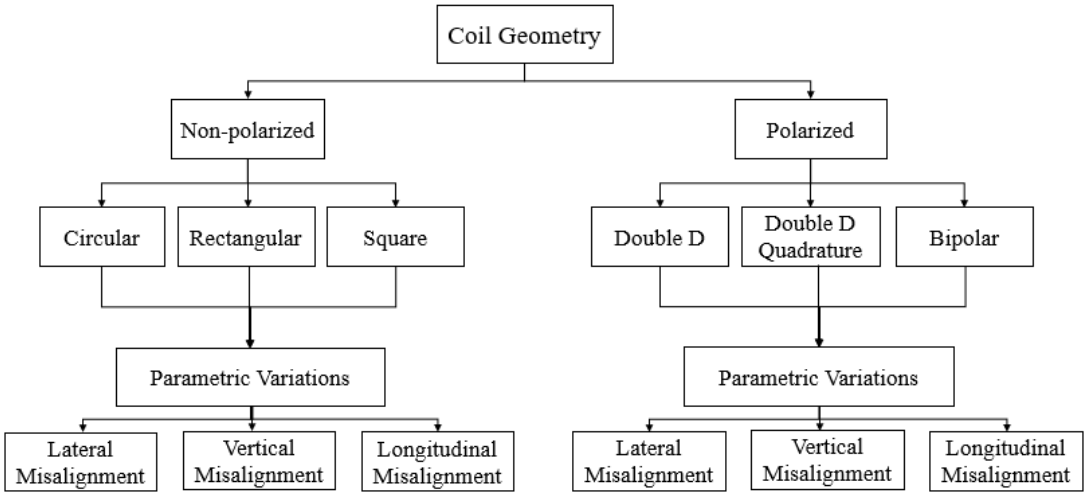

Figure 3.6: Mind map of different coil topologies.

Bipolar power pad exhibits a higher value of coupling coefficient, resulting in higher power transfer efficiency, and it requires 25-30% less copper to construct compared to DDQ power pads [51]. Double D Quadrature power pads are designed by adding a quadrature coil to DD power pads, resulting in excellent misalignment tolerance. For a similar size of the power pad structure, DDQ power pads result in a much larger charging zone which makes this power pad a protentional choice for the EV dynamic wireless charging system. However, the size of DDQ power pads is still an issue, as combining two different topologies increases the overall dimension of the power pad.

3.3.1. Rectangular coil. In Figure 3.7, each rectangular coil consists of N1=N2=7 turns of stranded copper wire. The area determined by the most outer turn is 0.48 m^2.

Rectangular and square coils have almost the same structure, but they differ hugely in performance; they form a double-sided polarized flux distribution [35]. This structure produces a higher flux path than the circular pad. When the coils are polarized, single-sided distribution flux is produced; this design has the highest magnetic coupling among all the other pad shapes.

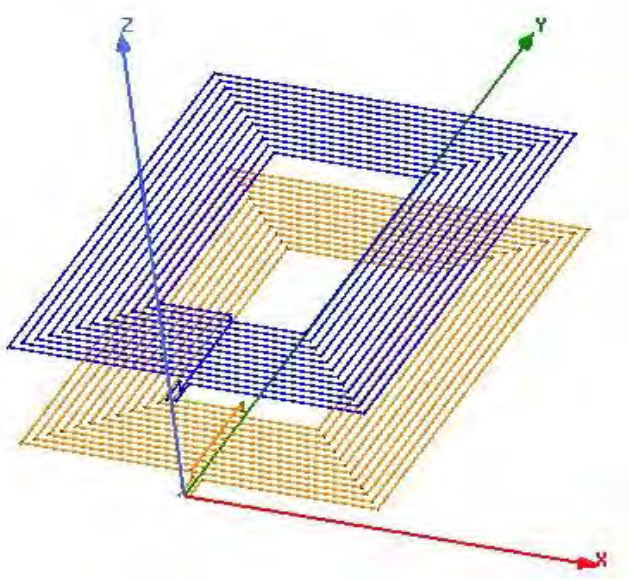

Figure 3.7: Rectangular coil (copper only).

A drawback of configuration that it is require more Litz wires to make a rectangular/square coil of the same area as that of a circular coil [18]. An analytic model built and validated experimental, to study and compare the performance of square pad with circular planar spiral pad, it was proved that square pad is the better choice for EV inductive charging.

3.3.2. Double-D coil. It is formed using two coils which are wound to form a north and south pole internally due to the layout of the coils and must be driven in series by a single-phase inverter. The coils are placed on the top of ferrite; this allows aluminum shielding to be placed under the ferrite without loss in quality factor. The main features of DD coil are single-sided flux paths, flux path height that is proportional to half of the length of the pad, resulting in a higher coefficient of coupling, lower losses in the aluminum shielding, and low leakage flux from the back of the coil. In addition, the no-load quality factor Q is improved [35], [53]. For the double-D winding, the losses in the eddy current shielding are significantly reduced. Due to the opposite winding sense of the two coils that form the double-D and their magnetic connection with the low-reluctance ferrite cores, the flux is naturally guided along the core without much leakage. DD power pads exhibit good performance. For the similar size power pads, the flux path height of DD power pads is doubled compared to circular power pads. The improved flux path height can significantly reduce the leakage flux and result in a higher coupling coefficient.

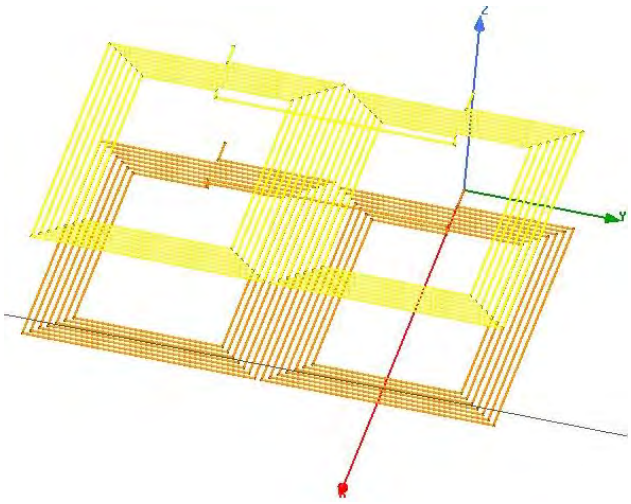

Figure 3.8: Double-D coil (copper only).

Double D power pad of two rectangular coils is shown in Figure 3.8, this is a single-sided polarized solenoid pad; this design merges advantages of both rectangular and flux pipe pads. Double-D pad (DDP) of square coils The DDP consists of two coils, magnetically in series and electrically in parallel to get low inductance. The coils also could be connected electrically in series using the same Litz wire. The DD structure has a flux pipe in the center, which usually made as long as possible; the remaining length of the coil has been minimized, in order to save copper, lowering the AC resistive losses, and controlling the flux height [34]. The flux height is directly proportional to the half-length of the pad.

3.3.3. Double-D quadrature coil. Double D quadrature (DDQ) coil is derived from DD coil by adding the quadrature coil as shown in Figure 3.9. The position of the coil is at the center of DD coil. The coils are placed such that DD coils capture the d-axis flux, and Q coil captures the q-axis flux. Therefore, this coil structure compensates the misalignment to a great extent. However, the size of the coils increases approximately three times with respect to the circular pad or the square coils [53].

A polarized flux pipe was reported in [53] that has better misalignment tolerance than a circular coil. The DDQ power pad is designed in this paper by combining rectangular and DD power pads inspired by double D quadrature (DDQ) power pads. The circular and DD power pads used in the DDC power pad design follow physical dimensions recommended in SAE J2954.

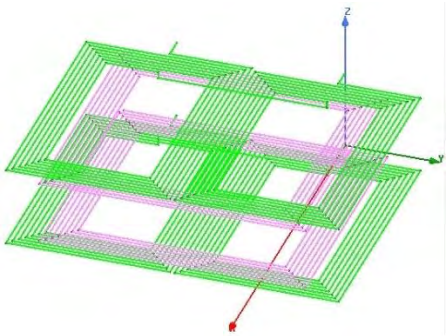

Figure 3.9: Double-D Quadrature coil (copper only).

Figure 3.9 The DDQ power pad is designed in this paper by combining circular and DD power pads inspired by double D quadrature (DDQ) power pads. The rectangular and DD power pads used in the DDQ power pad design follow physical dimensions recommended in SAE J2954. The DD coil and Q coil are used on the receiving side, and their outputs are connected in series. By determining the optimum turns of the receiver coil, a stable mutual inductance between the receiver coil and transmitters can be achieved when the receiver coil moves along transmitters. Based on the stable mutual inductance, a configurable compensation topology is used on the receiver side to achieve a constant output. The DDQ pad structure is same as DD, but has an additional quadrature coil, to enhance vertical misalignment tolerance. The flux height produced by DDQ structure is twice that those produced by circular pad structure [35].

3.3.4. Bipolar coil. The bipolar pad (BP) is a multi-coil coupler with two coils placed on the ferrite bar with an overlap as shown in Figure 3.10 [53], [54]. BP consists of two identical, partially overlapped, and mutually decoupled coils. The BP has high misalignment tolerance and high coefficient of coupling similar to DDQ pad. The main advantage of BP is that it requires 25% to 30% less copper as compared to DDQ pad [54]. A BP with reduced copper requirements was reported in [31]. It has the same misalignment characteristics as the DDQ coil. Bipolar base pads can be switched between circular and DD modes of operation. This means that public charging stations can effectively charge vehicles fitted with either circular rectangular or DD pads. DD pad flux path height is about half of the pad length and twice larger than circular pad in the same size and output power. Consequently, DD pad is efficient single sided pad which can be utilized in IPT.

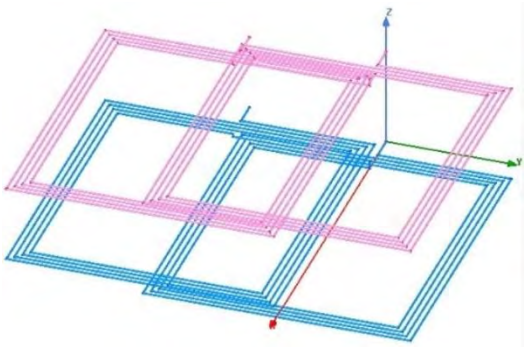

Figure 3.10: Bipolar coil (copper only).

BP pad, shown in Figure 3.10, has a construction identical to DD, except that the two coils here are overlapped [34]. It has proved that BPP provided an increase of misalignment tolerances [23]. Bipolar pads consisting of two largely coplanar, partially overlapping coils positioned such that there is no mutual inductance between them. This arrangement prevents interaction of the two coils and allows the currents within them to be independent in both phase and magnitude. By controlling the phase and magnitude of the two coil currents, the magnetic field can be shaped to assist in power transfer to a pickup underneath an EV.

3.4. Ferrite Geometry

The use of copper wires alone for the primary and secondary coils introduces significant losses for this high-power application, due to the inevitable flux leakage to surrounding ferrous materials such as the chassis of the car, surrounding infrastructure, etc., leading to eddy current losses and hysteresis losses [55] [56]. The use of ferrite, however, overcomes this problem and introduces significant improvements to the self and mutual inductances of the coils and to their coupling performance. This is because a ferrite layer helps to guide the magnetic field lines and constraints their path to within the area between the two coils, thereby reduces flux leakage to any surrounding magnetic materials. The ferrite layer is typically placed below the primary coil, with proper insulation between the copper wire and the ferrite surface, and on top of the secondary coil, as shown in Figure 3.11. magnetic permeability is significantly higher than that of the copper wire. Several ferrite material compositions can be used, of which Manganese-Zinc ferrites are most commonly used for power inductors and power transformer applications with relative magnetic permeability ranging from 1000 H/m to 3000 H/m depending on the material type [22]. The choice of the ferrite material and

the structure of the ferrite layer both determine the level of improvement in the self and mutual inductances of the coils in comparison to a ferrite-less structure. The arrangement of these ferrite pieces/bars directly impacts the inductance and coupling behavior of the coils. Three ferrite arrangements were reported in the literature in addition to the ferrite sheet structure. These are shown in Figure 3.11.

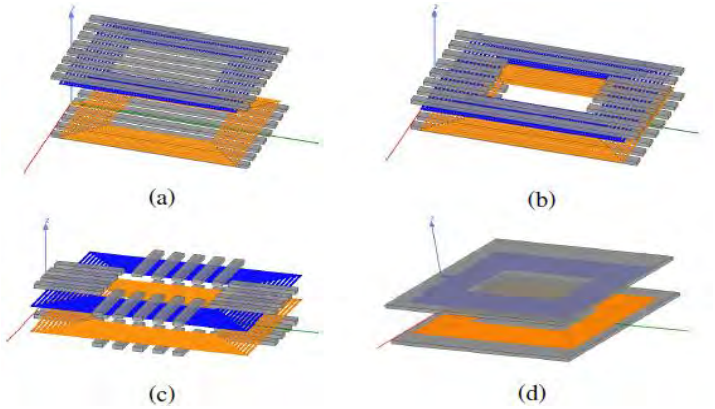

Figure 3.11: Ferrite geometries: (a) long ferrite bars across entire structure, (b) long ferrite bars along the length and short bars along the width, (c) short ferrite bars covering the conductor area, (d) ferrite sheet.

3.5. Aluminum Shielding

The most significant problem in WPT is the leakage field and its adverse effect on the surrounding material and human exposure. The WPT system should be compliant with different electromagnetic interference (EMI) standards. An aluminum is used for shielding the magnetic flux and also fix the physical structure of the pad. When aluminum shielding is used, its proximity to one side of the coil winding will result in intercepting flux and hence reducing the quality factor. This loss of quality factor lowers the efficiency of EV charging [53], [39]. Shielding can reduce the efficiency of a system by 1%–2% [57]. Typically, aluminum or copper is employed as a shielding material, as both of the material are highly conductive such that eddy currents induced in the material counteract the incident flux but also lead to losses in the shielding. To reduce losses in the shielding ferrite flux, guides with high permeability and high resistivity are used to divert the magnetic field into the coupling pad active zone, thereby minimizing flux entry into the shield [49], [50].

Shielding measures that redirect or absorb the magnetic field incur losses and reduce the efficiency of the WPT system. A proven method is to add aluminum shield

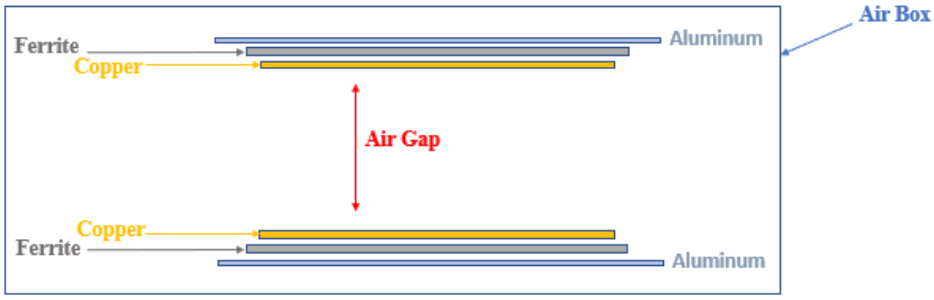

Figure 3.12: Detailed structure of power pad materials.

to the backside of the ferrite and coil. Figure 3.12 shows the circular coil with aluminum shielding. The presence of shielding affects the performance of the system by reducing coil inductance and increasing losses which requires further capacitance compensation to achieve resonance condition [57], [47].

3.6. System Model

The inductive power transfer system schematic diagram is shown in Figure 3.13, illustrating the basic series-to-series (S-S) compensation circuit of the WPT system.

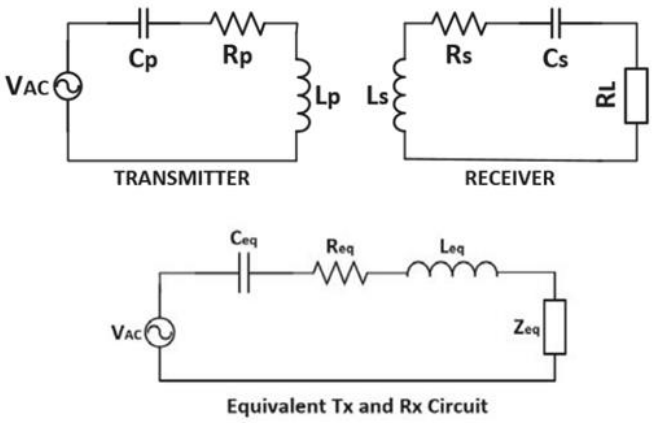

Figure 3.13: Series-series compensated circuit.

The schematic in Figure 3.13 consists of an input AC voltage V_{AC} connected to the primary and secondary resonant capacitors, C_p and C_s respectively, that resonate with the primary and secondary coil inductances L_p and L_s. The equivalent series resistance of the primary and secondary coils is denoted as R_p and R_s respectively, and RL is the equivalent load resistance on AC side of high-frequency rectifier. Equivalent resistance at the input of rectifier is given by

$$R_L = \frac{8}{\pi^2} R_o \,, \tag{3}$$

where R_o is the equivalent resistance of the battery.

$$R_o = \frac{V_o^2}{P_o}. \tag{4}$$

In this work, series compensation has been employed on both the transmitter and receiver sides due to its simplicity and reported effective performance in maximizing transferred power [36]. In order to maximize the power transferred from the primary to the secondary sides, the resonance condition needs to be established. This occurs by choosing the compensation capacitors to satisfy the condition in (5).

$$\omega = \frac{1}{\sqrt{Lp\ Cp}} = \frac{1}{\sqrt{Ls\ Cs}}. \tag{5}$$

From (5), it can be observed that the resonant frequency is independent of the mutual inductance *M* between the two coils, their coupling coefficient, *k* and the load resistance R_L which also indicates the independence of the capacitance values on these parameters. This, according to [58] [59], is a characteristic of S-S topologies over Series-Parallel (S-P), Parallel-Series (P-S) and Parallel-Parallel (P-P) networks. The coupling coefficient can be calculated from the self and mutual inductances using the expression:

$$k = \frac{M}{\sqrt{Lp\ Ls}}. \tag{6}$$

The output power across the load can be obtained using:

$$P_L = \frac{(\omega M)^2 \boldsymbol{V_{AC}}^2 R_L}{R_p\,(R_s + R_L) + \omega^2 M^2}\ . \tag{7}$$

The power transfer efficiency is defined as the ratio of output power across the load P_{RL} to the input power to the primary coil $P_{in,AC}$ and can be expressed as follows:

$$\eta = \frac{(\omega M)^2 R_L}{(R_s + R_L)(R_p\,(R_s + R_L) + (\omega M)^2)}. \tag{8}$$

By studying equations (4)-(6), it can be observed that the coils self and mutual inductances and their equivalent resistances directly impact their coupling performance and the power transfer efficiency. Since the geometry of the coils directly affects these

parameters, different coil geometries are compared in this work, particularly D, DD, Bipolar and DDQ coils at both the transmitter and receiver sides, in order to determine the most suitable geometry to provide a high efficiency dynamic wireless charging system.

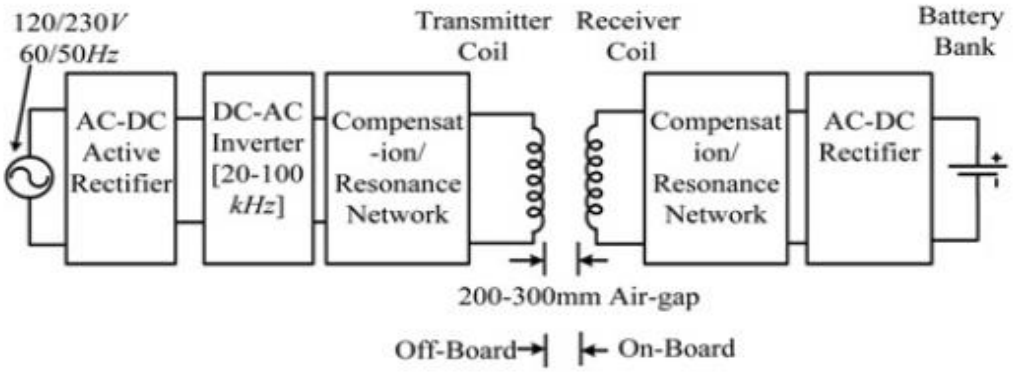

Figure 3.14: Block diagram of the Inductive Power Transfer system [70].

The block diagram of a classical EV wireless charging system is shown in Figure 3.14 following the standardized model for the wireless EV chargers presented in the SAE J2954 Standard. The end-to-end power transfer efficiency of this wireless EV charging system depends on the efficiency of each block in Figure 3.14. The modeling and co-simulation of the overall inductive power transfer system is implemented using the ANSYS Maxwell/Simplorer environments.

Besides the imported Maxwell 3D model of the coupling coils, previously created, the following models of the IPT system parts are built and added in Simplorer external circuit simulator: the system input DC power supply, the high frequency H-bridge inverter, the series tuned resonant capacitor on the transmitter coil side and the parallel capacitor on the receiver coil side, the diode bridge with the DC filtering capacitor, and the vehicle battery.

For this work, the inductive link efficiency is particularly investigated in order to evaluate the performance of the primary and secondary coils with different ferrite geometries. The link efficiency studied independently of the loading condition, depends on the coil quality factors, their self and mutual inductances and their coupling behavior. This efficiency is given by equation (7):

$$\eta = \frac{k^2 Q_p Q_s}{\left(1 + \sqrt{1 + k^2 Q_p Q_s}\right)^2}, \tag{9}$$

where *k* is the coupling factor and *Qp* and *Qs* are the quality factors of the primary and secondary coils, respectively. The coupling factor can be calculated from the self and mutual inductances as shown in equation (4), where *M* is the mutual inductance between the two coupling coils, and Lp and Ls are the self-inductances of the primary and secondary coils, respectively. The coil quality factors, Qp and Qs, on the other hand, are evaluated using the following expressions in (8) and (9):

$$\mathrm{Q_p} = \frac{\omega_0 \mathrm{L_p}}{\mathrm{R_p}}, \tag{10}$$

$$Q_s = \frac{\omega_0 L_s}{R_s}, \tag{11}$$

where ω denotes the operating frequency of the power transfer system, and *Rp* and *Rs* involves in the coil quality factor calculation. According to (7), increasing the inductive link efficiency can be achieved by increasing the coupling factor k and the respective coil quality factors Qp and Qs. The coupling factor *k* depends on the mutual and self-inductances of the two coils and is affected by the vertical distance between the two coils among other factors. The coil quality factors, on the other hand, are affected by resonance frequency ω, the self-inductances Ls and Lp, and the ESRs of the primary and secondary coils. The operating frequency of the inductive link for wireless EV chargers, ω, is selected based on industry standards and is used to design the different wireless power transfer (WPT) system parameters to establish resonant coupling conditions.

3.7. ANSYS Simplorer

The final design of the coupled coils shall be imported in ANSYS Simplorer for the overall inductive power transfer system model development. ANSYS Simplorer is another powerful platform that ANSYS provides, specifically for the aim of simulating system-level prototypes and models. ANSYS Maxwell was designed to provide an equivalent circuit for the model, which can be used as a part of the full system implemented on Simplorer. Simplorer enables verifying and optimizing the system's performance. In magnetic resonance WPT, the amount of transferred power depends

on the electrical characteristics of both the source and the load. The transmitting and receiving coils should be tuned to resonate at the same frequency. This can be achieved through adding some electrical components such as compensation capacitors to enable the tuning of compensation network and achieving resonance condition to guarantee maximum power transfer efficiency, in addition to the design of the coils, in terms of their geometry. ANSYS Simplorer makes it possible to simulate such a system, as it has the ability to solve electrical and magnetic fields at the same time, where it can account for the electrical components in the circuit, as well as the coils' geometry.

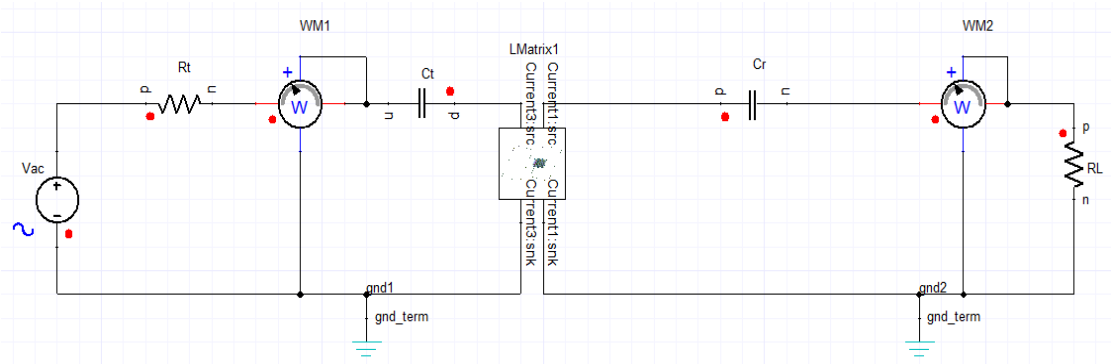

Figure 3.15: AC-AC inductive link circuit using Simplorer.

3.8. PSIM simulator for Inductive Link Efficiency Evaluation

In order to validate the simulated models, the proposed IPT system has been built in PSIM environment that is a circuit-oriented simulator model.

In Figure 3.15, is shown the PSIM circuit of the whole IPT system with a battery. The power supply has been modeled by a sinusoidal current generator at an operating frequency of 100 KHz, that supplies the primary coil of the inductive link.

The latter has been modeled by means of a two loosely coupled transformers, with a mutual inductance between them, where the first winding represents the rectangular primary coil and the other winding represents the rectangular secondary coil.

Figure 3.16 is the current and voltage waveforms generated for the primary and secondary sides using the proposed power pad design with an efficiency of 76%. The transferred power can be estimated from the input and output voltage and current of the wireless charging circuit.

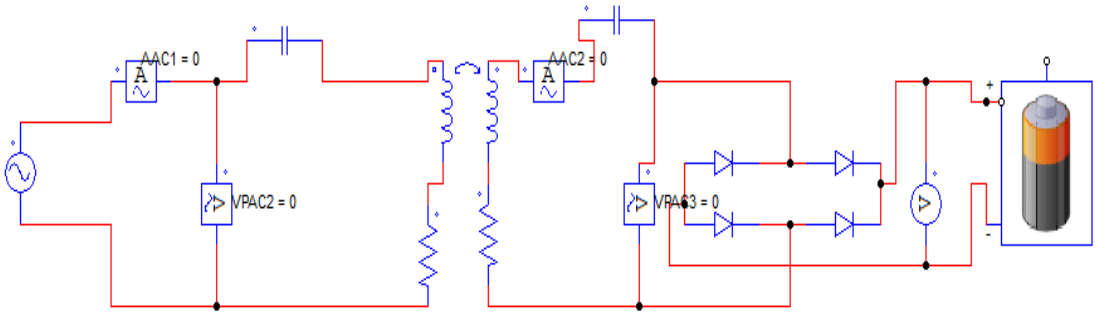

Figure 3.16: AC-AC inductive link circuit using PSIM.

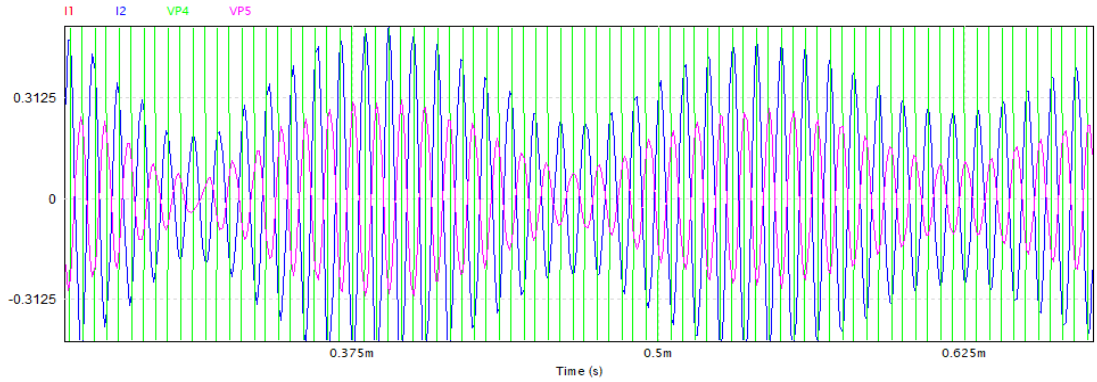

Figure 3.17: Input and output current and voltage using PSIM.

3.9. The Impact of Coupling and Loading Variations

This section outlines the analytical expressions of the inductive wireless power transfer system and discusses the details of the system model under investigation [6]. Nevertheless, the variation of mutual inductance does have an impact on the primary inverter current, which can be observed by analyzing the circuit in Figure 3.13 in the frequency domain, as follows:

$$-j\omega M I_s = V_{AC} - I_p R_p, \tag{12}$$

$$V_s = j\omega M \mathbf{I}_p = \mathbf{I}_s(R_s + R_L), \tag{13}$$

from which the secondary current $\mathbf{I}_s$ can be expressed in terms of the primary current *Ip* as:

$$\mathbf{I}_s = \frac{j\omega M \mathbf{I}_p}{R_s + R_L}, \tag{14}$$

which leads to the following expression for the primary current *Ip*:

$$\mathbf{I}_p = \frac{V_{AC}}{R_p + \frac{\omega^2 M^2}{R_s + R_L}}, \tag{15}$$

where $\mathbf{I}_p$, $\mathbf{I}_s$ and V_{AC} are the phasor representations of the corresponding signals. The voltage across the load V_L is expressed as follows:

$$V_L = \frac{j\omega M V_{AC}}{R_p(R_s + R_L) + \omega^2 M^2}. \tag{16}$$

The output power across the load is then calculated using the expression $P_{R_L} = \mathbf{I_s} \cdot 2R_L$. Then substituting $\mathbf{I}_s$ from (14) and $\mathbf{I}_p$ to obtain an expression for P_{R_L} in terms of the input AC voltage V_{AC} as follows:

$$P_{R_L} = \frac{(\omega M)^2}{\left(R_p(R_s + R_L) + (\omega M)^2\right)^2}. \tag{17}$$

On the other hand, the input power to the primary coil is expressed in terms of V_{AC} by substituting $\mathbf{I}_p$ from (15) into $P_{in,AC} = \mathrm{R}\{V_{AC}\mathbf{I}_p\}$:

$$P_{in,AC} = \frac{V_{AC}^2}{R_p + \frac{(\omega M)^2}{R_s + R_L}}. \tag{18}$$

From (15) and (17), it can be seen that the primary coil current and output power are inversely proportional to mutual inductance. This means that, in a DWPT scenario, when the EV has already passed over the primary coil segment, *M* is significantly reduced causing an undesirable increase in $\mathbf{I}_p$, i.e. a primary side overload. In addition, to maintain the same output power, the inverter primary current needs to be adjusted to offset the change in the mutual inductance caused by misalignment, which reduces the power transfer efficiency, which is defined as the ratio of output power across the load P_{R_L} to the input power to the primary coil $P_{in,AC}$ [6]. The expression for the power transfer efficiency is obtained using (17) and (18) as follows:

$$\eta = \frac{P_{R_L}}{P_{in,AC}} = \frac{(\omega M)^2 R_L}{(R_s + R_L)(R_p(R_s + R_L) + (\omega M)^2)}. \tag{19}$$

From (19), it is observed that the power transfer efficiency depends mainly on the resonance frequency ω, the mutual inductance *M* and the load resistance R_L. Hence,

in order to compensate for variations in efficiency caused by variations in mutual inductance, the resonance frequency and/or the load resistance can be varied. Nevertheless, changing the resonance frequency requires re-designing the inductive link parameters, particularly the capacitors *Cp* and *Cs*, which is practically difficult to implement. Instead, varying the AC equivalent load resistance R_L to compensate for changes in the mutual inductance is a suitable solution to maximize the power transfer efficiency. By differentiating the efficiency expression in (19) with respect to R_L, the optimum load resistance $R_{L_{Opt}}$ is given by:

$$R_{L_{Opt},S-S} = \sqrt{R_s^2 + \frac{R_s}{R_p}(\omega M)^2}\,. \tag{20}$$

By observing (20), it is noted that the load resistance needs to be varied according to variations in the mutual inductance in order to maintain the maximum transfer efficiency throughout the system operation. It should be noted that the load resistance in Figure 3.13 is the equivalent AC resistance of all circuits that are connected to the secondary coil, including the AC/DC rectifier circuit and the actual EV battery. Hence, controlling *RL* can be achieved by controlling the AC voltage across the load V_L to achieve $R_{L,Opt,S-S}$ in (20). The expression of optimum load voltage, $V_{L,Opt}$ can be obtained by substituting (20) in (16) as follows:

$$V_{L_{Opt},S-S} = \frac{j\omega M \mathbf{V}_{AC}}{R_p\left(R_s + \sqrt{R_s^2 + \frac{R_s}{R_p}(\omega M)^2}\right) + \omega^2 M^2}\,. \tag{21}$$

Based on the work in [59] and [60], the series–series compensation topology is the most common and convenient structure used to implement wireless power transfer for light weight electric vehicle. This topology is then selected for the simulations conducted in this work. In particular, the efficiency of the inductive link under different loading variations is specifically studied in order to evaluate the performance of the primary and secondary coils with various coupling and loading conditions.

3.10. Ferrite-Less Power Pad Weight and Cost Calculation

Litz wire made of copper material without ferrite or aluminum is considered.

3.10.1. Rectangular coil. Rectangular coil copper with circular cross section. The coil Length is calculated as follows:

$$\ell = 2t + via + (W - (N-1) * spacing) + N * spacing + \sum_{x=0}^{2N-1} (L - x * spacing) + \sum_{y=0}^{2N-2} (W - y * spacing). \quad (22)$$

Table 3.1 below shows the length, volume, and copper mass of the proposed rectangular power pad.

Table 3.1: Rectangular coil weight.

Length ℓ (m)	Volume (m^3)	Copper Mass (kg)
10.74	0.00013496	1.2079

$$R = \frac{\rho L}{A}, \quad (23)$$

where ρ is the resistivity, L is the coil length, and A is the cross-sectional area of the litz wires.

3.10.2. Double-D coil. Double-D coil copper with circular cross section, the coil Length is calculated as follows:

$$\ell = 2t + 2via + 2(W - (N-1) * spacing) + W + spacing + 2\sum_{x=0}^{2N-1} (L - x * spacing) + 2\sum_{y=0}^{2N-2} (W - y * spacing). \quad (24)$$

Table 3.2 below shows the length, volume, and copper mass of the proposed Double-D power pad. It is clear that the length, copper mass of the Double-D coil is higher that rectangular. This ensures that polarized magnetic couplers require more materials to be modelled. Hence, the performance of Double-D is expected to be better than non-polarized rectangular.

Table 3.2: Double-D coil weight.

Length ℓ (m)	Volume (m^3)	Copper Mass (kg)
15.296	0.000192	1.71947

3.11. Mutual Inductance Estimation

As part of coil parameter estimation, the mutual inductance is considered a critical parameter in the inductive link. Measuring the mutual inductance between too loosely coupled coils is not straightforward. Hence, in this research three different methods will be deployed to estimate the mutual inductance under misalignment variations.

3.11.1. Vectors Network Analyzer (VNA) evaluation/estimation. Measurement of coil S-parameters to calculate the self and mutual inductances of the implemented coils. The practical mutual inductance is estimated by substituting the Z parameters converted from S parameters. S_11 represents reflection coefficient and its dB value approaches zero tells that almost whole power fed is flowing back towards feed. The characteristic is between 6 and 12 GHz tells that it does not match in this band, in other words it may match somewhere. Equation (25) represents the Z parameter that is used to calculate the mutual inductance. Z_21 can be calculated from the S parameters obtained from the VNA.

$$Z_{21} = Z_o.\frac{2\,.S_{21}}{(1-S_{11})(1-S_{22})-S_{12}S_{21}}. \tag{25}$$

Mutual inductance can be calculated by

$$Z_{21} = j\omega M, \tag{26}$$

where ω is determined by $\omega = 2\pi f$ and f is at 85 KHz.

$$M_{21} = \frac{Z_{21}}{j\omega}. \tag{27}$$

3.11.2. Measurements using voltage gain. Calculation of Mutual inductance through voltage gain obtained experimentally using the following equations.

$$V_s = j\omega M_{Ip}, \tag{28}$$

where V_s is the voltage at the secondary side of the inductive link. Equation (29), the current at the primary side can be calculated by,

$$I_p = \frac{V_{AC}}{R_p + \frac{\omega^2 M^2}{R_s + R_L}}, \tag{29}$$

The voltage gain equation in (rms) is a function of M and R_L,

$$Voltage\ Gain = \frac{V_s}{V_{AC}} = \frac{\omega M}{R_p + (\frac{\omega^2 M^2}{R_s + R_L})}. \quad (30)$$

Since the value of R_p is very small, it can be neglected to simplify the equation as follows:

$$Voltage\ Gain\ (RMS) = \frac{V_s}{V_{AC}} = j\frac{R_s + R_L}{\omega M}. \quad (31)$$

Finally, the mutual inductance is calculated using the obtained values of V_s and V_{AC},

$$M = \frac{V_{AC}}{V_s} . \frac{(R_s + R_L)}{\omega}. \quad (32)$$

3.11.3. Finite Element Method simulation. The finite element method simulation is the most commonly used method for resolving electromagnetic problems. ANSYS Maxwell is used to model the mutual coupling between two loosely coupled coils an to estimate the design parameters.

3.12. Mutual Inductance and Dot convention

Mutual induction describes a phenomenon when a coil gets induced in electromotive force (EMF) across it due to the rate of change in current in the adjacent coil in a way that the flux of one coil current gets linked to another coil. This emf is the voltage drop across the coil. Mutual Inductance can be analyzed as the ratio between induced EMF across a coil (primary) to the rate of change of current of another coil (secondary) in such a way that two coils have flux linkage. This happens whenever there is a time varying current in a coil, the time varying flux will link with the coil itself and will cause a self-induced EMF across the coil. When a time varying current flows in the secondary coil placed at a certain air gap distance from the primary coil then the flux produced by the second coil will link the first coil.

This varying flux linkage from the second coil will also induce emf across the first coil. This phenomenon is called mutual induction. The mutually induced emf would be additive or subtractive depends on the relative polarity of the mutually coupled coils. The value of the mutual inductance depends on the amount of flux of one

coil links to another coil. The relative polarity of two mutually coupled coils is denoted by the dot convention.

It is represented with a dot mark at either end of a coil. If a current is entering a coil through dotted end, then mutually induced an emf to the other coil will have the positive polarity at the dotted end of the latter. If the current is leaving a coil through the dotted end, then mutually induced an emf to the other coil will have the negative polarity at the dotted end of the latter. If two currents are entering or leaving into the dot at the same time, then voltage generated due to mutual coupling will be positive. On the other hand, if one current is entering and another current is leaving or vice versa, then the voltage generated due to mutual coupling will be negative.

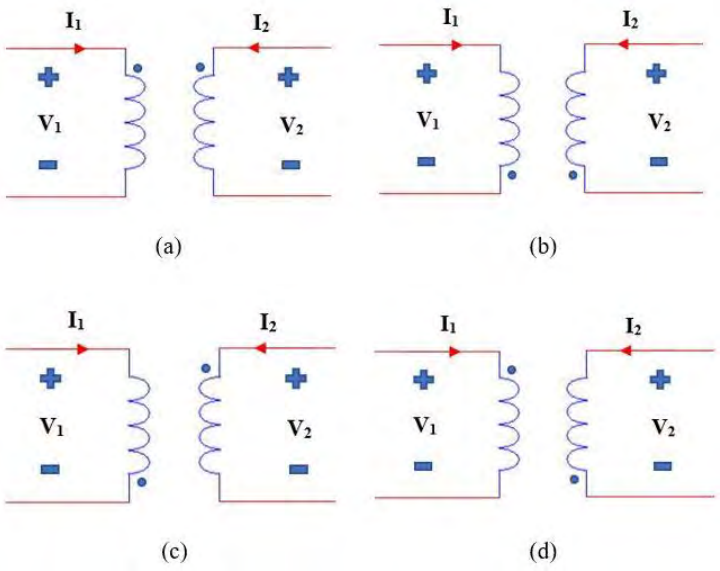

Figure 3.18: Dot notation and convention for two loosely coupled coils. (a) I_1 and I_2 are entering the dot (positive induced voltage), (b) I_1 and I_2 are leaving the dot (positive induced voltage), (c) I_1 leaving and I_2 entering the dot (negative induced voltage), (d)) I_1 entering, I_2 leaving the dot (negative voltage).

In Figure 3.18, for case (a), the voltage expression for the primary side voltage is given by

$$V_1 = L_1 \frac{di_1}{dt} + M \frac{di_2}{dt}. \tag{33}$$

where L_1 is the primary coil self-inductance, M is the mutual inductance between the two coils, i_1 and i_2 are the primary and secondary side current respectively.

For case (b), the voltage expression for the secondary side voltage is given by

$$V_2 = L_2 \frac{di_2}{dt} + M \frac{di_1}{dt}. \tag{34}$$

Similarly, for case (c), the voltage expression for the primary side voltage is given by

$$V_1 = L_1 \frac{di_1}{dt} - M \frac{di_2}{dt}. \tag{35}$$

Similarly, for case (d), the voltage expression for the secondary side voltage is given by

$$V_2 = L_2 \frac{di_2}{dt} - M \frac{di_1}{dt}. \tag{36}$$

Chapter 4. Simulation Results and Discussion

Among the several design parameters and optimization efforts required to maximize the power transfer efficiency of this wireless charging system, the design of the primary and secondary coils is of extreme importance, as it incorporates the electromagnetic aspect of the wireless power transfer process. The major drawback of a WPT system is that the power transfer efficiency is reduced significantly with the increment of the air gap distance between the transmitter and receiver. Several EV wireless charging topologies employed with a short air gap are provided. A short air gap configuration is also known as a near field power transfer system, where the transmitter and receiver remain in close proximity. Generally, the air gap ranges up to 40 cm.

4.1. Simulation Setup

In order to compare the different coil geometries, FEM simulations are conducted on ANSYS Maxwell simulation software to study the coupling performance of using D, DD, BP, and DDQ configurations for both transmitter and receiver coils. Each configuration is applied to both coils at a time and the simulation is conducted at 85 KHz frequency to ensure compliance with SAE J2954 standard [45]. To ensure a fair comparison between all different geometries under investigation, the outer dimensions of the coils are maintained at 80 x 60 cm^2, to make it possible for the secondary coil to fit at the bottom of the EV [9]. A copper wire (litz wire) is used for the coil construction, with a circular cross-section with 4 mm diameter. The number of turns is changing according to the inner-to-outer area ration and the vertical distance between the transmitter and receiver power pads (i.e. Air gap) is maintained at 200 mm for most of the simulations unless it is a variable. Ferrite layer is added to improve the coupling performance and reduce the leakage of flux to the surrounding ferrous materials [61], in the form of long ferrite bars inserted on the top of the secondary coil and below the primary coil in order to focus the magnetic field lines to the area between the two coils. In particular, eight (9) ferrite bars are used with a length of 900 mm and width equal to 37.5 mm. The ferrite thickness is 16 mm and the edge-to-edge bar spacing is set to 75 mm. The simulation is conducted on Eddy Current simulation mode and 50 A current was used as the primary and secondary excitation currents.

4.1.1. Design specifications. The primary and secondary coils of the WPT system are designed, simulated, and optimized using the ANSYS Maxwell simulation software. A parametric coil design process was conducted to observe the effect of different parameters on the value of inductance and the coupling factor. Parameters include coil length and width, turn-to-turn spacing, wire diameter, and air gap. Litz wires with a circular cross-section were used to model the primary and secondary coils. The value of inductance is observed to be smaller for larger wire diameters. The design specifications of primary and secondary coils are detailed in Table 4.1. Using Litz wires with circular shapes, rectangular-shaped coils were simulated using the 3D ANSYS Maxwell software. Two coil geometries are used for the analysis conducted in this work. The first design uses copper coils only with no ferrite or aluminum layers. Secondly, ferrite sheet structure was added under the primary coil and above the secondary. The third coil study was done to investigate the effect of adding aluminum shield on coupling and inductance. According to the SAE J2954 Standard for wireless power transfer systems, the operating frequency for EV charging systems should be up to 90 KHz in order to ensure compliance with magnetic field exposure limits. In particular, SAE J2954 standards recommends 85 KHz as the operating frequency for static EV chargers.

Table 4.1: Design specification of simulated primary and Secondary D & DD Coils.

Criteria	**Desired value**
Operating/Resonance Frequency, *f*	85 KHz
Excitation Current for Primary/Secondary	50 A
Number of Turns	4
Coil Dimensions (Length X Width)	60 X 80 cm^2
Turn Spacing	12 mm
Litz wire diameter	4 mm
Number of Ferrite bars	9
Ferrite Thickness	16 mm
Aluminum sheet thickness	1.2 mm

4.1.2. Lateral misalignment. The EV motion with a lateral displacement along axis y of Figure 4.1 reduces the power transferred to EV on account of the lower

value of the mutual inductances between track and pickup coils [13]. Effects of the lateral displacement in coil pair #1 have been evaluated by a FEM analysis, executing a parametric analysis of the mutual inductances between track and pickup coil for lateral displacements increasing from 0 up to 800 m, the lateral dimension of the pickup coil. A simulation model was created to investigate flux paths produced in a rectangular and DD pad system comprising identical transmitter and receiver (vertically aligned) with an air gap of 200 mm.

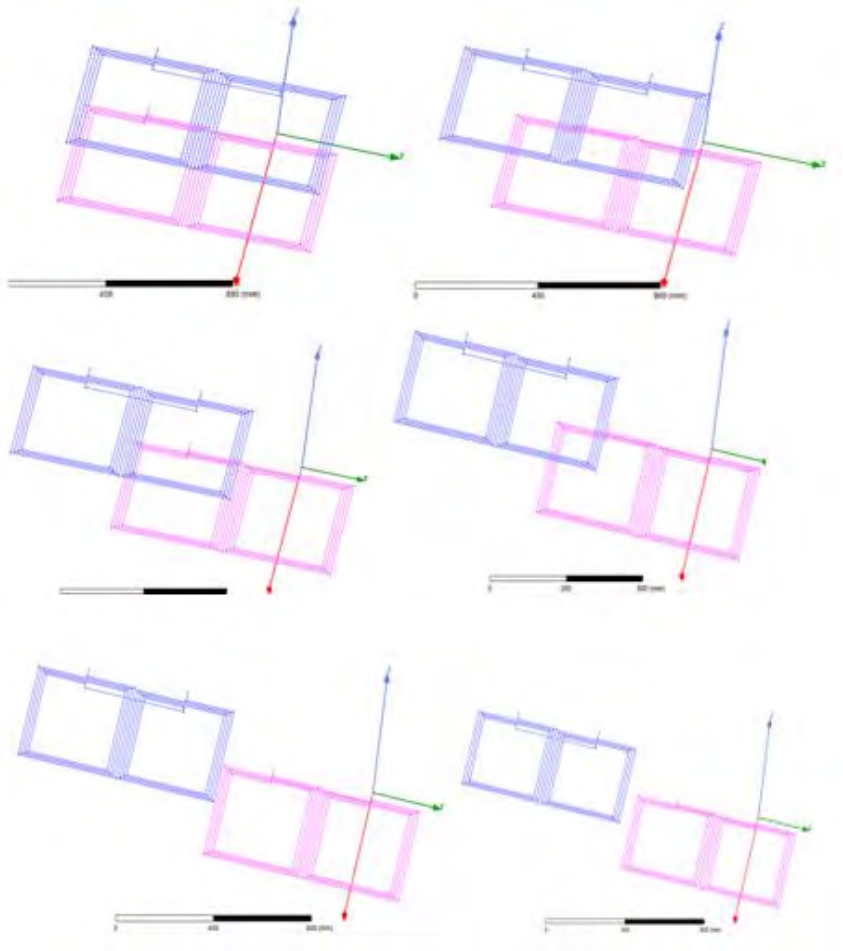

Figure 4.1: Lateral misalignment variations from 0 to 850 mm for DD coil.

4.2. Preliminary Results

In this section, the simulation is conducted for both Double-D and rectangular power pads as shown in Figure 4.2. The dimensions of each power pad were introduced in Table 4.1. to allow fair comparison between each geometry, the outer dimension, number of turns, wire diameter, and number of ferrite bars for rectangular and DD coils are identical.

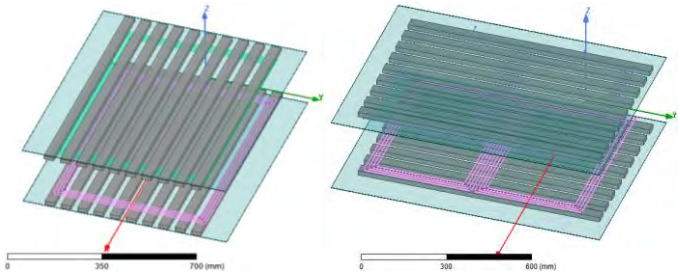

Figure 4.2: Rectangular coil simulated in this section (left) and Double-D coil (right).

Based on the simulation setup presented in the previous section, the D and DD coils are simulated at different lateral misalignment positions varies from -800 mm up to 800 mm, and their coupling factors are obtained and plotted. Furthermore, vertical misalignment variations from 100 mm to 300 mm coupling factor and efficiency will be further studied [64].

Figure 4.3 - Figure 4.6 simulate the difference between rectangular and DD coils with the variation of wire diameter: 4 mm, 6 mm, and 8 mm, along various lateral and vertical misalignment conditions. Figure 4.3 describes the effect of air gap on coupling and quality factors. It is obvious that the maximum coupling factor can be achieved at the minimum value of vertical misalignment. Hence, the relationship between air gap and k, Figure-of-Merit is inversely proportional.

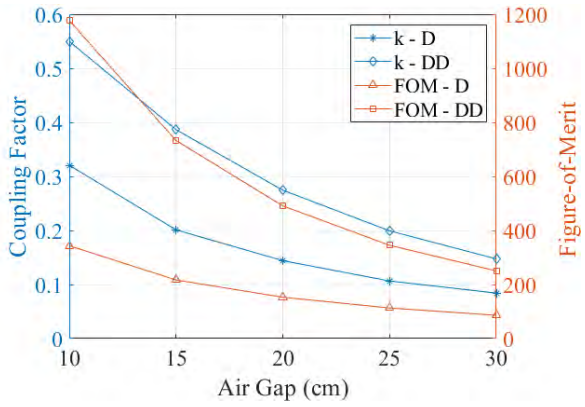

Figure 4.3: Rectangular vs DD: air gap variation with coupling factor and Figure-of-Merit.

Figure 4.4 illustrates the impact of air gap on the inductive link efficiency and the Figure-of-Merit. It can be concluded that air gap has huge potential in increasing or decreasing the power transfer efficiency of an IPT system. FOM was calculated based on equation (2). As a result, it was found that the higher the value of the air gap the lower the mutual inductance and coupling factor values. Hence, the overall system

efficiency decreased. The results indicate acceptable results at an air gap of 10 cm. Practically, air gap shall be larger in case of EV charging.

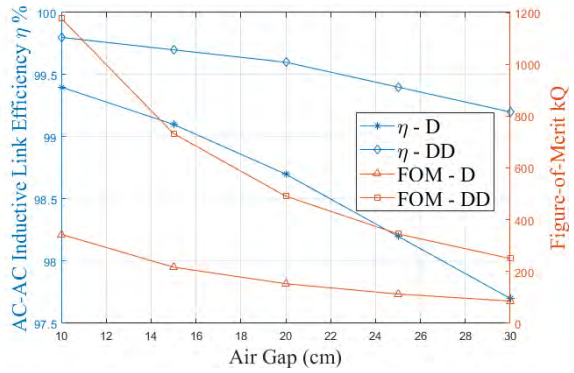

Figure 4.4: Rectangular vs DD: Air Gap variation η and FOM.

The next parametric simulation estimates the influence of lateral misalignment between the transmitter and the receiver coils for rectangular and Double D. Variations in lateral misalignment were shown earlier in Figure 4.1. The results were obtained and presented in Figure 4.5 and Figure 4.6 at an air gap of 20 cm. Based on the literature, it is expected that Double D will perform better at different misalignment conditions. The effect of lateral displacement on coupling and quality factors is presented. It is clear that with the variation in lateral distance, the coupling factor fluctuates and decreased extremely after 200 mm of misalignment. It became negative at 300 mm and above.

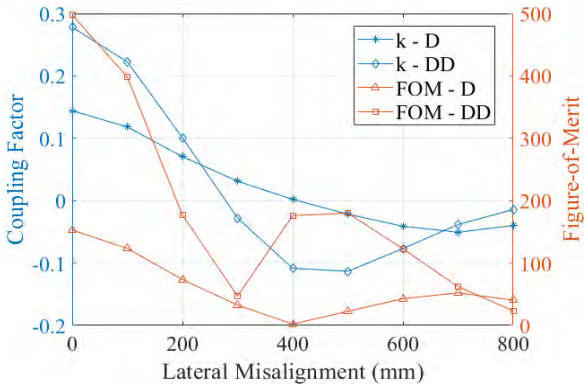

Figure 4.5: Rectangular vs DD: lateral misalignment variation with Coupling factor and Figure-of-Merit.

In addition, Figure 4.6, indicates the efficiency variations with lateral misalignment for rectangular and Double D coils. The center point represents the location of perfect alignment and hence provides the highest coupling. The AC-AC power transfer efficiency is then calculated using (7) for each data point in Figure 4.4

and the corresponding efficiency values are plotted in Figure 4.6 as follows. Rectangular (D) and Double-D coil geometries were designed, simulated and compared using the same design specifications. The following set of results are focusing on Double D geometry under various wire diameter options.

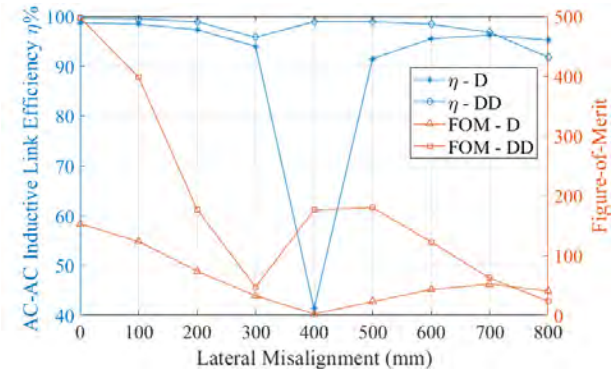

Figure 4.6: Rectangular vs DD: lateral misalignment variation with efficiency and Figure-of-Merit.

Figure 4.7-Figure 4.10 represent the variation of coupling coefficient, quality factor, and inductive link efficiency for Double D power pads under different litz wire diameters with the vertical displacement ranging from 100 mm to 300 mm between Ground assembly and vehicle assembly and lateral displacement ranging from -800 mm to 800 mm. The value of the coupling coefficient indicates the condition of flux linkage between transmitting and receiving power pads. A greater value of coupling coefficient indicates stronger coupling between transmitting and receiving sides of power pads, which is very crucial for EV wireless charging systems.

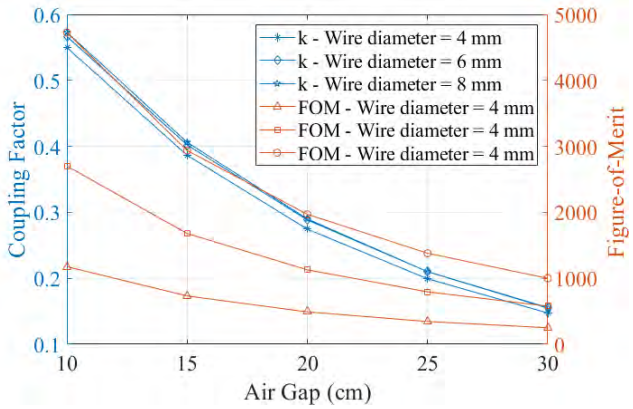

Figure 4.7: Double-D: air gap variation with coupling factor and Figure-of-Merit for various wire diameters.

Figure 4.7 illustrates the performance of the Double D power pad against air gap variation. Each line graph represents different wire diameter that forms the coil. The diameter of copper wires was found to be an important factor that affects the coupling performance and inductive link efficiency. It can be observed that the higher the litz wire diameter the better the coupling performance and overall system efficiency. In fact, the larger the wire diameter the more complex is to form the coil in the desired shape. Moreover, large wire diameter for coil windings results in extra losses of magnetic flux. Hence, magnetic field losses cause a drastic drop in the coupling factor. At the lowest value of air gap, the AC-AC efficiency of the inductive link was calculated to be approximately 100%, as shown in Figure 4.8. The efficiency is almost 100% for all air gaps and for all wire diameters. This was obtained when the wire diameter was set to be 8 mm. For experimental setup, it is recommended to use smaller wire diameter to be able to shape them, and maintain the turn spacing to be fixed at a value of 12 mm.

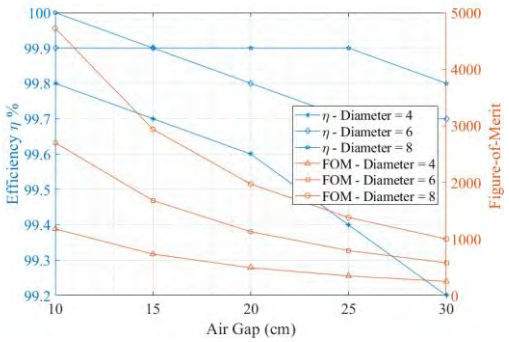

Figure 4.8: Double-D: air gap variation with efficiency and Figure-of-Merit for various wire diameter options.

Apart from vertical misalignment, lateral misalignment is a major challenge of the dynamic wireless charging system. This is due to the variations in mutual inductance between primary/secondary power pads that occurs due to horizontal misalignment. Figure 4.9 and Figure 4.10 describe the impact of lateral displacement on the coupling characteristics of the Double D power pad. Under fixed turn-to-turn spacing, varying wire diameter with lateral displacement is shown in Figure 4.9. It can be observed that when the value of wire diameter is relatively high (8 mm), the coupling coefficient performs slightly better at various misalignment distances. On the other hand, the Figure-of-Merit decreases vary rapidly from perfect alignment scenario at a value of 1981.68 to a value of 98.2 at y=±800 mm. Double D geometry is acknowledged

to have misalignment tolerance. Hence, Figure 4.9 and Figure 4.10 indicate that DD can tolerate the lateral misalignment up to 200 mm. The null point is defined to be the point where there is no mutual coupling between transmitter and receiver. It happens at y = ±300 mm and y = ±300 mm, where the coupling factor value is almost zero -0.027 and -0.0147 respectively. The coupling factor becomes negative at y =±400 mm, y=±500 mm and y=±600 mm. The negative sign of the coupling coefficients is negative indicates the flipped direction of the magnetic flux lines. The positive direction of the magnetic flux linkage can be defined when two transmitter coils are perfectly aligned.

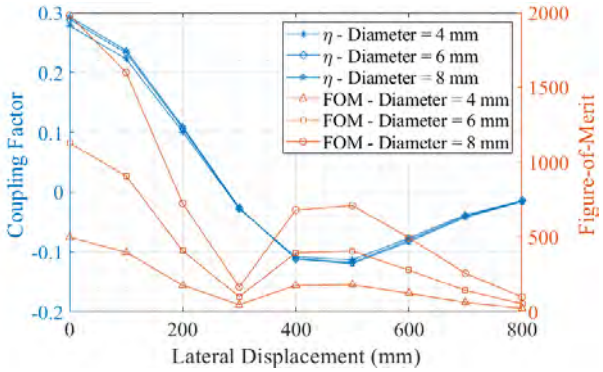

Figure 4.9: Double-D: lateral misalignment variation with coupling factor and Figure-of-Merit for various wire diameter options.

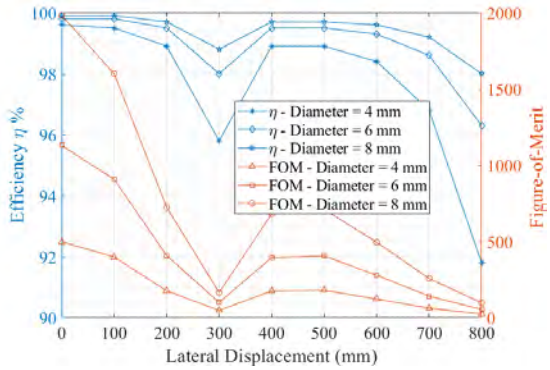

Figure 4.10: Double-D: lateral misalignment variation with efficiency and Figure-of-Merit for various wire diameter options.

In Figure 4.10, the inductive link efficiency against lateral displacement is presented. When the wire diameter is 8 mm, the efficiency is more stable along different horizontal distances. The maximum power transfer efficiency at perfect alignment for different wire diameter options 4 mm, 6 mm, 8 mm is 99.6%, 99.8%, 99.9% respectively.

4.3. Discussion

The initial comparative study focused on analyzing two coil geometries: rectangular (D) coil with Double-D coil. The simulation was done with a fixed wire diameter to 4 mm and turn-to-turn spacing to 12 mm. Ferrite bars and aluminum sheet were added to improve the coupling characteristics. In case of DD power pad comparison with rectangular, the extracted parameters using the Maxwell/Eddy Current solver for the DD are: L1=74.36 µH, L2=74.23 µH, M=20.655 µH, k=0.2779, and coils resistances fairly small, R1=R2= 22.149mΩ. The results obtained were as expected based on the conducted literature survey, Figure 4.5 reveals that the DD coils provides better tolerance to lateral misalignments in contrast to D coils. This is despite the fact that the outer dimensions, wire type, number of turns and other design variables are held constant to ensure a fair comparison as explained in Table 4.1. In addition, by studying the section of the efficiency graph in Figure 4.6 for misalignments between +/- 300 mm, over which the coupling factor is positive, it is observed that the DD coil maintains a more stable power transfer efficiency over this misalignment range, which would also translate to better charging performance. Hence, further investigation into the structure of the DD coils needs to be conducted and the comparison needs to be held for different outer dimensions, different number of turns and different wire diameters in order to draw reliable conclusions on the coupling performance of the DD geometry compared to the polarized D. Therefore, DD coil was simulated for different wire diameter values to investigate the effect on the inductive link performance. It is found that the change in wire diameter of the coil doesn't affect the coupling factor and mutual inductance. The efficiency remains high for all variations of wire diameter. Wire diameter has a great impact on the value of the coil resistance. At 4 mm wire diameter, the resistance of the coils was extracted to be 22.3 mΩ. on the other hand, the coil resistance of 8 mm wire diameter was found to be 5.4 mΩ. to conclude this, the main factor that varies with wire diameter is quality factor and the Figure-of-Merit. This can be validated from the relationship between R and Q discussed earlier. The effects of the lateral displacement in coil have been evaluated by a FEM analysis, executing a parametric analysis of the mutual inductance between transmitter and receiver coil for lateral displacements increasing from 0 up to the lateral dimension of the pickup coil (800 mm).

4.4. Comparative Study Plan Comparative Study using FEM Simulation

Maxwell simulation plan that shall be followed as part of the comparative study of the effect of the coil geometry on the coupling performance of WPT inductive links. The following primary-secondary coil geometry combinations are to be investigated: (DD,DD), (DD,DDQ), (DDQ, DDQ), (DD, Bipolar), (DDQ, Bipolar), (Bipolar, Bipolar), (Rectangular, DD), (Rectangular, DDQ), (Rectangular, Bipolar). For each of the abovementioned combinations, starting with (DD, DD), the following parametric simulations will be conducted:

- Vary the Air gap from 100-300 mm in steps of 50 mm.
- Vary the lateral misalignment variation from 0 to +800 mm in steps of 100 mm, making sure the coils are symmetric about the y-axis. This shall cover all the required dimension/geometry variations.
- Number of turns varies with turn spacing and inner & outer dimensions:
    - Inner dimension: 0%, 15%, 25%, 50% of the outer dimension
    - Turn-to-turn spacing: 6, 8,10, 12,14, 16 mm
    - Wire diameter: 4,6, 8 mm
- Ferrite thickness and geometry: 8, 16, 20 mm
- Aluminum thickness: 1.2, 1.6, 2.0 mm

Fixed parameters:

- Coil length and width: 800X600 mm.
- Ferrite and Aluminum length and width.

Ferrite Geometry Check:

This study aims at choosing the most optimum geometry selected above and simulate the ferrite sheet performance. Compare it with the 9-bars used for all the simulations. 12 mm, 16 mm, 20 mm.

Aluminum Shield Thickness:

The most optimum geometry selected above and simulate the effect of the Aluminum Shield Thickness (increase to 1.2mm, 1.6mm, and 2.0 mm).

Design of a Ferrite-Less and Aluminum-less Power Pad:

The power pads shall be simulated considering the effect of litz wire on the coupling performance of the inductive link neglecting the effect of ferrite core and

aluminum shielding. Using copper-only coils shall reduce the weight and the complexity of the design. It can be considered for cases where losses in magnetic field is not a major issue.

Variation of Inner to outer area ratio between the power pads:

Inner Dimension Variations and Turn-Spacing-to-Wire Diameter Variations with air gap and lateral displacement. Spacing shall be varied between 6,8,10,12,14, and 16 mm.

- At inner dimensions 0%,15%,25%, and 50% of the outer dimensions & wire diameter 4mm, reduce center-to-center spacing to 6 mm edge-to-edge and add more turns.
- At inner dimensions 0%,15%,25%, and 50% of the outer dimensions & wire diameter 4mm, increase center-to-center spacing to 8mm edge-to-edge and reduce the number of turns.
- At inner dimensions 0%,15%,25%, and 50% of the outer dimensions & wire diameter 4mm, increase center-to-center spacing to 10mm edge-to-edge and reduce the number of turns.
- At inner dimensions 0%,15%,25%, and 50% of the outer dimensions & wire diameter 4mm, increase center-to-center spacing to 12mm edge-to-edge and reduce the number of turns.
- At inner dimensions 0%,15%,25%, and 50% of the outer dimensions & wire diameter 4mm, increase center-to-center spacing to 14mm edge-to-edge and reduce the number of turns.
- At inner dimensions 0%,15%,25%, and 50% of the outer dimensions and wire diameter 4mm, increase center-to-center spacing to 16mm edge-to-edge and reduce the number of turns.

4.4.1. Inner to outer area ratio (0%). Identical Double-D coils are simulated for both primary and secondary varying the spacing between the turns. Table 4.2 indicates the simulated coil characteristics along with material weight and cost calculation.

Increasing the spacing between the turns from 6 mm to 16 mm reduces the number of turns maintaining the inner area almost equal to zero.

Table 4.2: 0% inner to outer area ratio at 20 cm air gap and perfect alignment.

Spacing (mm)	Inner area	Outer area (m^2)	# of turns	Coil length	Volume (m^3)	copper mass	Material cost ($)	L (uH)	M (uH)	k	R (mΩ)	Q
6	0	0.48	34	81.968	0.001	9.2189	67.2	1347.4	419.924	0.31153	120.8	5957.0
8	0	0.48	26	62.208	0.00078	6.9965	51.01	762.961	239.415	0.313866	90.9	4482.6
10	0	0.48	21	50.2	0.00063	5.6459	41.16	496.609	156.023	0.314165	72.88	3639.2
12	0	0.48	17	41.712	0.00052	4.6913	34.2	351.718	110.2586	0.313455	60.73	3093.2
14	0	0.48	15	36.28	0.000455	4.0804	29.75	263.382	82.47778	0.313064	52.69	2670.9
16	0	0.48	13	31.84	0.000401	3.581	26.1	206.092	64.291	0.31188	46.21	2382.9

Figure 4.11 to Figure 4.16 represent coil parameters such as self-inductance (L), coupling factor (k), Mutual inductance (M), Quality factor (Q), and inductive link efficiency.

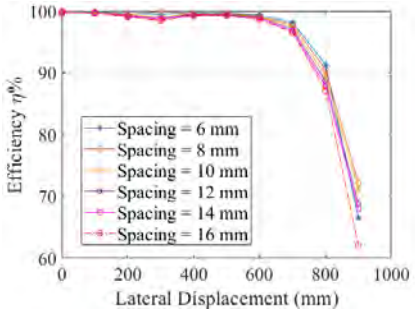

Figure 4.11: Double-D: lateral misalignment variation with efficiency for various turn spacing.

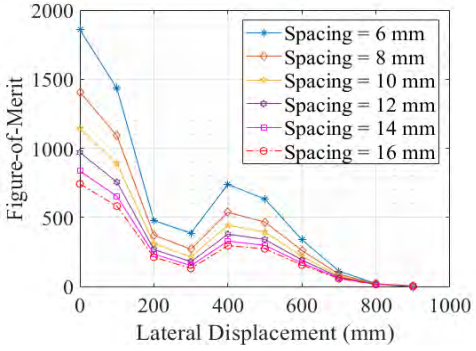

Figure 4.12: Double-D: lateral misalignment variation with Figure-of-Merit for various turn spacing.

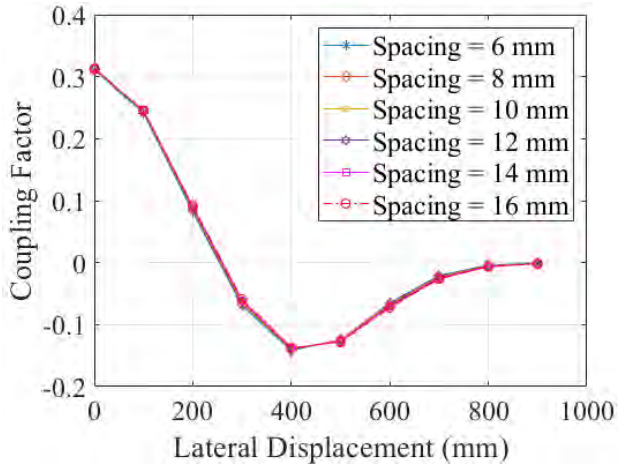

Figure 4.13: Double-D: lateral misalignment variation versus coupling factor for various turn spacing.

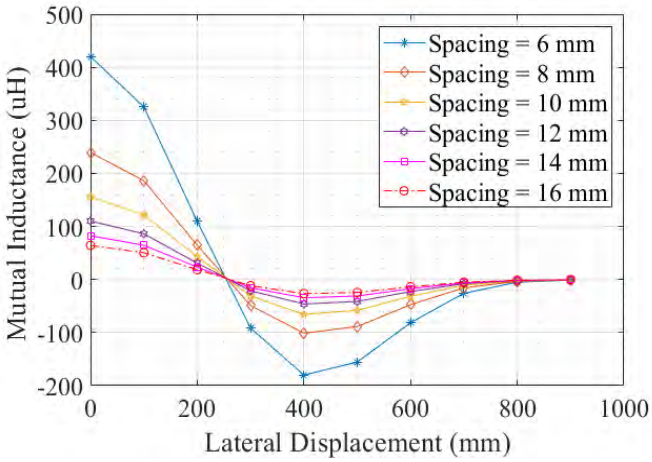

Figure 4.14: Double-D: lateral misalignment variation versus mutual inductance for various turn spacing.

The following figures corresponds to coils designed to have the maximum number of turns maintain the same outer area. It can be observed that all the above-mentioned parameters reduce with the increase in the turn spacing. The quality factor is maximized when spacing is twice and a half the value of the wire diameter. Hence, at spacing = 6mm, the coils exhibit higher quality factor along lateral displacement. The value of Q shall change the FOM accordingly.

The coupling coefficient between the power pads when the coils are made of the maximum number of turns for a fixed outer dimension, does not change with varying the turn spacing. Hence, increasing the number of turns to the maximum possible does not necessarily improve the coupling in the inductive link. On the other

hand, more turns result in higher inductance value which in turn improve the quality factor and the FOM.

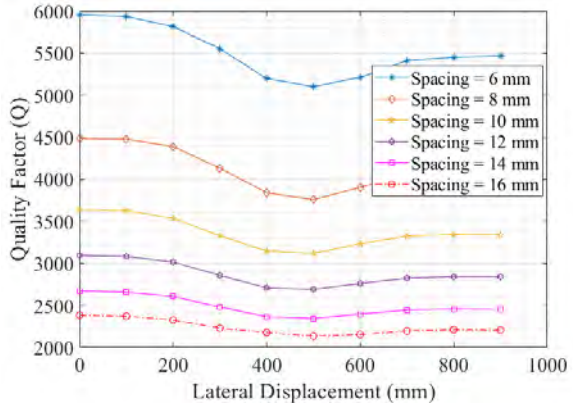

Figure 4.15: Double-D: lateral misalignment variation versus quality factor for various turn spacing.

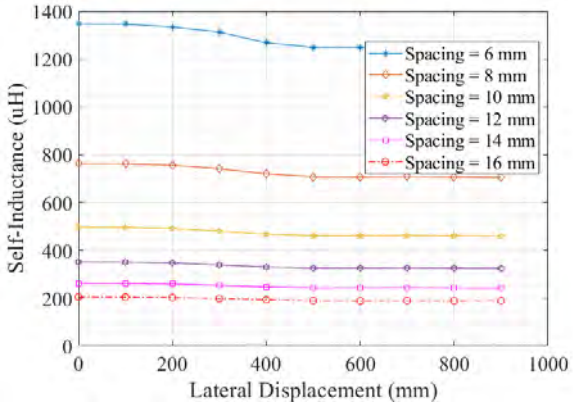

Figure 4.16: Double-D: lateral misalignment variation versus self-inductance for various turn spacing.

4.4.2. Inner to outer area ratio (15%). Identical Double-D coils are simulated for both primary and secondary varying the spacing between the turns. Figure 4.17 to Figure 4.22 indicate the power pad characteristics when the inner area is 15% the outer area.

Similarly, the coupling coefficient only changes lightly with the change in the spacing. Hence, other design parameters shall be observed to monitor the variation of k over lateral misalignment in order to minimize it.

The following figures represent the coils mutual inductance and quality factor. It can be noticed that the increase in spacing between the coil turns smoothen the mutual inductance curve along lateral displacement.

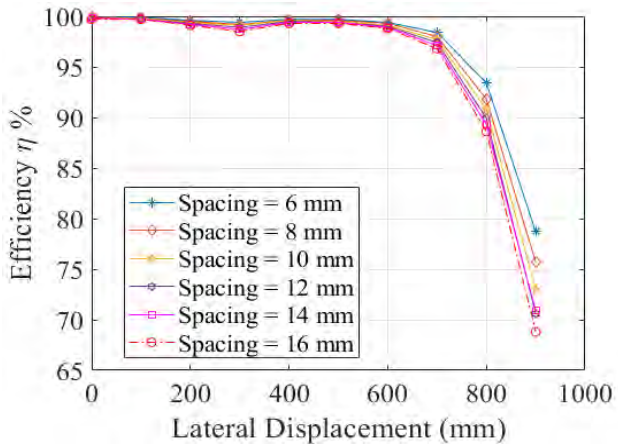

Figure 4.17: Double-D: lateral misalignment variation versus efficiency for various turn spacing.

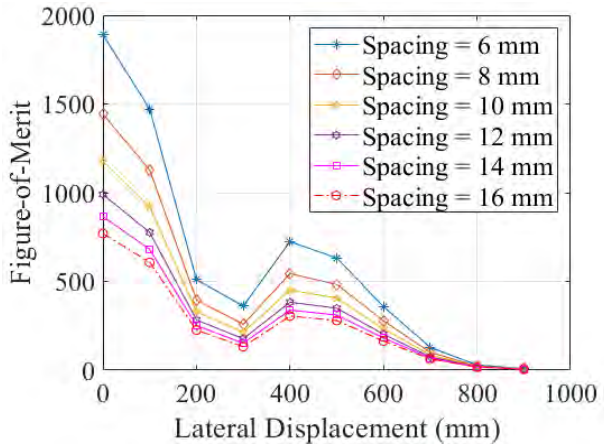

Figure 4.18: Double-D: lateral misalignment variation with Figure-of-Merit for various turn spacing.

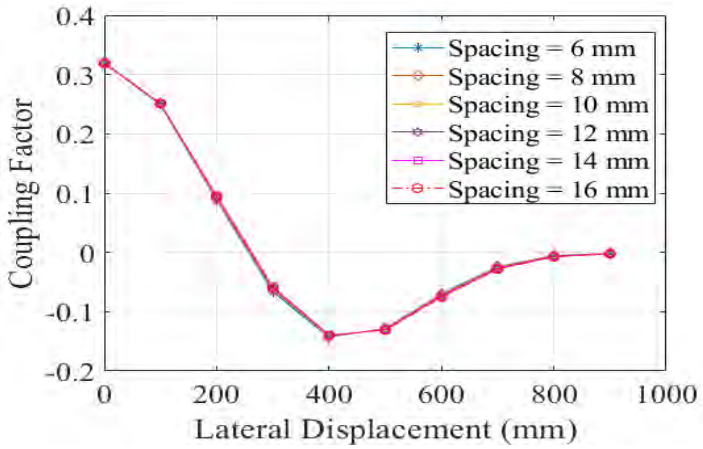

Figure 4.19: Double-D: lateral misalignment variation with coupling factor for various turn spacing.

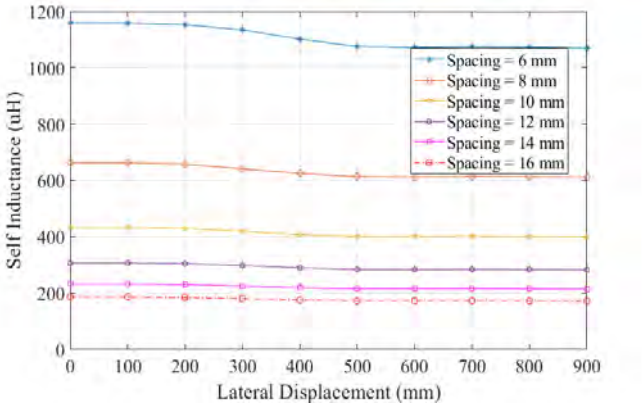

Figure 4.20: Double-D: lateral misalignment variation with self-inductance for various turn spacing.

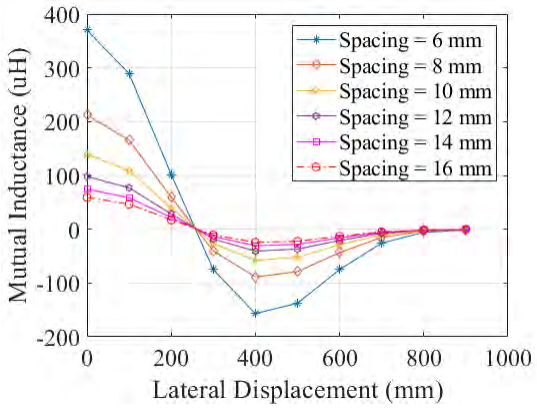

Figure 4.21: Double-D: lateral misalignment variation with mutual inductance for various turn spacing.

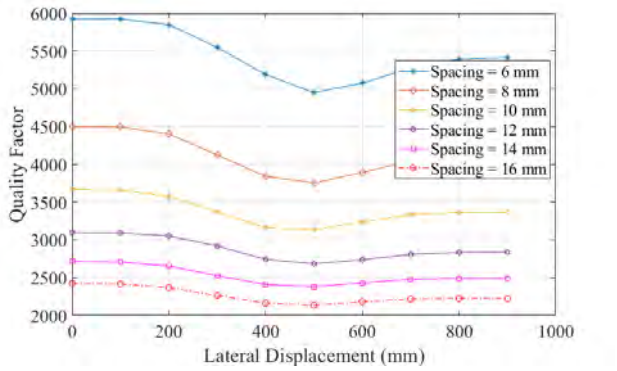

Figure 4.22: Double-D: lateral misalignment variation with quality factor for various turn spacing.

Table 4.3 shows the simulation results of inductive link power pads having a 15% inner-to-outer area ratio. Increasing the inner-to-outer area ratio from 0% to 15% reduces cost and weight, minimizes the losses of the primary and secondary coils, and hence increases the quality factor of each coil.

When the turn-to-turn spacing is 8 mm, the quality factor when considering a ratio of 15% was slightly higher (4497.063), where 0% gave a Q of (4482.553). This result indicated that increasing the number of turns to the maximum shall not necessarily enhances the coupling characteristics of the coils. As a result, an extra increase in the inner area is investigated in the coming results. The six figures below represent the coupling factor, self and mutual inductances, quality factor, Figure-of-Merit and the inductive link efficiency.

Table 4.3: 15% inner to outer area ratio at 20 cm air gap and perfect alignment.

Spacing (DD)	**Inner area** (mm^2)	**Outer area** (mm^2)	**Number of turns**	**Coil length (m)**	**Volume (m^3)**	**Copper mass(kg)**	**Material cost ($)**	**L (uH)**	**M (uH)**	**k**	**R (mΩ)**	**Q**
6 mm	72000	480000	25	71.24	0.00089523	8.0123	58.42	1159.7	370	0.319244	104.612	5921.236
8 mm	68200	480000	19	54.144	0.00068039	6.0895	44.3	662.053	211.947	0.3201	78.64	4497.063
10 mm	76800	480000	15	43.24	0.00054337	4.8632	35.45	433.94	138.939	0.3203	63.02	3675.78
12 mm	77376	480000	13	37.04	0.00046546	4.1659	30.37	306.5133	98.0347	0.31981	52.87	3096.85
14 mm	76800	480000	11	31.704	0.0003984	3.5657	25.99	233.123	74.402	0.31908	45.86	2716.084
16 mm	69888	480000	10	28.48	0.00035789	3.2031	23.35	186.44	59.278	0.318	41.094	2423.032

4.4.3. Inner to outer area ratio (25%). The following set of figures have been generated for a 25% inner-to-outer area ratio for various turn-to-turn spacing values. It can be noticed that increasing the spacing between the turns could increase the misalignment tolerance of the inductive link.

However, when spacing is relatively small compared to the wire diameter (6mm), self and mutual inductances, FOM and Quality factor are extremely higher than larger spacing distance. This concludes that there should be a tradeoff when choosing the turn spacing with respect to wire diameter.

Also, turn spacing has considerably impacted the coupling performance in a way that reflects on the values of coupling factor and FOM.

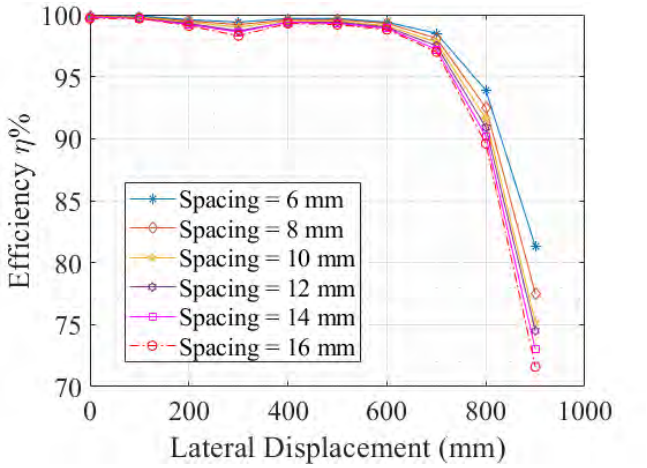

Figure 4.23: Double-D: lateral misalignment variation with efficiency for various turn spacing.

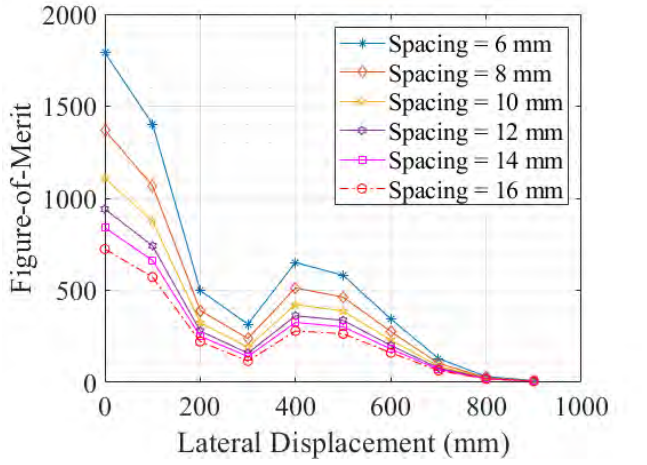

Figure 4.24: Double-D: lateral misalignment variation with Figure-of-Merit for various turn spacing.

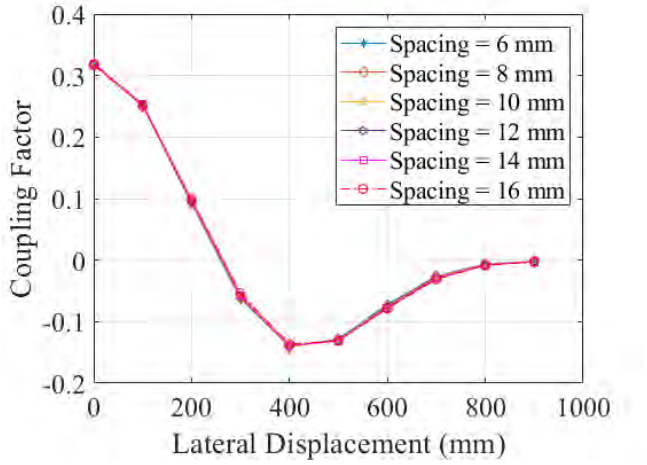

Figure 4.25: Double-D: lateral misalignment variation with coupling factor for various turn spacing.

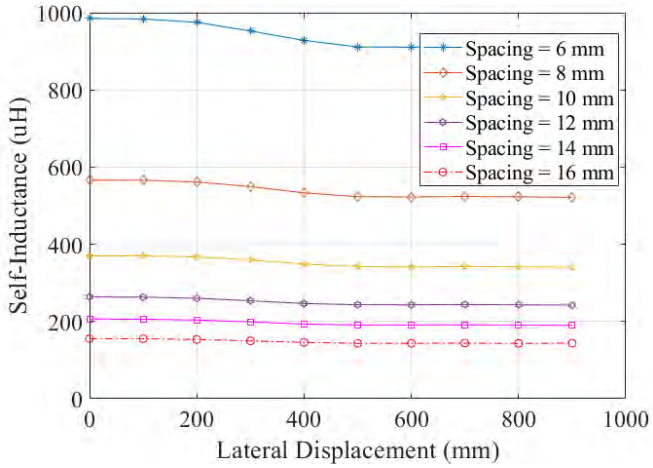

Figure 4.26: Double-D: lateral misalignment variation with self-inductance for various turn spacing.

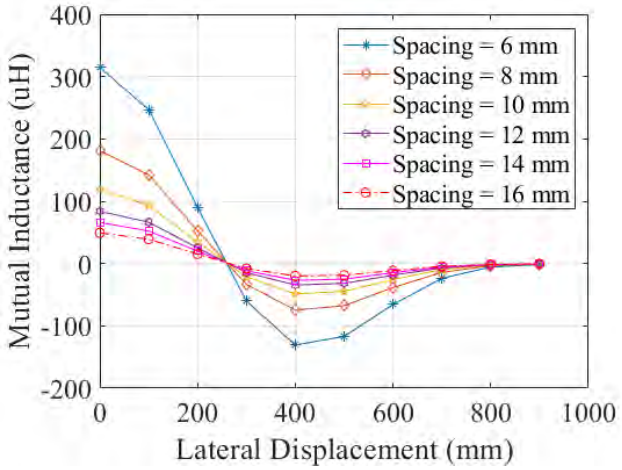

Figure 4.27: Double-D: lateral misalignment variation with mutual inductance for various turn spacing.

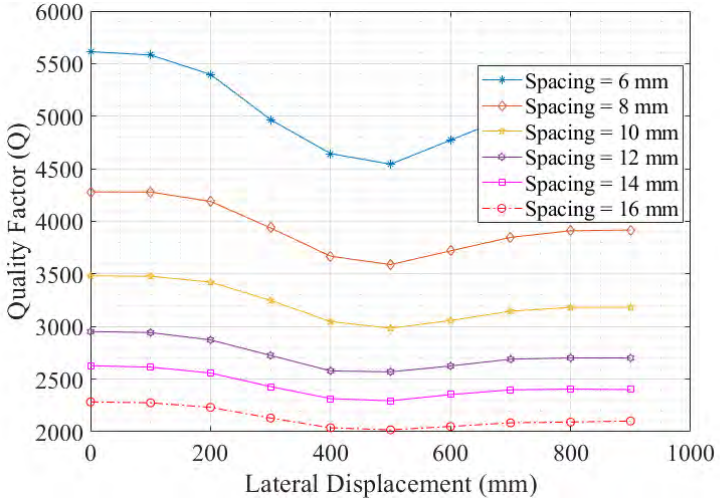

Figure 4.28: Double-D: lateral misalignment variation with quality factor for various turn spacing.

Table 4.4 below, indicates that Q decreased further with increasing the inner area, this concludes that the most suitable inner-to-outer area ratio for Double-D ranges between 0% to 25%. However, the determining factors that changes the area ratio are number of turns, turn spacing, and wire diameter. These in turn are to be studied to obtain the factor that has the most dominant effect on the overall coupling characteristics.

Further increase in the area ratio was observed to guarantee the accuracy of the abovementioned conclusion. 50% inner-to-outer area ratio study was simulated, and the results were concluded and plotted in the following Figures.

Table 4.4: 25% inner to outer area ratio at 20 cm air gap and perfect alignment.

Spacing	Inner area (mm^2)	Outer area (mm^2)	Number of turns	Coil length (m)	Volume (m^3)	Copper mass	Material cost ($)	L (uH)	M (uH)	k	R (mΩ)	Q
6 mm	121512	480000	21	63.976	0.00080395	7.1953	52.46	985.17	314.657	0.3194	93.73	5613.83
8 mm	123648	480000	16	48.768	0.00061284	5.4849	39.989	565.88	180.92	0.3197	70.6	4280.354
10 mm	125800	480000	13	39.64	0.00049813	4.4583	32.5	369.86	118.39	0.3201	56.79	3481.508
12 mm	127968	480000	11	33.552	0.00042163	3.7736	27.51	263.724	83.997	0.318555	47.69	2952.45
14 mm	117288	480000	10	30	0.00037699	3.3741	24.6	206.374	66.017	0.31981	41.994	2627.756
16 mm	126720	480000	9	26.848	0.00033738	3.0196	22.01	155.52	49.2829	0.31695	36.39	2283.721

4.4.4. Inner to outer area ratio (50%). In the following set of simulation results, the inner area of primary and secondary power pads is half the outer area. Expectedly, varying turn spacing from 6 mm to 16 mm results in a change in the number of turns. Hence, the inductive link parameters changes with lateral misalignment is plotted. Variations of mutual inductance over lateral displacement is reduced as turn spacing with respect to wire diameter increases. As a result, a smoother mutual inductance curve is achieved. Hence, coupling performance can be enhanced. On the other hand, the minimum the turn spacing the higher the quality factor of the power pad.

It is confirmed that any further decrease in the number of turns from the inner area shall have a negative impact on the coil characteristics. Hence, number of turns is a determining factor in terms of inductive link performance. However, for the same number of turns (13 turns), In Table 4.4, 10 mm turn spacing, the quality factor was 3481, where, on the other hand, for 13 turns, at 6 mm turn spacing, the quality factor is extremely higher (4483.82) as shown in Table 4.5, considering fixed wire diameter (4 mm) for the simplicity of forming and bending.

An important finding has to be highlighted here, is that there is a combination of factors that have to be optimized simultaneously in order to design the most optimum power pads for a specific application.

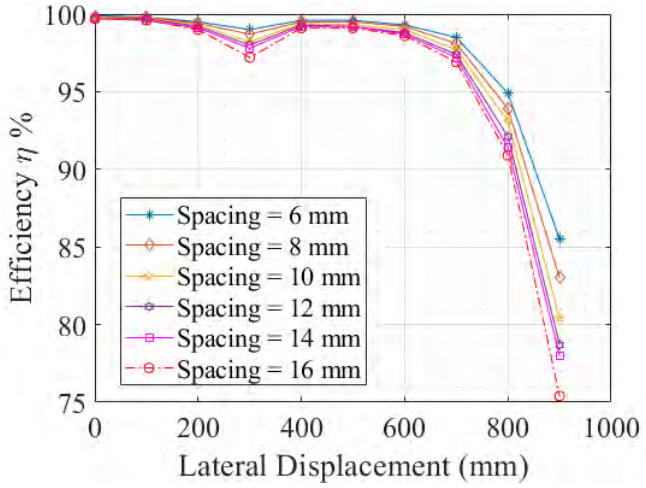

Figure 4.29: Double-D: lateral misalignment variation with efficiency for various turn spacing.

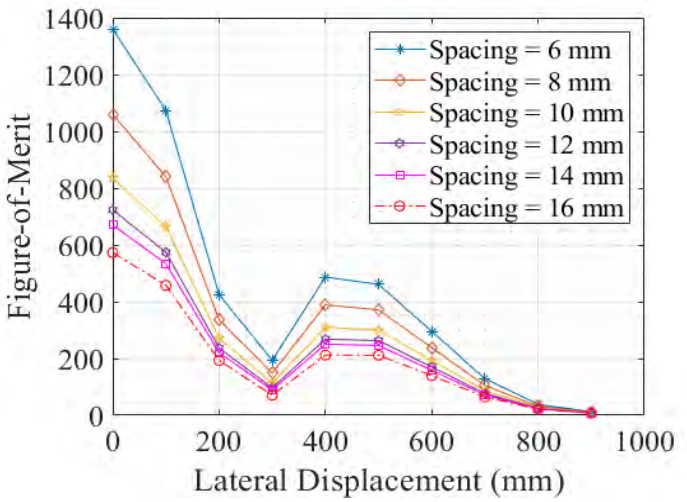

Figure 4.30: Double-D: lateral misalignment variation with Figure-of-Merit for various turn spacing.

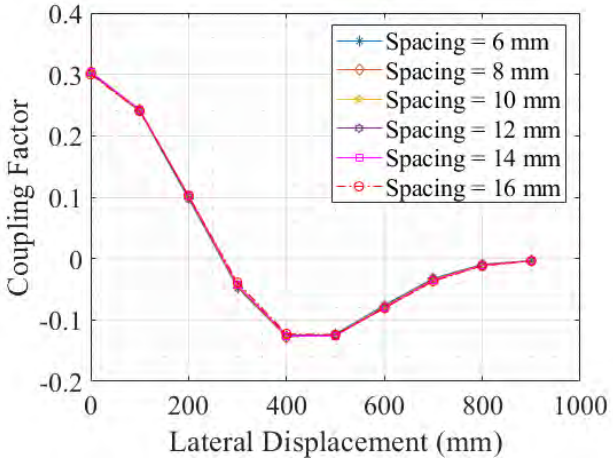

Figure 4.31: Double-D: lateral misalignment variation with coupling factor for various turn spacing.

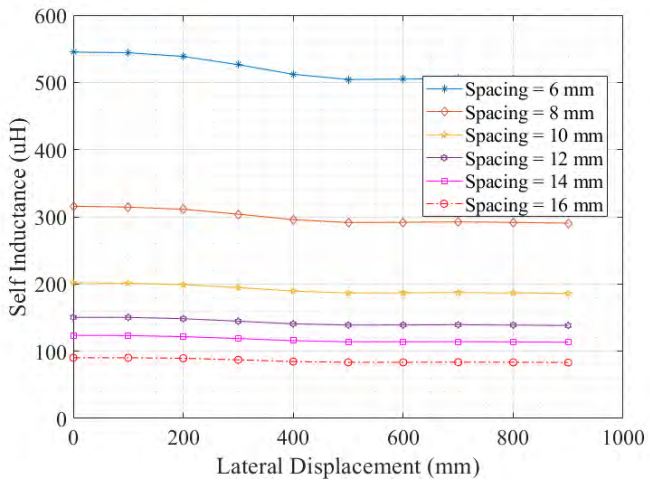

Figure 4.32: Double-D: lateral misalignment variation with self-inductance for various turn spacing.

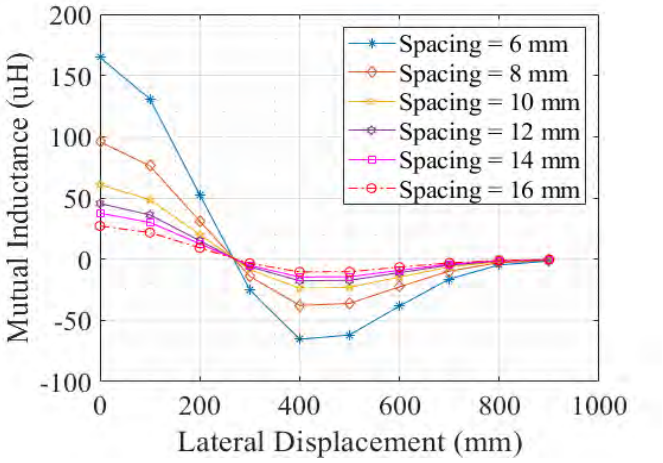

Figure 4.33: Double-D: lateral misalignment variation with mutual inductance for various turn spacing.

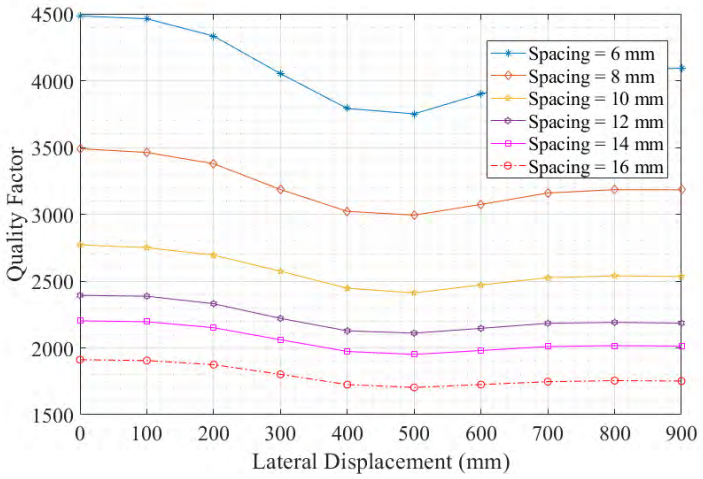

Figure 4.34: Double-D: lateral misalignment variation with quality factor for various turn spacing.

Table 4.5: 50% inner to outer area ratio at 20 cm air gap and perfect alignment.

Spacing	Inner (area) (mm^2)	Outer area (m^2)	Number of turns	Coil length (m)	Volume (m^3)	copper mass (kg)	Material cost ($)	L (uH)	M (uH)	k	R (mΩ)	Q
6 mm	242088	0.48	13	44.84	0.00056348	5.0431	36.77	544.96	164.75	0.3026	64.94	4483.82
8 mm	244992	0.48	10	34.56	0.00043429	3.8869	28.34	315.57	95.78	0.3034	48.31	3490.527
10 mm	248400	0.48	8	27.84	0.00034985	3.1311	22.8	201.72	60.86	0.30164	38.88	2771.417
12 mm	247912	0.48	7	24.272	0.000305	2.7298	19.9	150.43	45.41	0.30187	33.55	2392.96
14 mm	239200	0.48	6	20.944	0.00026319	2.3556	17.17	123.53	37.56	0.304	29.96	2202.594
16 mm	256768	0.48	5	17.76	0.00022318	1.9974	14.56	90.28	27.093	0.29997	25.26	1911.862

4.5. Comparative Study Design Considerations

The simulations described above shall be conducted for each of the following cases. Control Simulation Set to which all other results shall be compared. A primary & secondary coil pair, with outer dimensions of 800 mm x 600 mm, net inner dimension of 120mmx90mm (15% of outer dimensions), wire diameter: 4mm and turn-to-turn spacing: 4 mm (Edge-to-Edge) with As Many Turns as would fit. Ferrite geometry consists of 9 ferrite bars, each with dimensions 900mm x 37.5mm and thickness 16 mm, placed at 1mm spacing from the coils (fixed for all simulations). Ferrite magnetic permeability is $\mu_r = 3000$. Aluminum sheet with dimensions 1000mm x 800mm and thickness 1.2 mm, placed at 5mm spacing above and below the ferrite bars accordingly (fixed for all simulations).

Since the outer dimensions are based on the available space at the bottom of the vehicle, the dimensions of the Aluminum shield and Ferrite layer can be considered the maximum possible, acknowledging the available area. The last step is to set inner dimensions to 0% - i.e. Fill up the entire coil area with turns, with wire diameter 4mm, 4mm turn-to-turn spacing and as many turns as required.

The target plan is to choose the inner dimensions percentage that provides the most superior performance for all turn spacings and # of turns - This shall be used for all subsequent simulations. Moreover, the turn spacing-to-wire diameter ratio that provides the most superior performance in terms of Figure-of-Merit over lateral and longitudinal misalignments at 20cm air gap is to be chosen.

Double-D pads generate single-sided flux with less flux leakage which can be nullified by adding aluminum backing sheet with less impact on the efficiency. .DD power pads have high misalignment tolerance in horizontal direction, when compared to non-polarized pad. Since, Double D exhibits high misalignment tolerance than rectangular, and since it is the simplest polarized coupler design, this geometry will be considered in the following set of results.

4.5.1. Variation of litz wire diameter (4,6,8 mm) with turn spacing. The effect of varying wire diameter at a fixed turn spacing has been studied above. It's concluded that the higher the wire diameter the higher the Figure-of-Merit and the maximum inductive link efficiency. Table 4.6 and represents the effect of varying air gap and lateral misalignment with the coil parameters. The following figures have been generated to indicate the effect of varying turn-to-turn spacing by fixing the litz wire diameter at 4 mm and varying the space accordingly. The combinations to be considered in this study are as follows:

Table 4.6: Double-D with 4 mm diameter and 12 mm spacing: Air Gap variations with k, L, M, Q, FOM, and η.

AirGap (cm)	k	Lp (uH)	Ls (uH)	M (uH)	Rp (mΩ)	Rs (mΩ)	Qp	Qs	FOM	η
10	0.54778	89.816	89.839	49.206	22.169	22.163	2163.705	2160	1190	99.8
15	0.386424	79.195	79.1608	30.596	22.107	22.1168	1913.163	1910	739	99.7
20	0.276265	74.517	74.447	20.577	22.113	22.13	1799.76	1800	496	99.6
25	0.201	72.1744	72.054	14.496	22.143	22.1438	1740.783	1740	349	99.4
30	0.149	70.84	70.75	10.542	22.174	22.1746	1706.19	1700	254	99.2

Table 4.7: Double-D- Ferrite lateral, with 4 mm diameter and 12 mm spacing: Lateral Misalignment variations with k, L, M, Q, FOM, and η.

Starty (mm)	k	Lp (uH)	Ls (uH)	M (uH)	Rp (mΩ)	Rs (mΩ)	Qp	Qs	FOM	η
0	0.276265	74.5175	74.447	20.5768	22.1127	22.1304	1799.76	1800	496	99.6
100	0.222056	74.3654	74.2997	16.506	22.1654	22.1722	1791.82	1790	397	99.5
200	0.099195	73.5338	73.48	7.2915	22.3	22.312	1761.266	1760	174	98.9
300	-0.02908	71.8136	71.755	-2.087	22.52	22.53	1702.973	1700	49.5	96.0
400	-0.108916	69.599	69.532	-7.57	22.79	22.83	1630.63	1630	177	98.9
500	-0.112677	68.218	68.18	-7.684	22.87	22.94	1592.88	1590	179	98.9
600	-0.07518	68.435	68.438	-5.145	22.709	22.714	1609.41	1610	121	98.4
700	-0.036815	68.7515	68.725	-2.53	22.46	22.48	1634.85	1630	60.1	96.7
800	-0.013165	68.7945	68.799	-0.9057	22.28	22.28	1648.9	1650	21.7	91.2
900	-0.004932	68.6788	68.637	-0.3386	22.21	22.209	1651.15	1650	8.14	78.3

- **Double-D power pad with wire diameter=4, spacing(12,16,8mm)**

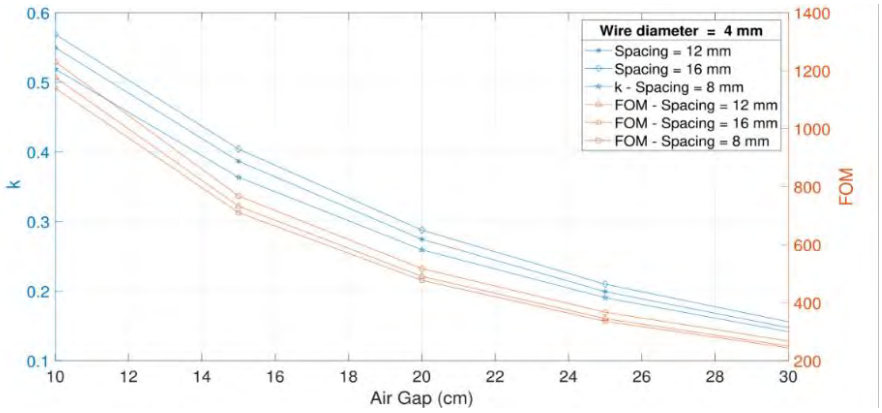

Figure 4.35: Double-D with different turn spacing and diameter = 4 mm: air gap versus coupling factor and Figure-of-Merit.

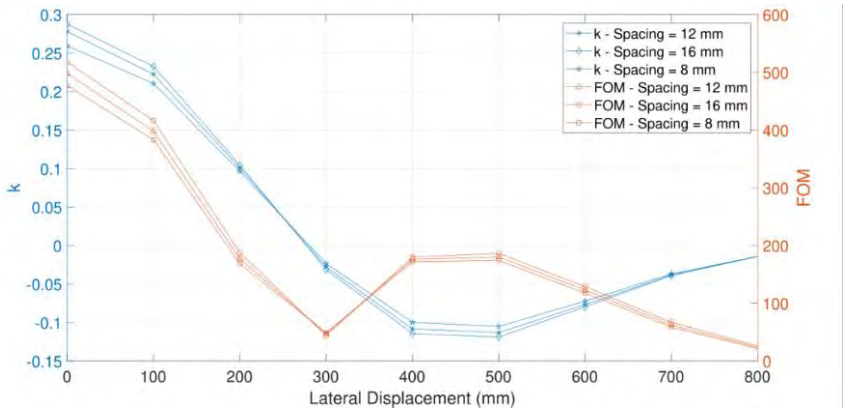

Figure 4.36: Double-D with different turn spacing and diameter = 4 mm: lateral misalignment versus coupling factor and Figure-of-Merit.

At a fixed litz wire diameter, 4-turn Double D power pads were simulated for different values of spacing. Figure 4.35 and Figure 4.36 were plotted to show the impact of spacing on vertical and lateral misalignment. The coupling factor shows smoother performance when the spacing is relatively small. Furthermore, the impact of turn spacing on the Figure-of-Merit with lateral misalignment is insignificant as they share the same value at 300 mm lateral displacement.

- **Double-D power pad with wire diameter=6, spacing(12,16,8mm)**

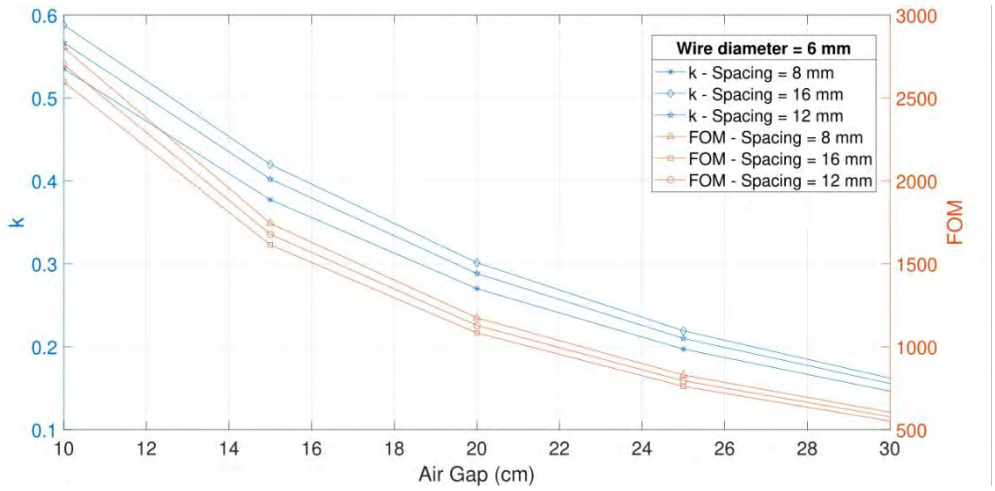

Figure 4.37: Double-D with different turn spacing and diameter = 6 mm: air gap versus coupling factor and Figure-of-Merit.

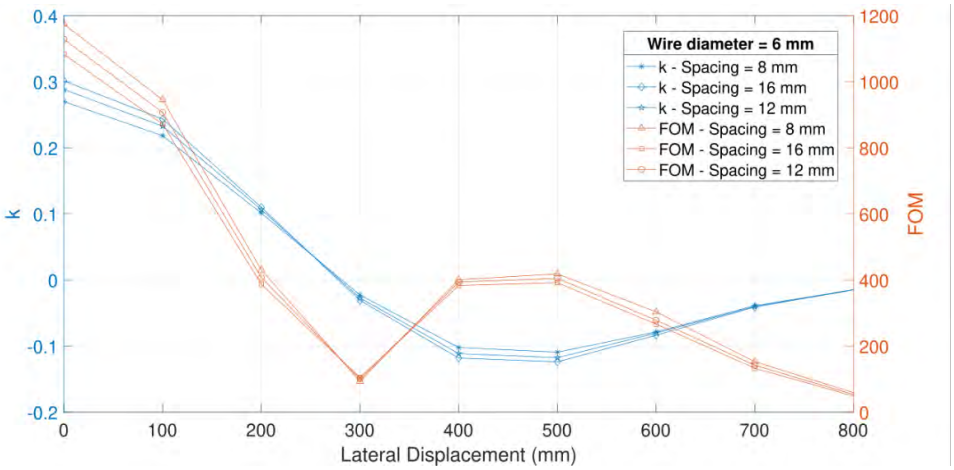

Figure 4.38: Double-D with different turn spacing and diameter = 6 mm: lateral misalignment versus coupling factor and Figure-of-Merit.

Figure 4.37-Figure 4.40 concludes that spacing is an important factor that impacts the coupling performance including Figure-of-Merit and coupling factor of the power pads. Hence, the relationship between wire diameter and turn spacing for the most optimized coupling performance is given by:

Spacing = (2.5) * wire diameter

- **Double-D power pad with wire diameter=8, spacing (12,16 mm)**

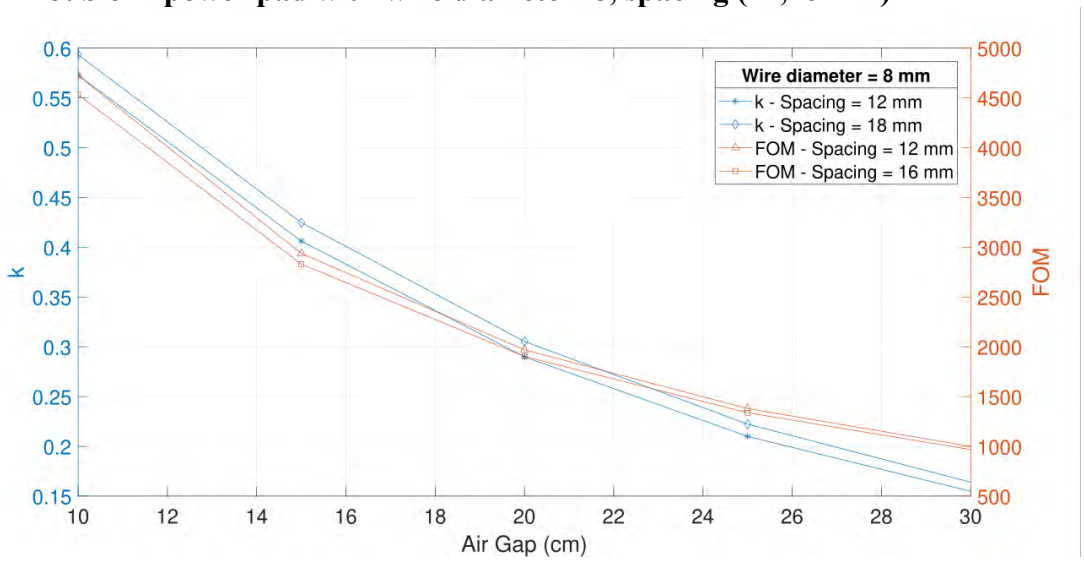

Figure 4.39: Double-D with different turn spacing and diameter = 8 mm: air gap versus coupling factor and Figure-of-Merit.

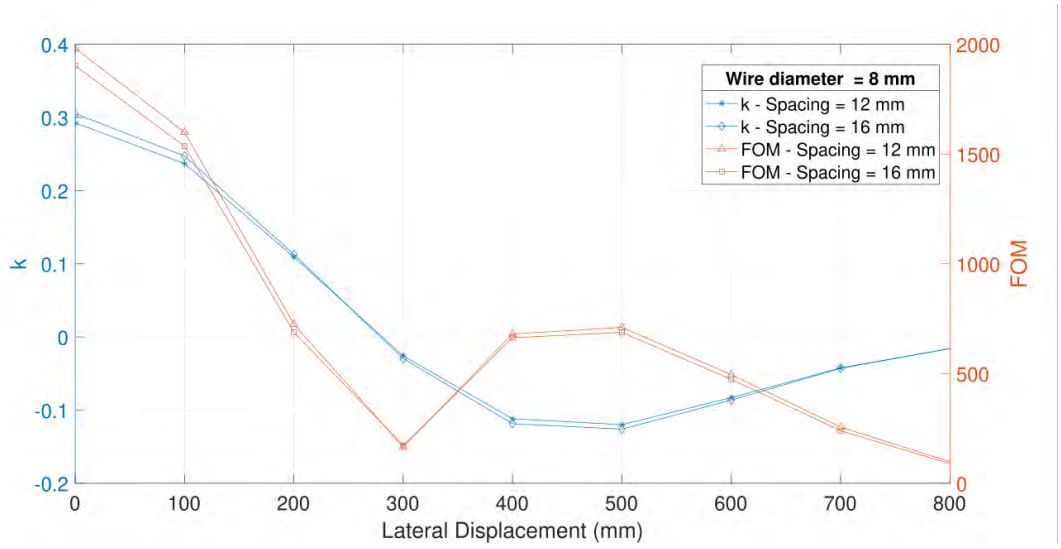

Figure 4.40: Double-D with different turn spacing and diameter = 8 mm: lateral misalignment versus coupling factor and Figure-of-Merit.

By observing the variation of coupling factor over lateral misalignment at different wire diameter values, it can be concluded that there is an obvious dependency on wire diameter and turn spacing values. The relationship is directly proportional which results in enhanced coupling factor curve. Figure 4.36 indicates that the magnetic null point happens at 300 mm irrespective of the wire diameter. Furthermore, the coupling factor at 300 is approximately -0.12 for different spacing values. On the other hand, Figure 4.38 and Figure *4.40* exhibit similar performance at 300 mm shift on y-axis and a coupling factor of -0.15 for all spacing values.

4.5.2. Variation of number of turns. The study shall investigate the impact of number of turns on the coupling factor and the Figure-of-merit of the transmitting and receiving coils. The tested numbers varied from 4 turns to 15 turns to facilitate the process. FEM simulations were conducted using ANSYS Maxwell to obtain the required results. Table 4.8 below illustrates the inductive link parameter variations with respect to number of turns of both primary and secondary coils. It can be noticed that the increase in the number of turns shall enhance the coupling characteristics and hence improve the performance of the inductive link. However, there must be a tradeoff when increasing the number of turns in terms of coil weight and length, which resulted in extra losses and complexity of the coils.

Table 4.8: Double-D: variable turn ratio at 20 cm air gap and perfect alignment for Double-D, 4 mm diameter, 12 mm spacing.

Double D	Inner area (mm)	Outer area (m^2)	Ratio Inner-to-outer ratio	Coil Length (m)	Volume (m^3)	Copper mass (kg)	Material cost ($)	k	Q
4 Turns	339552	0.48	70.74%	15.296	1,922e-4	1.7203	12.54	0.27799	1790.6
7 Turns	227808	0.48	47.46%	24.272	3.05e-4	2.7298	19.9	0.307466	2495.51
11 Turns	111072	0.48	23.14%	33.55	4.216e-4	3.7736	27.5	0.321734	3132.57
15 Turns	31200	0.48	6.5%	39.76	4.996e-4	4.4718	32.6	0.318333	2989.25

The variation of number of turns with respect to lateral and vertical misalignments is presented in Figures below. Figure shows the impact of coil turn ratio versus the air gap. It is concluded that 15 Turns power pads obtained higher coupling performance (higher k and kQ) when compared to 4-Turns. Double-D designed to tolerate misalignment variation; however, other design factors shall be studied to

understand the reasons behind the major drop in the inductive link performance when increasing or decreasing number of turns, litz wire diameter, and turn-to-turn spacing.

It can be observed clearly that the larger the number of turns, the better the Figure-of-Merit. Hence, there should be a tradeoff when increasing the number of turns to maintain smooth coupling factor curve and high FOM.

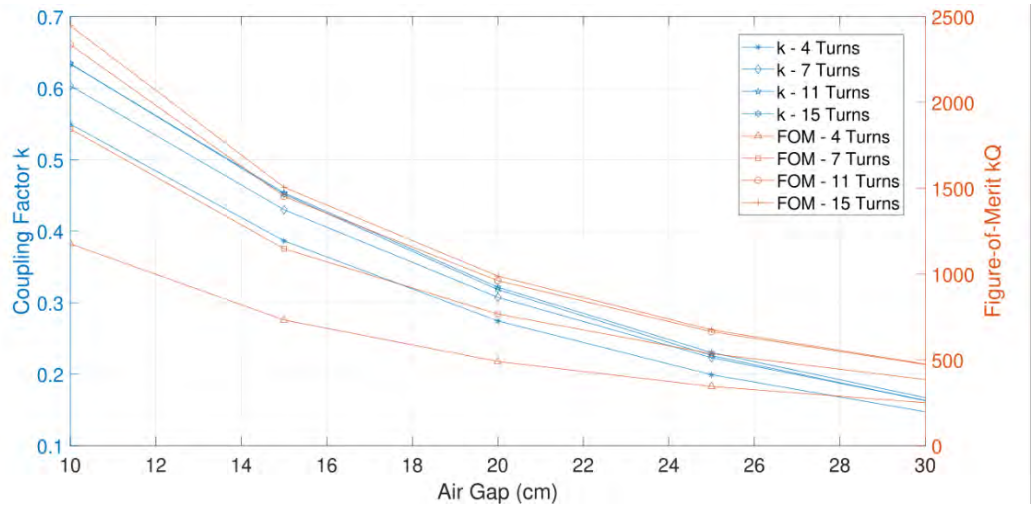

Figure 4.41: Double-D with different number of turns: air gap versus coupling factor and Figure-of-Merit.

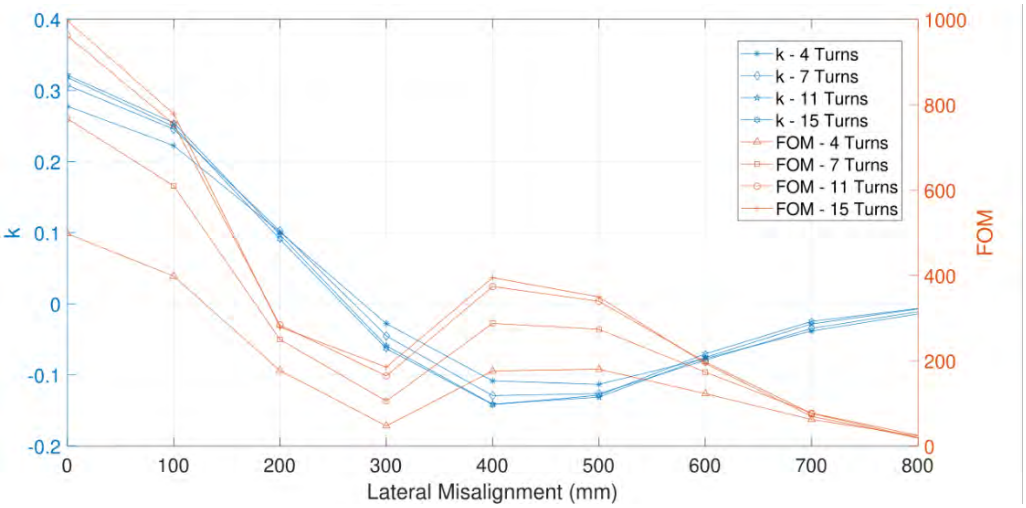

Figure 4.42: Double D with number of turns: lateral misalignment versus coupling factor and Figure-of-Merit.

4.5.3. Aluminum thickness. The following set of Double D power pads with fixed diameter and spacing varying the thickness of aluminum sheet to 1.2 mm, 1.6

mm, and 2.0 mm. Figure 4.43 represents the self-inductance change with increasing the aluminum thickness. It can be observed that the aluminum thickness should range from 1.2 mm to 1.6 mm. Figure 4.44 indicates the quality factor versus misalignment. The most optimum aluminum thickness value is 1.6 mm. this value is subject to change under any change in the coil design specifications. This conclusion was found based on the FEM simulations done in ANSYS Maxwell.

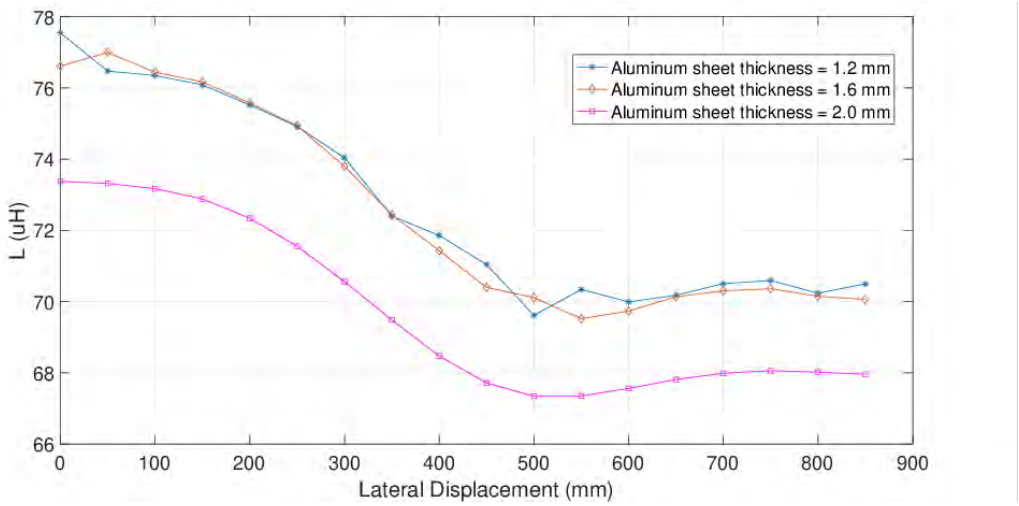

Figure 4.43: Various aluminum sheet thicknesses: self-inductance versus lateral misalignment.

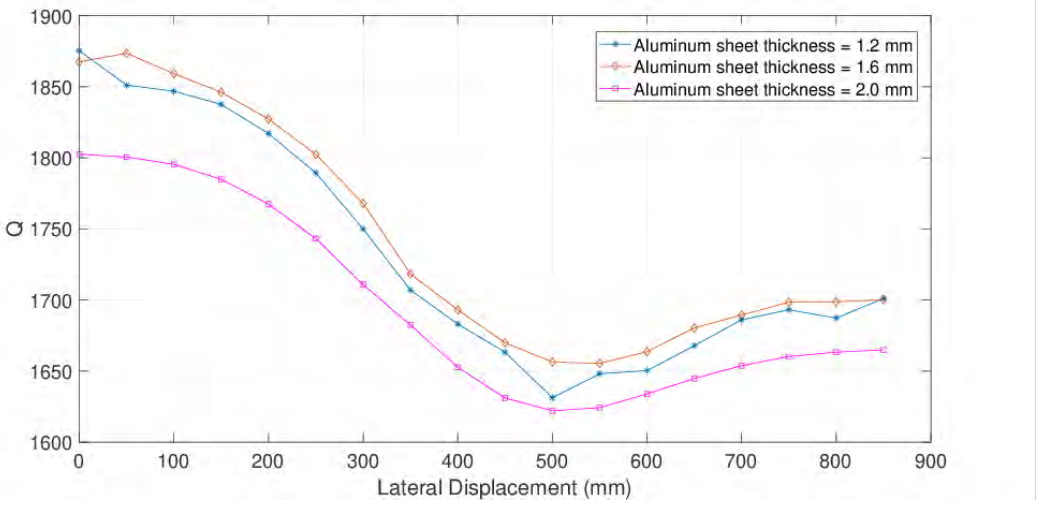

Figure 4.44: Various aluminum sheet thickness: quality factor versus lateral misalignment.

Adding aluminum plate will result in high eddy current losses as high amount of flux is generating from backside of core. Hence, optimizing the sheet dimension is essential to minimize eddy current losses.

4.5.4. Bipolar design. The design of bipolar magnetic couplers is challenging. In literature, different bipolar designs were observed and studied. The following set of figures compare between three different bipolar designs that have the same outer dimension, number of turns, diameter and spacing. The first design was to form two separate rectangular coils and put them on the top of each other with 50% overlapping between each other. The second design is to put them at a vertical distance of 16 mm maintaining the same overlapping percentage. Finally, the third design consists of two connected rectangular coils forming one bipolar. The results obtained are shown in Figure 4.45 and Figure 4.46 below. It is observed that in case of self-inductance, it is expected that the third design will exhibit higher inductance due to the fact that current is flowing in two rectangular coils instead of one. On the other hand, the coupling performance would be improved along lateral misalignment in the second design due to the smoother curve of k.

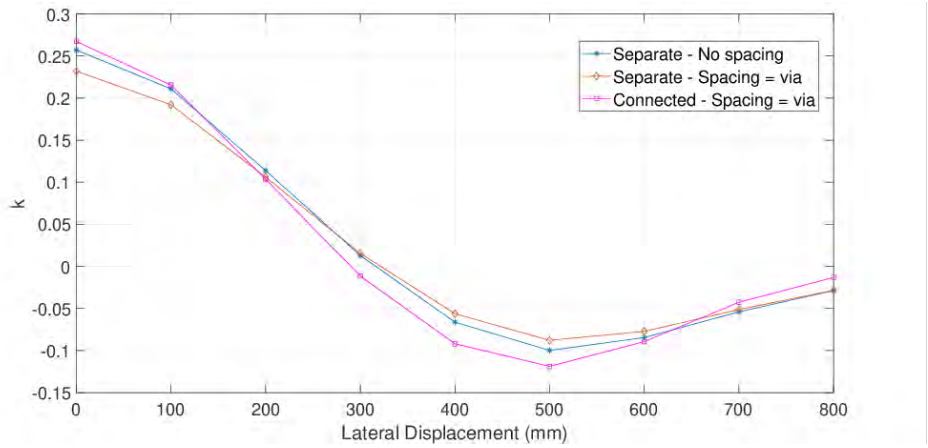

Figure 4.45: Bipolar design: coupling factor versus lateral misalignment.

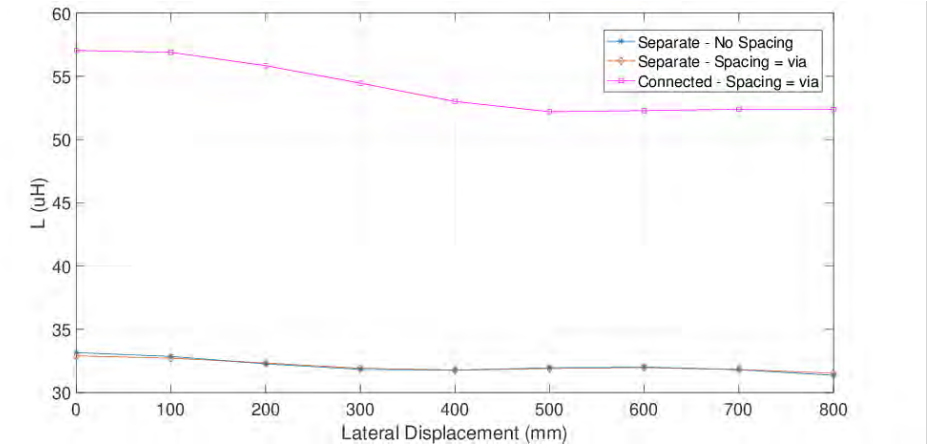

Figure 4.46: Bipolar design: self-inductance versus lateral misalignment.

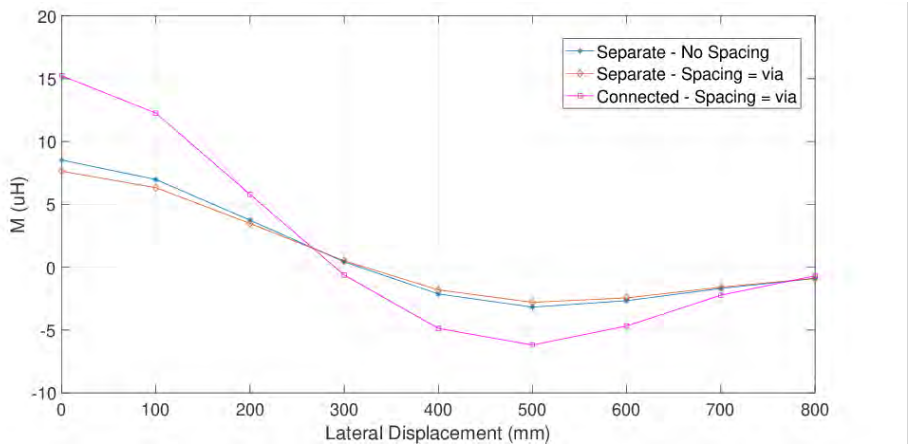

Figure 4.47: Bipolar design: mutual inductance versus lateral misalignment

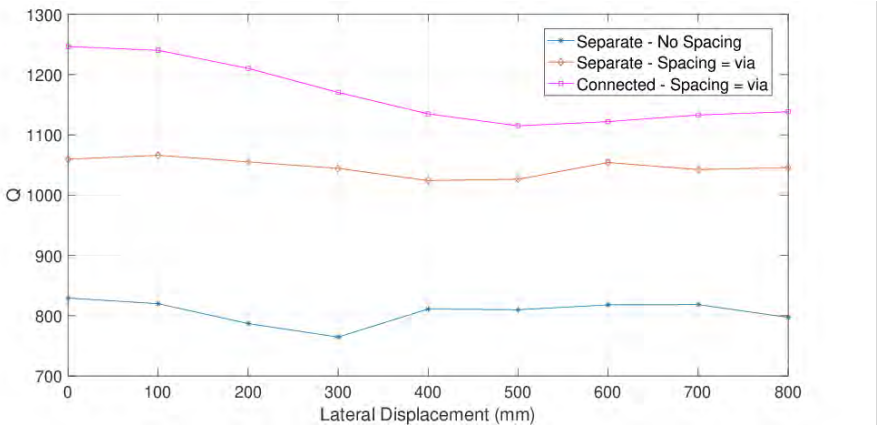

Figure 4.48: Bipolar design: quality factor versus lateral misalignment.

It can be observed from Figure 4.47 and Figure 4.48, that the value of M and Q is significantly dependent on the self-inductance. Hence, the third design of bipolar is preferred over the second in case of low probability of misalignment.

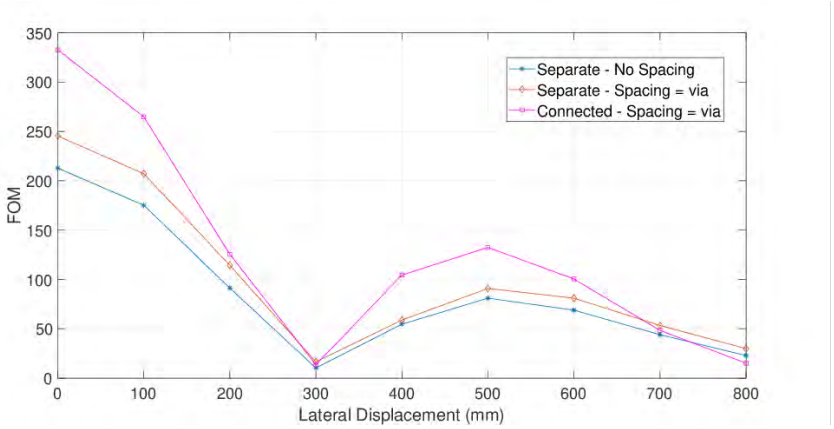

Figure 4.49: Bipolar design: Figure-of-Merit versus lateral misalignment.

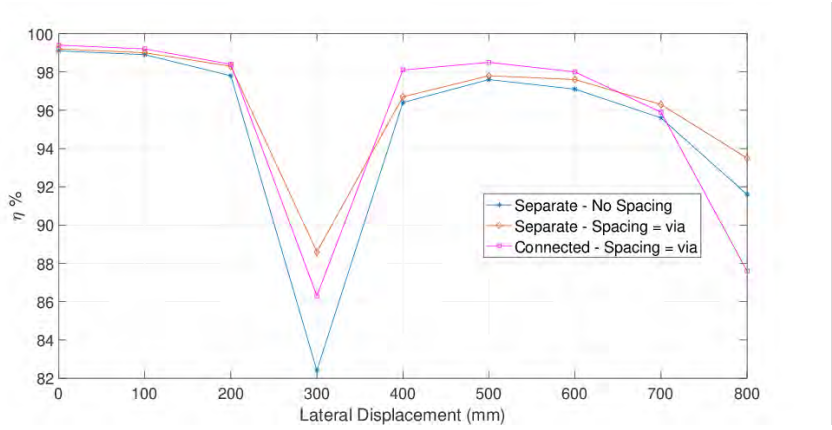

Figure 4.50: Bipolar design: efficiency versus lateral misalignment.

The maximum efficiency of the inductive link shows higher value in case of second bipolar design. There exists a drastic drop at a misalignment of 300 mm. This is because of the overlapping between the coils forming the bipolar in the middle of the power pad. This drop shall be shifted to further misalignment value if the overlapping percentage changes to higher or lower value.

4.5.5. Double-D quadrature design. DDQ pads differs from DD pads in which they are considered interoperable along with having high misalignment tolerance in lateral and horizontal directions. The main design limitation of DDQ pads is the requirement of high amount of copper.

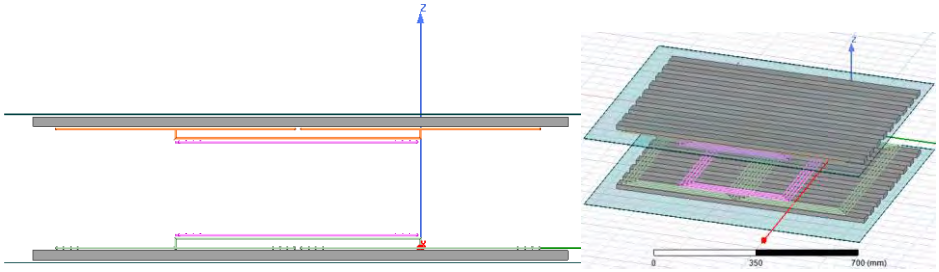

(a)

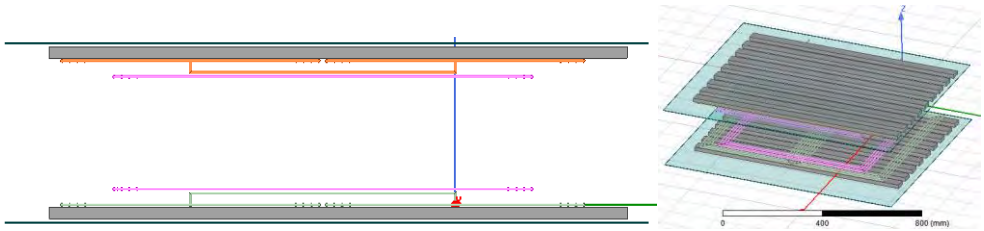

(b)

Figure 4.51: DDQ design: (a) Q size is 50% of DD size placed in the middle. (b) Q size 85% of the DD size placed in the middle.

DDQ is formed by adding a rectangular coil named Q on the top of the DD pad. The size of the Q and the position impacts the performance of DDQ pad. In Figure 4.51, two different sizes of Q are presented. It can be noticed that under vertical misalignment, the larger the Q size the better the quality factor and hence, the better the FOM. On the other hand, Figure 4.53 and Figure 4.54 showed an opposite behavior in which the small Q behaved better in terms of quality factor and FOM.

The quality factor along with the coupling factor combine the concept of the Figure-of-Merit which determines the performance of the inductive link. Lateral displacement varies with the quality factor as shown in Figure 4.52. It can be observed that with DDQ structure the size of Q coil matters in a way that changing it along with lateral displacement might drop the quality factor and thus reduce the FOM.

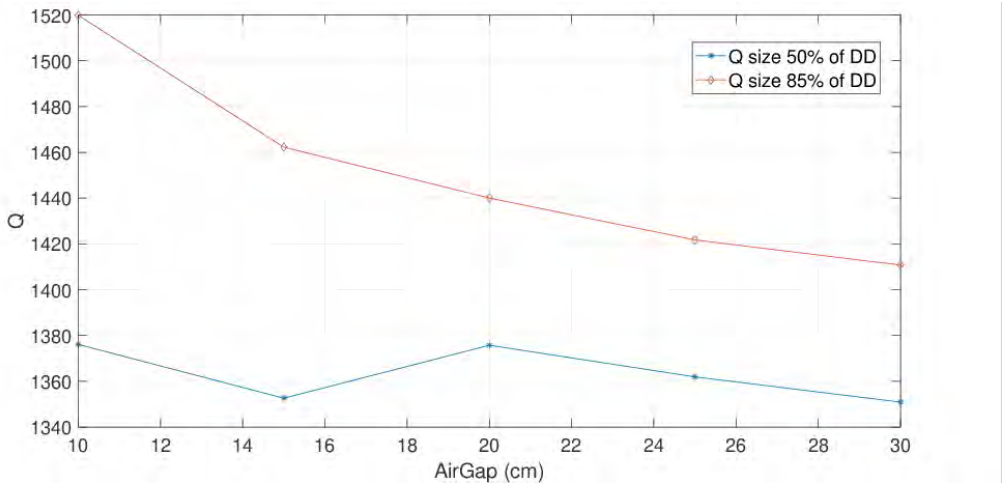

Figure 4.53: DDQ design: quality size versus air gap

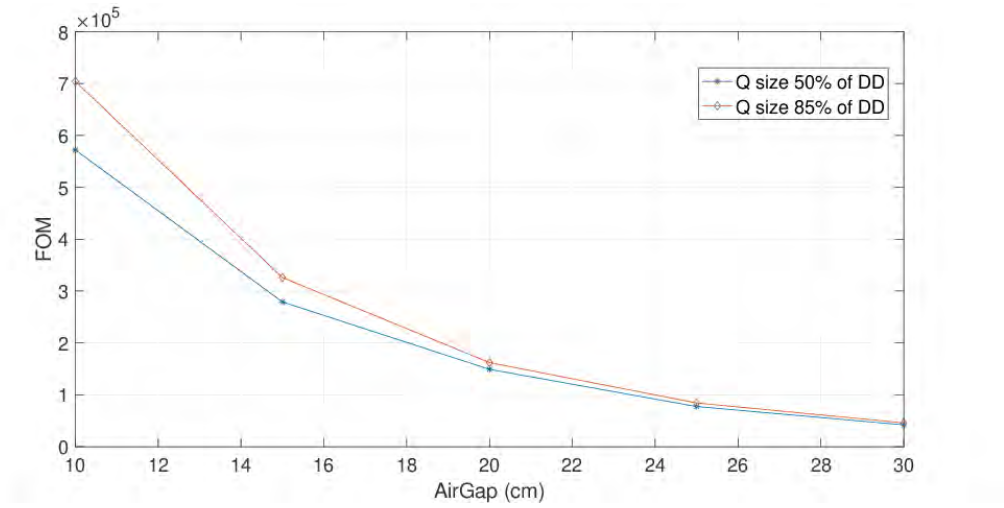

Figure 4.54: DDQ design: Figure-of-Merit versus air gap.

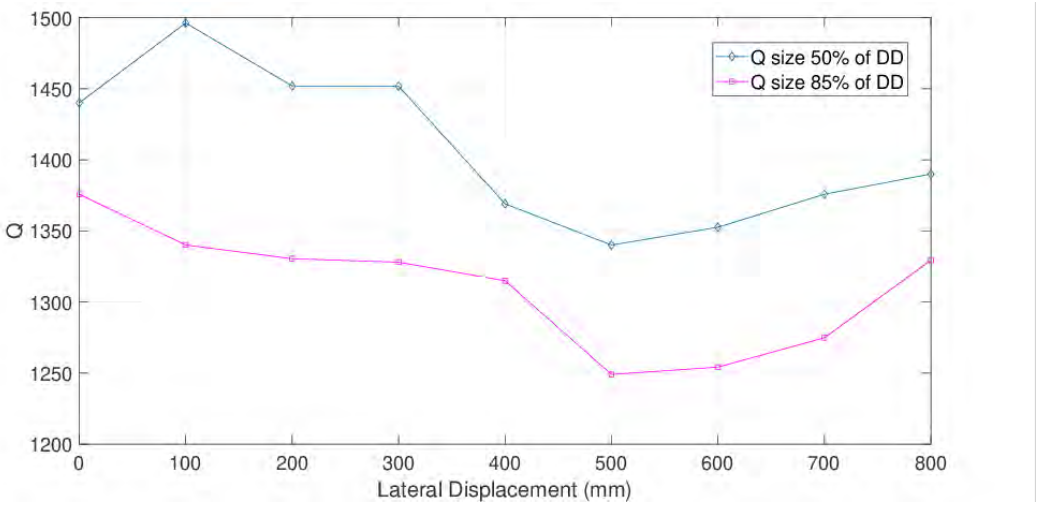

Figure 4.55: DDQ design: quality factor versus lateral misalignment.

Hence, DDQ with a Q size equal to half of the DD size will be carried out throughout this study to maintain high misalignment tolerance. At a distance of 300 mm, the FOM reaches zero due to the magnetic null phenomena which will be discussed at the end of this chapter.

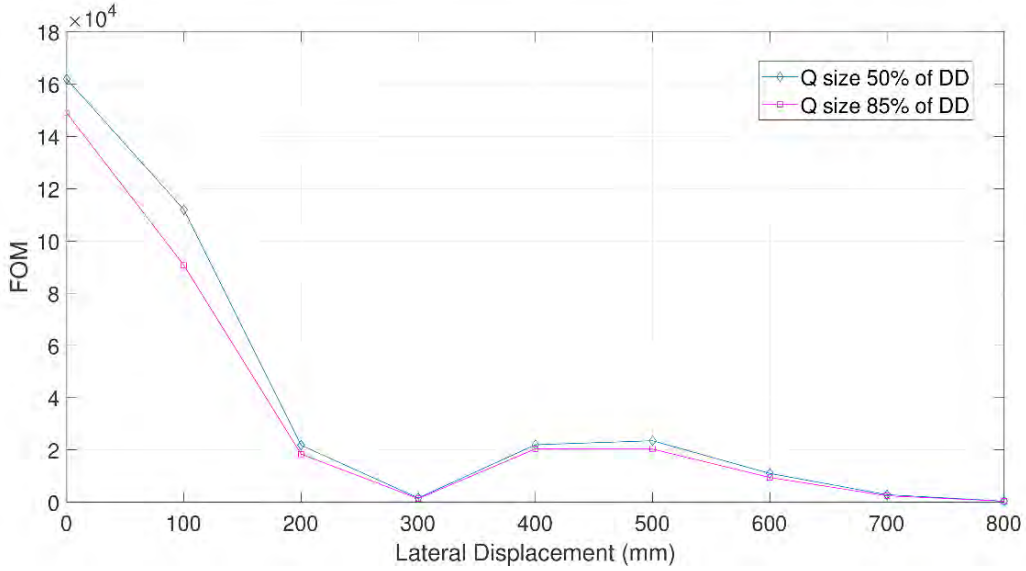

Figure 4.56: DDQ design: Figure-of-Merit versus lateral misalignment.

4.5.6. Double-D quadrature vs. bipolar power pads. Bipolar pad is developed in which it has the same advantages of DDQ pad with less requirement of copper. The coupling factor of the most optimized Bipolar and DDQ designs obtained from previous results are plotted against air gap and lateral misalignment.

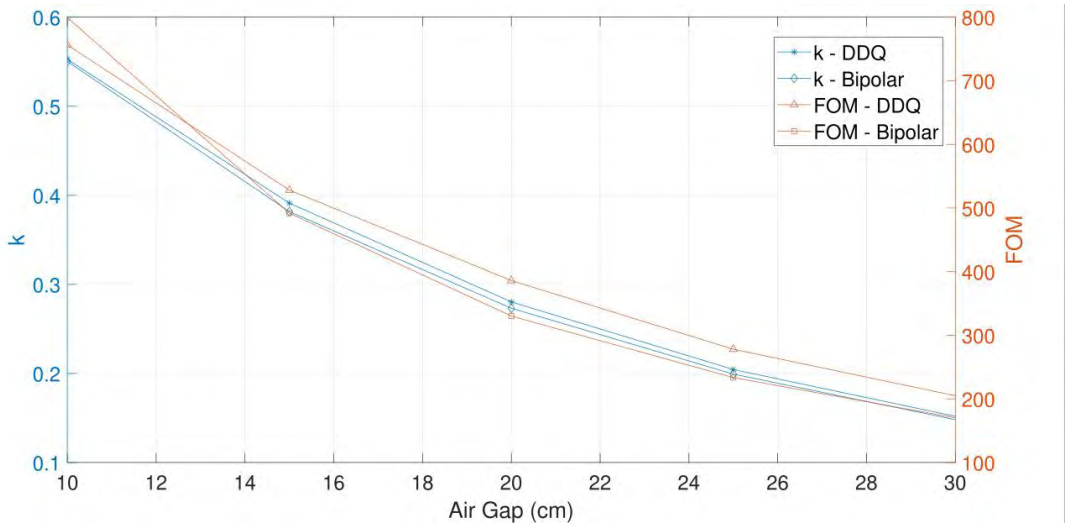

Figure 4.57: DDQ and bipolar: air gap versus coupling factor and Figure-of-Merit.

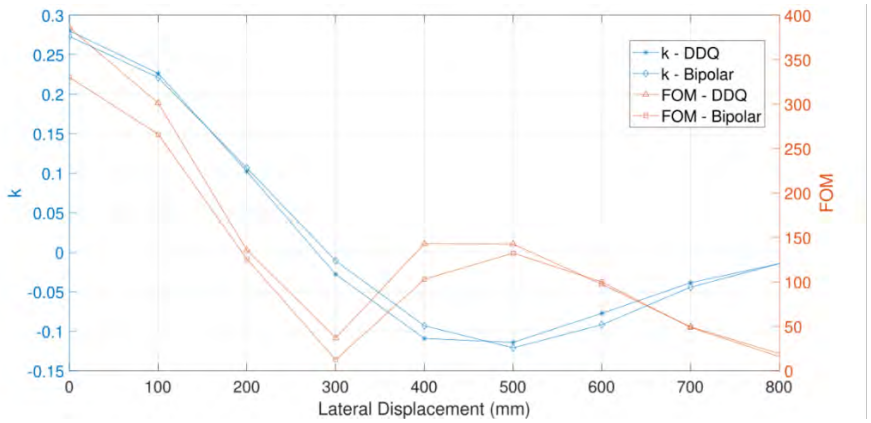

Figure 4.58: DDQ and bipolar: lateral misalignment versus coupling factor and Figure-of-Merit.

The performance of DDQ and Bipolar pads in terms of vertical and horizontal misalignment is identified in Figure 4.57 and Figure 4.58 although DDQ has better coupling factor under misalignment, Bipolar can be considered in some applications where coil weight and cost shall be optimized.

4.6. Non-Identical Asymmetric Primary and Secondary Geometry Combinations

In the previous sections, rectangular, DD, DDQ, and Bipolar pads were simulated for both transmitting and receiving coils. In this section, asymmetric transmitter and receiver power pads is a promising technique to enhance the coupling performance. Polarized and non-polarized power pad combinations are considered to reduce the problem of negative coupling coefficient under lateral misalignment as shown in

Figure 4.59 The power pad combinations can be categorized into polarized-polarized, and non-polarized to polarized for the transmitter and the receiver power pads respectively.

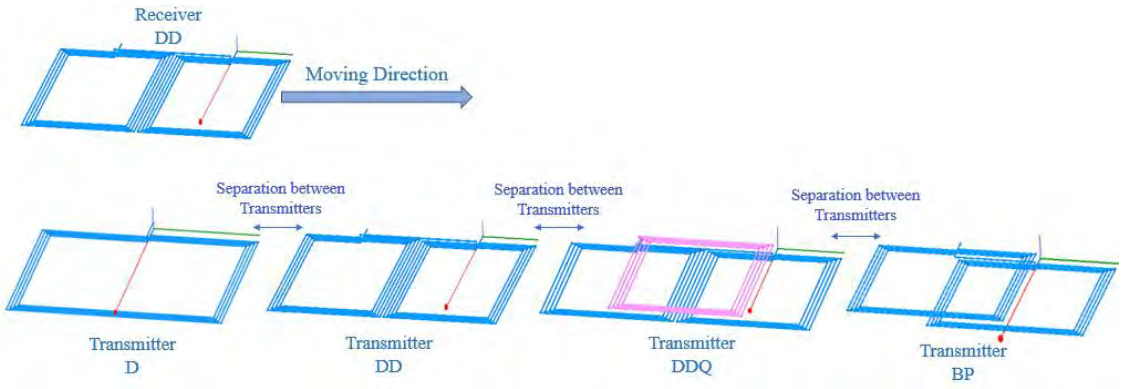

Figure 4.59: Power pad combinations: transmitter geometries (D, DD, DDQ, and BP), receiver (DD).

4.6.1. Polarized-polarized asymmetric geometry combinations. To begin with the first set of power pad combinations consists of DD-BP, DDQ-BP, DD-DDQ, DD-DD, DDQ-DDQ, and BP-BP. Figure 4.60 - Figure 4.65 represent the four turn pads under lateral misalignment variation.

The mutual inductance of the Bipolar-Bipolar combination ranges between -6 and 15uH. On the other hand, it performed lower quality factor (1250) compared to other combinations. DD-DDQ, DD-DD, and DD-Bipolar showed the best performance in terms of FOM, quality factor, and efficiency. The magnetic null point occurs at 300 mm misalignment where k, M, and FOM drops dramatically due to flux cancelation in the power pads.

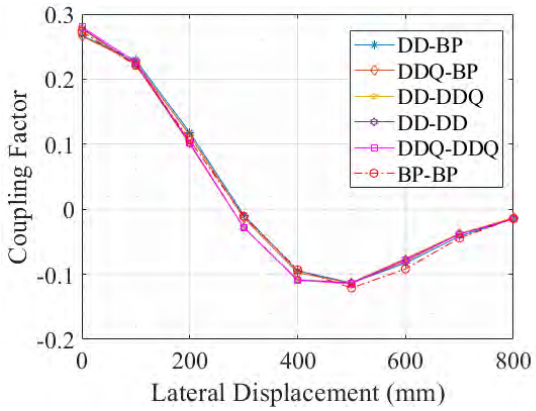

Figure 4.60: Different Tx-Rx combinations: coupling factor versus lateral misalignment.

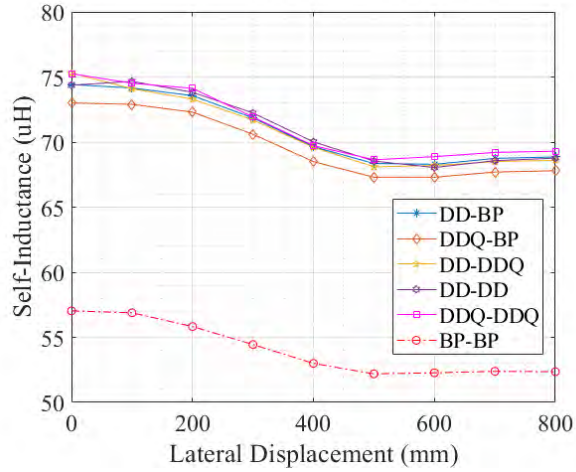

Figure 4.61: Different Tx-Rx combinations: self-inductance versus lateral misalignment.

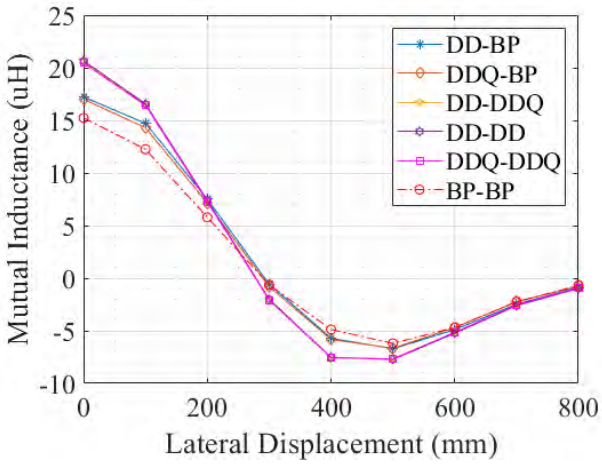

Figure 4.62: Different Tx-Rx combinations: mutual inductance versus lateral misalignment.

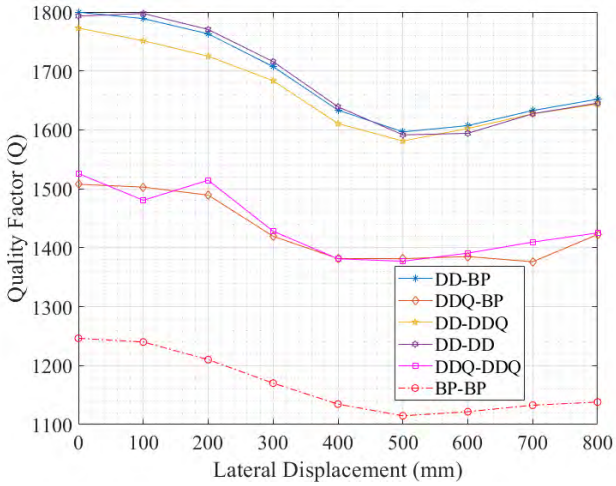

Figure 4.63: Different Tx-Rx combinations: quality factor versus lateral misalignment.

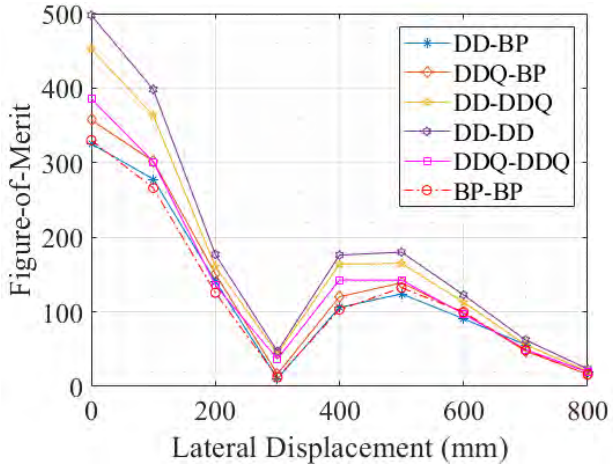

Figure 4.64: Different Tx-Rx combinations: Figure-of-Merit versus lateral misalignment.

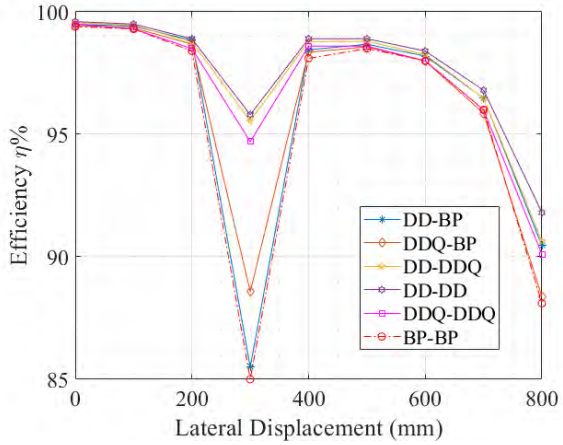

Figure 4.65: Different Tx-Rx combinations: efficiency versus lateral misalignment.

4.6.2. Non-polarized vs polarized rectangular combinations. To begin with the first set of power pad combinations consists of DD-D, DDQ-D, Bipolar-D, and D-D. Figure 4.66 - Figure 4.71 represent the four turn pads under lateral misalignment variation. As mentioned in the literature, the non-polarized magnetic couplers cannot tolerate the misalignment between the primary and secondary coils. However, merging non polarized with polarized pads improved the inductive link performance and pushed the magnetic null point to 700+ mm.

As shown in Figure 4.66 indicates the variation in coupling coefficient with lateral misalignment. The coupling factor starts at zero and increases with lateral misalignment. Until it drops back to zero. This is because of the nature of polarized and non-polarized power pads whenever they are merged. The mutual inductance exhibits

similar to the coupling factor as shown in Figure 4.68. DD-D and DDQ-D has very similar coupling performance.

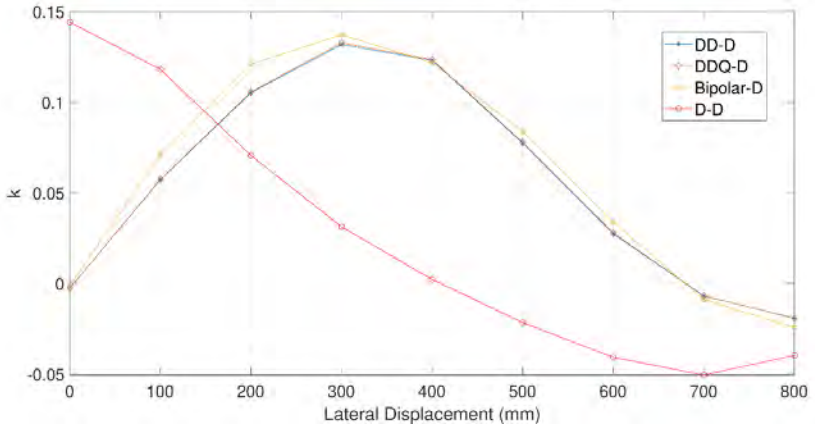

Figure 4.66: Different Tx-Rx combinations: coupling factor versus lateral misalignment.

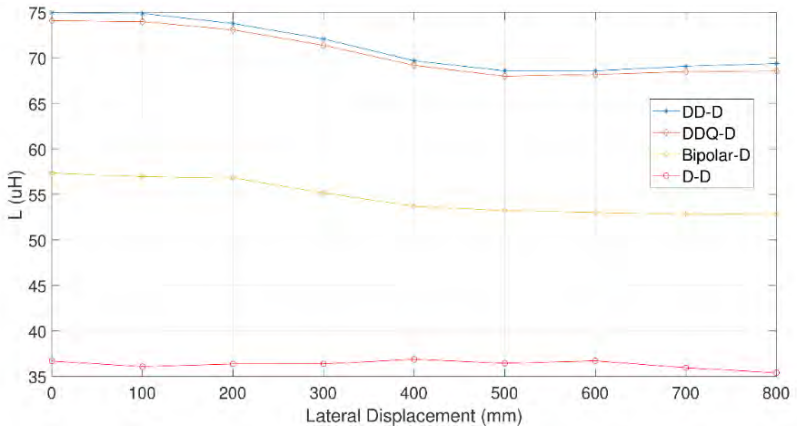

Figure 4.67: Different Tx-Rx combinations: self-inductance versus lateral misalignment.

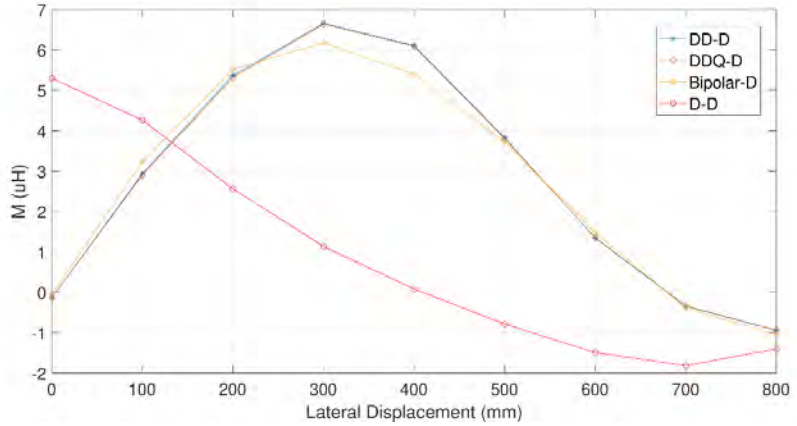

Figure 4.68: Different Tx-Rx combinations: mutual inductance versus lateral misalignment.

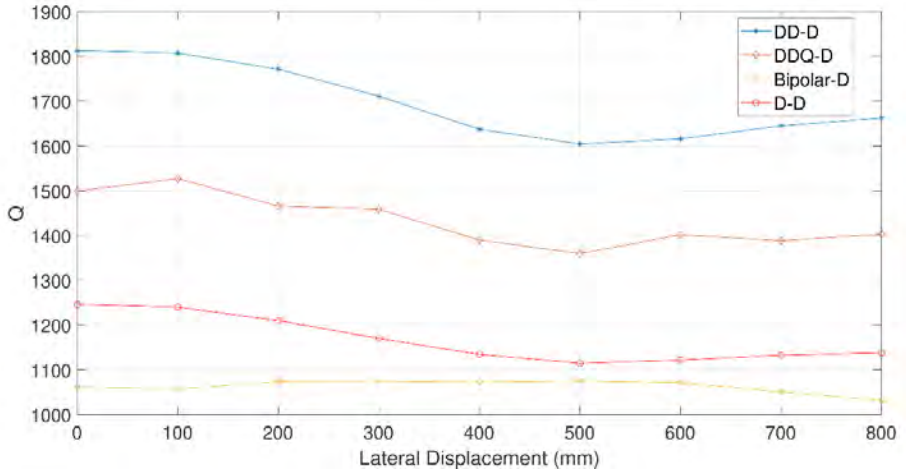

Figure 4.69: Different Tx-Rx combinations: quality factor versus lateral misalignment.

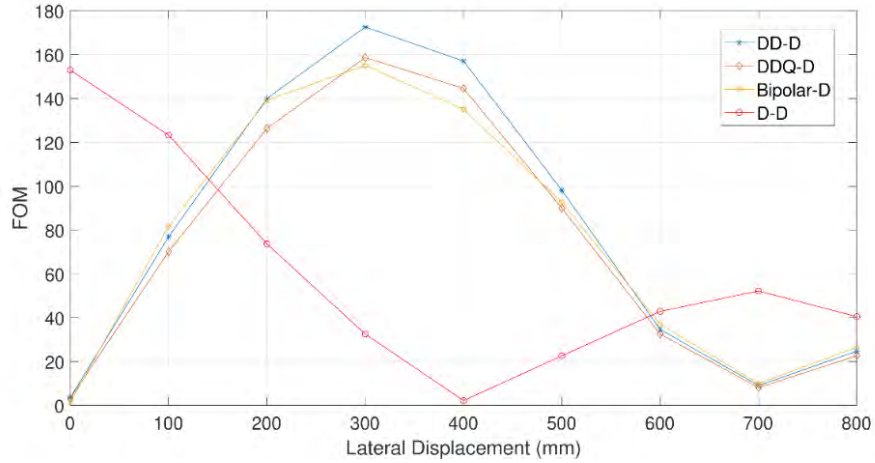

Figure 4.70: Different Tx-Rx combinations: Figure-of-Merit versus lateral misalignment.

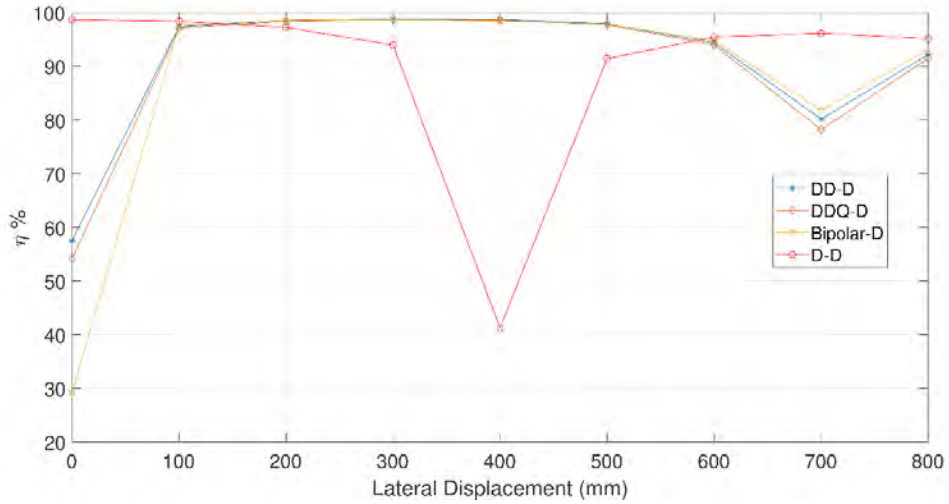

Figure 4.71: Different Tx-Rx combinations: efficiency versus lateral misalignment.

DD-D is chosen to be the most optimized non-polarized to polarized power pad combination due to the high Q factor and Figure-of-Merit. Rectangular geometry is not suggested to be used in dynamic charging systems.

4.7. Implementation and Experimental Validation

This comparative study was conducted for different power pad geometries and various coil specifications under vertical and horizontal misalignment using ANSYS Maxwell (3D FEA simulation). The simulation results shall be compared with the experimental prototypes that has been chosen to be implemented for the wireless charging system.

4.7.1. Copper only double-d power pads. Double-D power pads were implemented and tested using different methods to obtain their characteristics. Ferrite-less power pads are considered to be implemented.

4.7.1.1. *Simulation.* The 13-turn Double-D power pads were simulated for primary and secondary coils with 12 mm center-center spacing. **Table 4.9** shows the simulation results under air gap. As vertical distance between the power pads increases, the coupling factor decreases, and hence, mutual inductance decreases accordingly.

Table 4.9: Air gap variation.

AirGap (cm)	k	Lp (uH)	Ls (uH)	M (uH)	Rp (mΩ)	Rs (mΩ)	Qp	Qs	FOM	η %
10	0.3731	198.08	198.065	73.8955	55.72207	55.7214	1898.505	1.90E+03	708.3098	99.7
15	0.245889	198.0856	198.0446	48.7019	55.72	55.719	1898.63	1.90E+03	466.808	99.6
20	0.166485	198.083	198.000	32.9709	55.7228	55.721	1898.509	1.90E+03	316.0122	99.4
25	0.11519	198.085	197.936	22.81	55.7237	55.719	1898.498	1.90E+03	218.6149	99.1
30	0.08118	198.0865	197.8464	16.0714	55.7269	55.726	1898.403	1.90E+03	154.0202	98.7

The Finite Element Method simulation of the implemented DD coils is shown in Table 4.10 for various lateral displacement distances. These results shall be compared to the measured using the measurement methods presented in Chapter 3.

Ferrite-less power pads show a significant drop in the values of coupling factor and mutual inductance. At perfect alignment, the value of the coupling factor is 0.166 and the mutual inductance is 32.97 uH.

Table 4.10: Lateral misalignment.

Lateral misalignment (mm)	k	Lp (uH)	Ls (uH)	M (uH)	Rp (mΩ)	Rs (mΩ)	Qp	Qs	FOM	η %
0	0.166485	198.083	198.000	32.9709	55.7228	55.721	1898.509	1900	316.0122	9.94
100	0.12892	198.0845	198.0006	25.532	55.724	55.721	1898.483	1900	244.7071	9.92
200	0.041724	198.0841	197.996	8.263	55.722	55.7225	1898.547	1900	79.197	97.5
300	-0.04277	198.0853	197.997	-8.4713	55.7232	55.722	1898.518	1900	81.18237	97.6
400	-0.0844	198.0889	197.993	-16.7166	55.7247	55.719	1898.501	1900	160.2029	98.8
500	-0.07783	198.088	197.99	-15.413	55.724	55.7195	1898.516	1900	147.729	98.7
600	-0.04638	198.088	197.98	-9.186	55.721	55.721	1898.618	1900	88.03391	97.8
700	-0.01684	198.09	197.97	-3.33519	55.725	55.72	1898.501	1900	31.96631	93.9
800	-0.00162	198.0912	197.95521	-0.32176	55.7237	55.7231	1898.557	1900	3.084113	52.8

4.7.1.2. ***Measurements using programmable LCR meter.*** The LCR meter was used to measure the inductor parameters such as self-inductance, ESR series resistance, and corresponding capacitance.

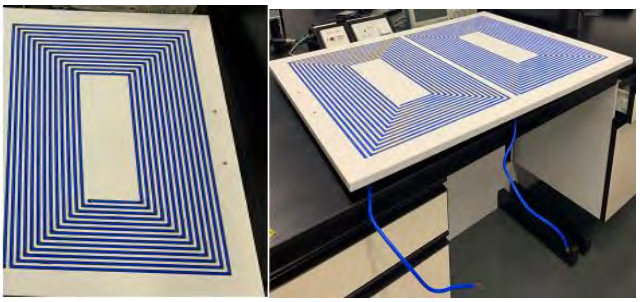

(a) (b)

Figure 4.72: Implemented coils: (a) Rectangular, (b) Double-D.

The implemented coils are slightly different than each other due to fabrication mismatching. Table 4.11 shows coil parameter values for both coils. Figure 4.72 shows the proposed design of Double-D coil. This coil was measured using LCR meter and the results are shown in Table 4.11.

Table 4.11: Double-D coil measurement using programmable LCR meter.

Parameter/Value	L	C	Q	ESR
DD1 (red)	169.5 uH	13.89 nF	190	605 mΩ
DD2 (blue)	161.4 uH	15.7 nF	176.8	574 mΩ

4.7.1.3. ***Vectors Network Analyzer for mutual inductance evaluation.*** The mutual inductance between two loosely coupled coils is to be estimated from the S parameters for each coil measured using the VNA. At 100KHz, the VNA setup was established to measure both terminals of the coils. The relations mentioned in Chapter 3 are used to calculate the mutual inductance accordingly from the Z parameters. Table 4.12 indicates the S parameters for the Double D coils used to calculate Z_{21} in order to estimate the value of mutual inductance. The input impedance of the VNA is 50 **Ω**. The coupling factor was calculated for each value of mutual inductance across variable lateral misalignment.

Table 4.12: Lateral misalignment for the implemented 13-Turn DD using VNA.

Lateral Misalignment (mm)	S11	S12	S21	S22	Z21	M (uH)	k
0	0.6233	0.49945	0.5407	0.653	18.001	28.65	0.173
100	0.4341	0.3233	0.351	0.4544	14.137	22.5	0.136
200	0.4975	0.1899	0.1887	0.5115	10.304	16.4	0.0992
300	0.3556	0.1456	0.1422	0.3774	1.96	3.12	0.0189
400	0.1998	0.10045	0.1078	0.2098	6.2015	-9.87	-0.0597
500	0.1878	0.0995	0.0988	0.1799	4.115	-6.55	-0.0396
600	0.154	0.256	0.2111	0.1447	2.73	-4.34	-0.0262

4.7.1.4. ***Voltage gain method for mutual inductance evaluation.*** The mutual inductance calculation using voltage gain ratio can be done using a sinusoidal AC input signal representing the input voltage from the function generator at 100 kHz. This voltage shall be supplied to a primary side compensation capacitor of a rating

(C_p=97.5nF). C_p in turn is connected to a primary power pad to supply a current signal through the coil. The receiver power pad is connected to a secondary side compensation capacitor C_s=95.3nF. The secondary capacitor is also connected to load resistance of 20Ω. Finally, the compensation capacitor in the receiver side is connected to oscilloscope to measure the output voltage. Table 4.13 included the design parameters of the implemented WPT system.

Figure 4.73 and Figure 4.74 indicates the comparison of mutual inductance for simulated, estimated using voltage gain, and measured using VNA mutual inductance versus lateral displacement for 13 turn ferrite-less Double D primary and secondary coils.

Table 4.13: Experimental design parameters for 13-turn DD-DD.

Design Parameters	**Value**
Output Voltage (rms) (V_o)	534 mV
Input Voltage (rms) (V_i)	401 mV
Load Resistance (R_L)	20 Ω
Primary Capacitance (C_p)	97.5 nF
Secondary Capacitance (C_s)	95.3 nF
Operating Frequency	100 KHz
Air Gap	15 cm
Primary Self-inductance Lp	169.5 uH
Secondary Self-inductance Ls	161.4 uH
Primary ESR	605 mΩ
Secondary ESR	574 mΩ
Lateral Misalignment	0

It can be noticed that the estimated mutual inductance using voltage gain method and the measured mutual inductance using VNA are almost the same across lateral misalignment.

On the other hand, simulated mutual inductance is slightly lower than the experimental results. This is due to the surrounding environment in the ANSYS Maxwell.

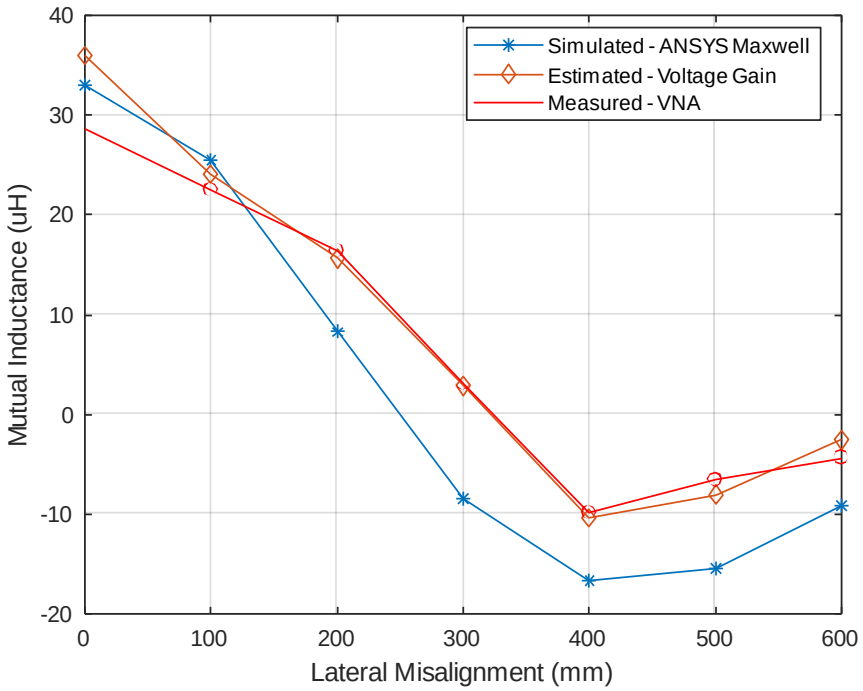

Figure 4.73: Mutual inductance (simulated, estimated, and measured).

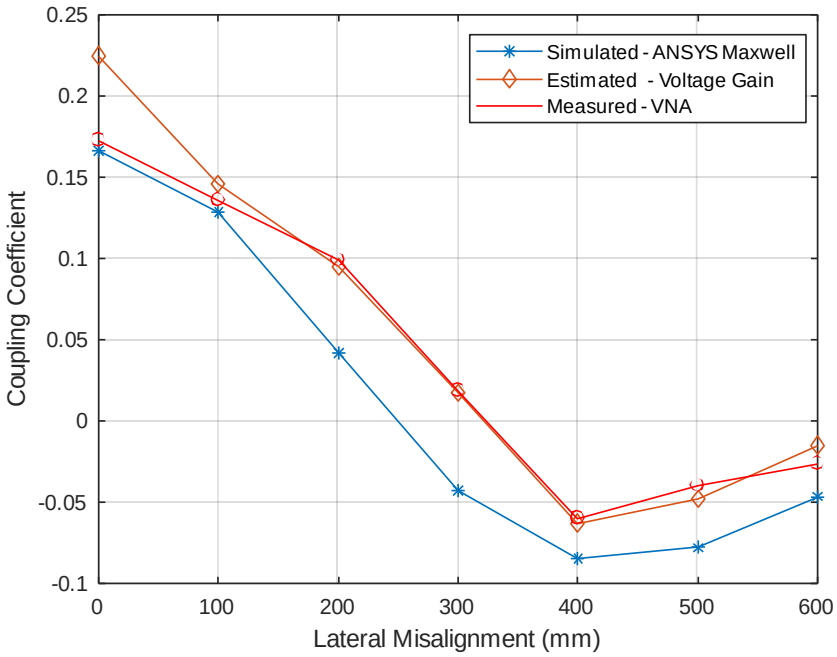

Figure 4.74: Coupling coefficient (simulated, estimated, and measured).

4.7.2. Copper-only rectangular power pads. Rectangular (D) power pads were implemented with a 15-turn primary and secondary and tested using different methods to obtain their characteristics. Ferrite-less power pads are considered to be implemented and compared with simulation results.

4.7.2.1. *Simulation.* The 15-turn D power pads were simulated for primary and secondary coils with 12 mm center-to-center spacing. Table 4.14 shows the simulation results under lateral misalignment variations, where Table 4.15 presents the air gap variation. Simulation was conducted using ANSYS Maxwell observe the characteristics of the power pads such as their self and mutual inductance, series resistance, coupling and quality factors. Moreover, the Figure-of-Merit and the maximum inductive link efficiency were calculated to investigate their variations along lateral and vertical misalignment.

Table 4.14 represents the variation of primary and secondary coil parameters.

Table 4.14: 15-Turn rectangular power pads under lateral misalignment.

Lateral misalignment (mm)	k	Lp (uH)	Ls (uH)	M (uH)	Rp (mΩ)	Rs (mΩ)	Qp	Qs	FOM	η %
0	0.33485	144.675	144.449	48.40696	42.5127	42.507	1817.498	1810	608.200	99.7
100	0.30789	144.685	144.469	44.5152	42.5121	42.5062	1817.64	1820	559.273	99.6
200	0.24481	144.675	144.445	35.3896	52.5128	42.5067	1471.386	1810	400.050	99.5
300	0.172	144.684	144.456	24.866	42.5119	42.5074	1817.637	1810	312.405	99.4
400	0.10067	144.679	144.434	14.552	42.5143	42.5094	1817.479	1810	182.815	98.9
500	0.03539	144.686	144.431	5.1154	42.5133	42.5066	1817.607	1810	64.266	96.9
600	-0.0140	144.689	144.396	-2.02613	42.513	42.508	1817.67	1810	25.454	92.4
700	-0.0376	144.687	144.3768	-5.4327	42.513	42.511	1817.638	1810	68.251	97.1
800	-0.0387	144.692	144.31567	-5.59866	42.513	42.5071	1817.701	1810	70.338	97.2
900	-0.0314	144.690	144.2476	-4.535	42.5117	42.494	1817.73	1810	56.983	96.5

It can be observed that at perfect lateral alignment and 15 cm air gap the coupling factor and the mutual inductance are approximately 0.335 and 48.4 uH respectively. In rectangular structure, the magnetic null phenomena describe the point where coupling factor and mutual inductance becomes negative. The magnetic null

occurs when lateral misalignment between the power pads reaches the 600 mm and beyond (i.e. 75% of the coil length).

Table 4.15: 15-Turn rectangular power pads under vertical misalignment.

Air Gap (cm)	k	Lp (uH)	Ls (uH)	M (uH)	Rp (mΩ)	Rs (mΩ)	Qp	Qs	kQ	Ƞ %
10	0.4593	144.663	144.565	66.423	42.513	42.506	1817.331	1820	834.486	99.8
15	0.3349	144.675	144.449	48.40696	42.513	42.507	1817.498	1810	608.155	99.7
20	0.25065	144.679	144.253	36.2097	42.515	42.512	1817.442	1810	454.887	99.6
25	0.1916	144.684	144.001	27.662	42.5133	42.509	1817.582	1810	347.516	99.4
30	0.1491	144.711	143.645	21.495	42.513	42.507	1817.93	1800	270.073	99.3

4.7.2.2. ***Measurements using programmable LCR meter.*** The LCR meter was used to measure the inductor parameters such as self-inductance, ESR series resistance, and corresponding capacitance for the implemented rectangular coils. Both coils have 15 turn windings with different spacing but same wire diameter. In *Table 4.16*, the coil parameters of the implemented coils are shown.

Table 4.16: Rectangular coil parameter measurements using LCR meter.

Parameter/Value	L (uH)	C (nF)	ESR (mΩ)	Q
D1 (red)	146.5	17.8	358	237
D2 (blue)	174	14.55	778	140

Two rectangular coils with the same design specifications were implemented, and their magnetic characteristics were measured. Self-inductance, capacitance, series resistance and quality factor vary a little bit due to mismatching in the making procedure of the turns. The above Figure 4.75 indicates the programmable LCR meter used in this measurement and one of the rectangular coils.

4.7.2.3. ***Measurements of rectangular power pads using VNA*****.** Measurement of coil S-parameters to calculate the self and mutual inductances of the implemented coils. Where Zo=50Ω. Figure 4.76 shows the measured rectangular coils and the VNA used to measure their S-parameters. Z parameters can be obtained directly from the VNA or calculated using the abovementioned equations.

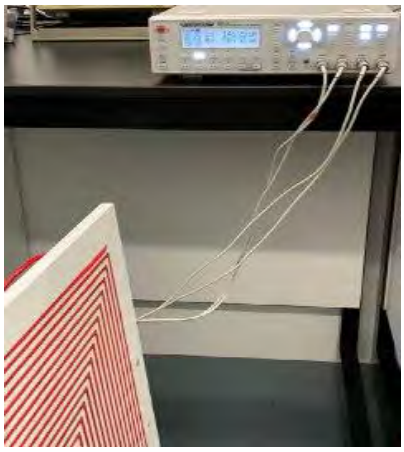

Figure 4.75: Measuring coil parameters using programmable LCR Meter.

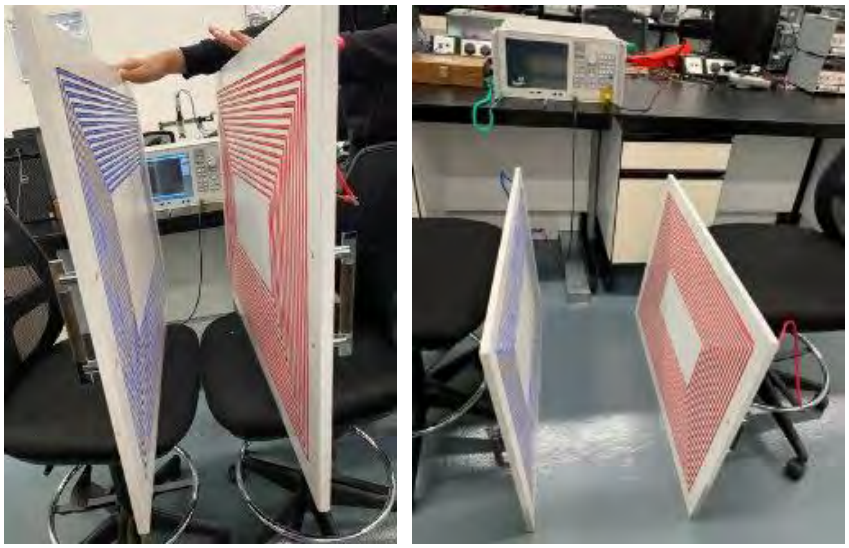

(a) (b)

Figure 4.76: Measurement of S-parameters for two loosely coupled coils: (a) Rectangular-Rectangular at 20 cm air gap. (b) Rectangular-Rectangular at 30 cm air gap.

Table 4.17: Rectangular-Rectangular under vertical misalignment.

Air Gap (cm)	S_{11}	S_{12}	S_{21}	S_{22}	Z_{21}	M (uH)
10	0.939723	0.399945	0.400867	0.93111	37.32	59.4
15	0.6089	0.2356	0.2216	0.6109	25.32	40.3
20	0.4975	0.1899	0.1887	0.5115	18.93	30.13
25	0.3556	0.1456	0.1422	0.3774	12.43	19.79
30	0.1998	0.10045	0.1078	0.2098	3.71	5.9

Table 4.17 presents the S-parameters measured over vertical distance variation between the two rectangular coils. Z_{21} is calculated for each air gap and the mutual inductance is then estimated accordingly.

Table 4.18: Rectangular-Rectangular under lateral misalignment.

Lateral Misalignment (mm)	S_{11}	S_{12}	S_{21}	S_{22}	Z_{21}	M (uH)	k
0	0.2012	0.321	0.345	0.2009	26.3	44.9	0.28
100	0.4975	0.1899	0.1887	0.5115	18.93	30.13	0.1887
200	0.3556	0.1456	0.1422	0.3774	12.43	19.79	0.124
300	0.2245	0.1661	0.1644	0.2326	8.22	13.08	0.082
400	0.1998	0.10045	0.1078	0.2098	-3.99	-6.3	-0.039
500	0.2012	0.162	0.151	0.2010	-9.07	-14.44	-0.0905
600	0.3055	0.211	0.198	0.31j	-5.08	-8.09	-0.051

Table 4.18 presents the S-parameters measured over lateral distance variation between the two rectangular coils. Z_{21} is calculated for each air gap and the mutual inductance is then estimated accordingly. These results were obtained for a 15 cm air gap at perfect lateral alignment between the two coils. It is concluded that the coupling factor is 0.28 and the mutual inductance is approximately 45 uH, comparing to the simulated results obtained for k and M which are 0.335 and 48.4 uH respectively.

4.7.2.4. ***Measurements using voltage gain.*** The calculation of Mutual inductance using voltage gain was done following the steps below:

- Input Voltage (Vac) from function generator: a sinusoidal signal at 100 kHz.
- Vac was connected to primary side compensation capacitor (Cp=100nF or 0.1uF).
- Cp is connected to Lp (primary coil the red one of Lp= 146.5 uH measured using LCR meter).
- Secondary coil (blue) Ls=174uH is connected to secondary side compensation capacitor Cs=100nF.
- The secondary capacitor is connected to load resistance of 20Ω.

- The capacitor in the receiver side must be connected to oscilloscope to measure the output voltage (V_o).
- Calculate the voltage gain ratio.

Table 4.19: Experimental design parameters for 15-turn Rectangular to Rectangular.

Design Parameters	**Value**
Output Voltage (rms) (V_o)	511 mV
Input Voltage (rms) (V_i)	359 mV
Load Resistance (R_L)	20 Ω
Primary Capacitance (C_p)	30 nF
Secondary Capacitance (C_s)	20 nF
Operating Frequency	100 KHz
Air Gap	15 cm
Primary Self-inductance Lp	146.5 uH
Secondary Self-inductance Ls	174 uH
Primary ESR	358 mΩ
Secondary ESR	778 mΩ
Lateral Misalignment	0

Table 4.19 included the design parameters of the implemented WPT system. Varying lateral misalignment at 15 cm air gap and 100 KHz is shown in Table 4.20. It can be observed that the measured values of mutual inductance and coupling factor showed a great match when compared to the simulation results stated above.

The mutual inductance can be estimated using the ratio of input-to-output voltage of the inductive link circuit. Table *4.20* shows the different values of mutual inductance and coupling coefficient at various lateral misalignment distances. These results shall be compared to simulation results.

The difference between the values of coupling factor and mutual inductance obtained from ANSYS Maxwell and measured using Voltage gain method is relatively small. This proves that the voltage gain method using to estimate the mutual inductance is highly promising and easy to implement.

Figure 4.77 and Figure 4.78 represent the difference between simulated and measured mutual inductance and coupling factor values along various lateral misalignment distances.

In Table 4.21, indicates the coil parameter values of simulated using ANSYS Maxwell and measured using LCR meter and voltage gain method power pads. Results are compared and the percentage error is calculated to measure the feasibility of voltage gain method in estimating the mutual inductance and the coupling factor.

Table 4.20: 15 turns rectangular to rectangular, 14 mm, 15 cm air gap, at 100 KHz.

Lateral Misalignment (mm)	**Vo (V_{RMS})**	**Vi (V_{RMS})**	**M (uH)**	**k**
0	511	359	47.0945	0.295
100	488	376	42.9414	0.269
200	555	520	35.3129	0.223
300	492	76.2	21.3626	0.134
400	500	106	15.6066	0.0977
500	489	126	12.8405	0.0804
600	552	270	6.76425	0.045
700	494	350	2.541932	0.00966
800	533	365	3.14797	0.00135
900	535	370	3.6648	0.000232

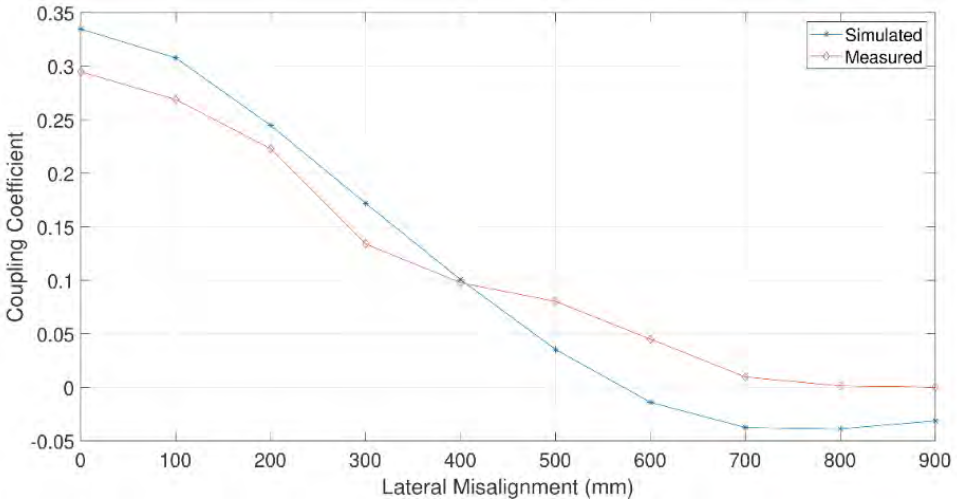

Figure 4.77: Coupling factor versus lateral misalignment.

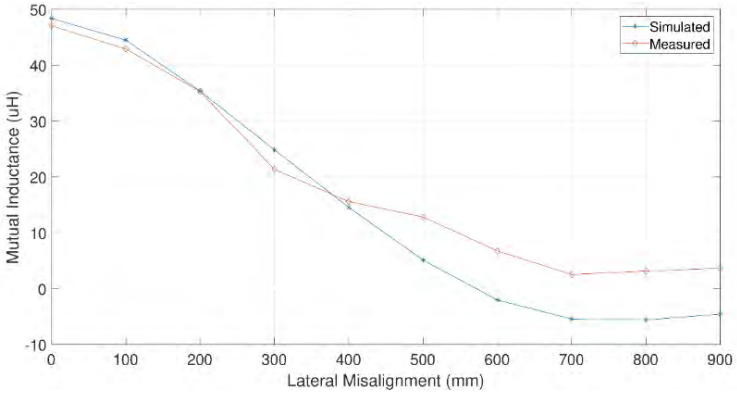

Figure 4.78: Mutual inductance versus lateral misalignment.

The coupling factor indicated a percentage error of 3.27% between simulated and measured. Where on the other hand, the mutual inductance differs slightly more from simulated to measured values by a difference of 11.8%.

Table 4.21: At perfect alignment and 100 KHz using ANSYS Maxwell.

ANSYS Maxwell (Simulated)	**Value**	**Experimental results (measured and calculated)**	**Value**
Mutual inductance (M)	41.5132 uH	**Mutual inductance (M)**	47.0945 uH
Coupling factor (k)	0.305263	**Coupling factor (k)**	0.295
Lp	135.6053 uH	**Lp D1 (red)**	146.5 uH
Ls	136.3786 uH	**Ls D2 (blue)**	174 uH
Rp	137.0135 mΩ	**Rp**	358 mΩ
Rs	133.49 mΩ	**Rs**	778 mΩ

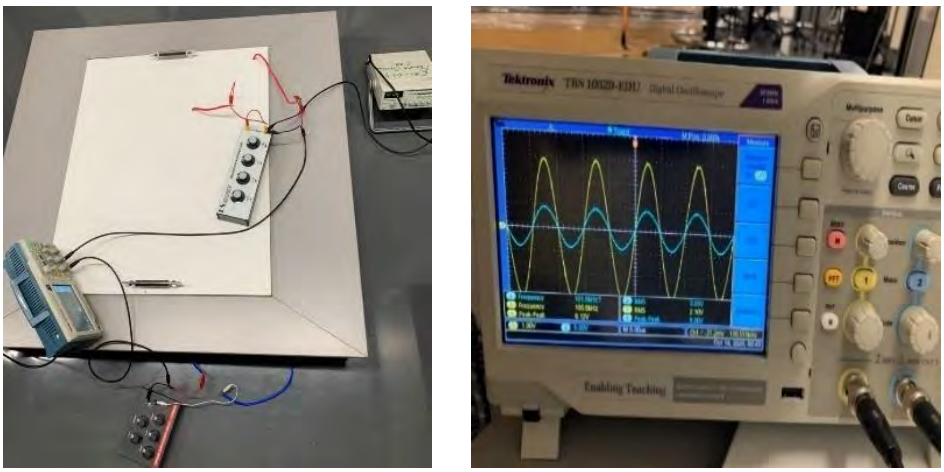

Figure 4.79: Voltage gain method to estimate mutual inductance: Rectangular-Rectangular at 15 cm air gap.

Figure 4.79 and Figure 4.80 show the experimental setup of the inductive power transfer AC-AC circuit. It consists of a voltage source represented in a sinusoidal signal

at 100KHz generated from the function generator. Furthermore, primary compensated capacitor is placed in series with an inductor (coil) at the transmitter side. On the other hand, secondary coil on the receiver side is placed in series with a compensated capacitor connected to a load resistance.

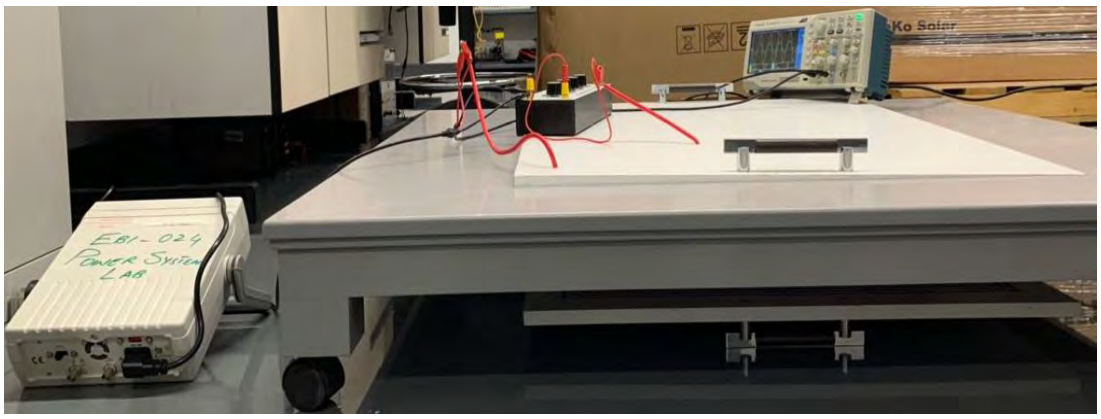

Figure 4.80: Experimental setup for WPT system.

In Figure 4.81 and Figure 4.82, the mutual inductance and the coupling factor for the 15-turn rectangular power pads between simulated, estimated by voltage gain, and measured with VNA. It can be noticed that the mutual inductance curve is very close to linear in case of simulated mutual inductance. Furthermore, voltage gain method shows that the behavior of mutual inductance and coupling factor is very similar to the simulated results obtained by ANSYS Maxwell.

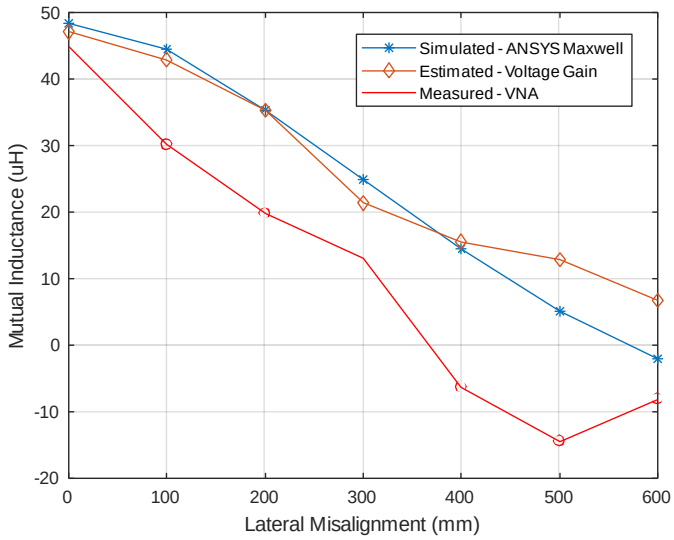

Figure 4.81: Mutual Inductance (simulated, estimated and measured).

On the other hand, the measured mutual inductance using VNA happened to be the least accurate method as the results were lower than those obtained by simulation and experimentation.

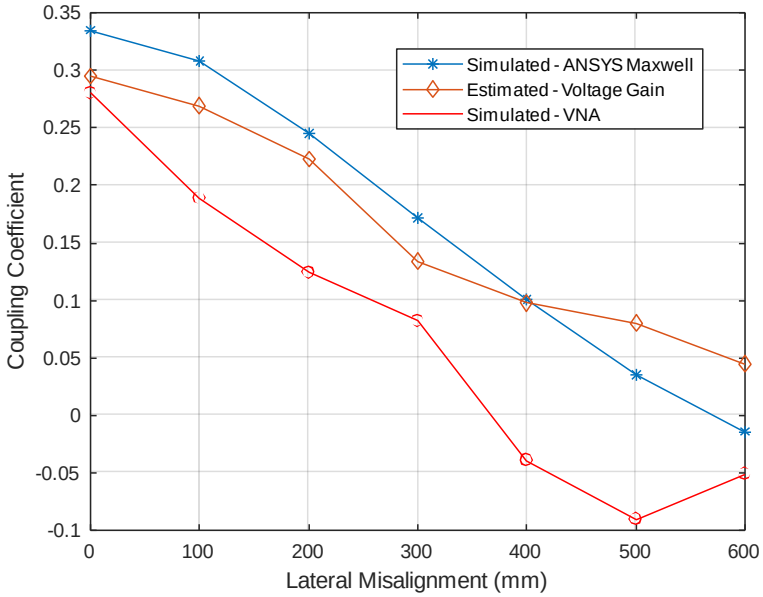

Figure 4.82: Coupling Coefficient (simulated, estimated and measured).

4.8. Comparison of simulated, measured, calculated Rectangular power pads

As part of the comparative study for various coil geometries and design specifications, some reference studies from the literature were used as a benchmark to build stronger findings and draw reliable conclusions.

Furthermore, authors in [32] have presented the magnetic null problem with DD and D coils. It can be observed from Figure 4.83 that the coupling factor has a null point at around 40% of the length of the pad. The null point occurs at 432 mm.

Authors in [32], presented the problem of magnetic null phenomena that occurs due to lateral misalignment. This phenomenon shall impact the coupling performance of the inductive link and cause a drop in the coupling coefficient to negative values.

Several methods were tested trying to reduce the impact of the magnetic null phenomena with lateral misalignment. Some authors used asymmetric coil geometries as well as non-identical outer dimensions between the primary and secondary charging pads.

It is necessary to study the impact of the coil geometry on the magnetic null point location at different lateral misalignment distances. For example, the null point in non-polarized geometry such as rectangular is at 600 mm where in DD is at 300 mm.

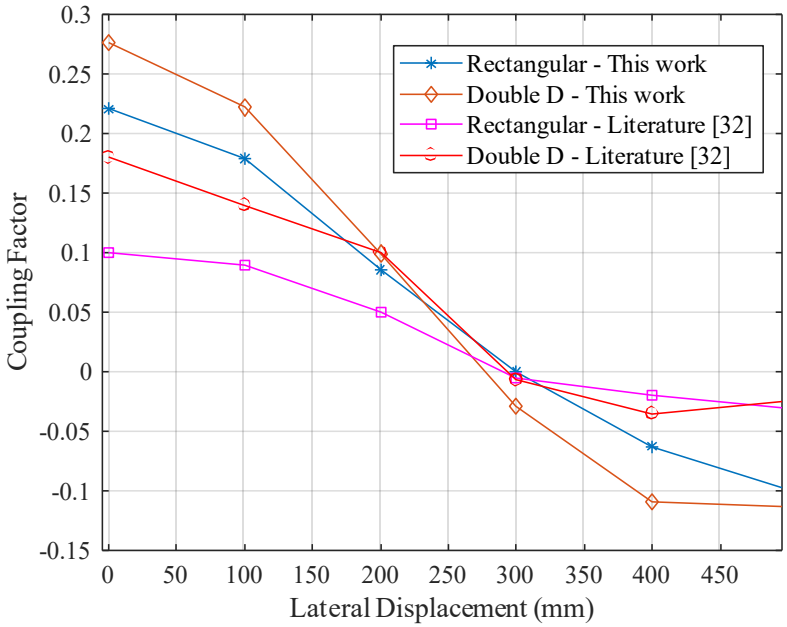

Figure 4.83: Lateral misalignment versus coupling factor for rectangular and Double D power pads.

A 720 x 440 mm Double-D power pad has a null point when misaligned in the lateral direction, at 34% of its length [32]. This is due to the transmitter being linked with only one section of the receiver without inducing a voltage. In this study, the null point occurs at 285 mm of lateral misalignment as shown in Figure 4.84, which is 35.6% of the power pad length.

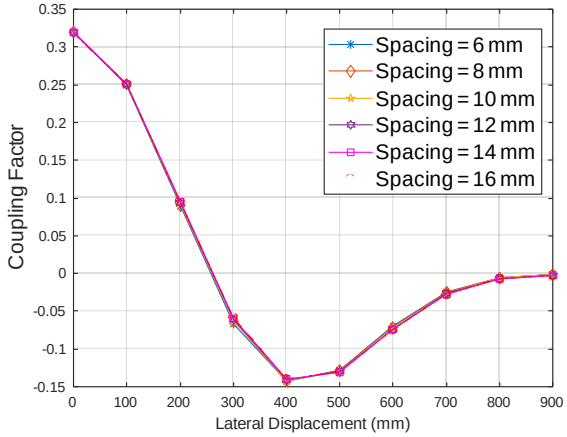

Figure 4.84: Magnetic null point location at lateral misalignment.

The outer dimensions of litz wires coils used in this work are 600x800 mm^2 and nine ferrite bars of 16 mm thickness each were compared to similar dimensions presented in previous work from the literature [36]. This to ensure the use of practical coil dimensions that is suitable for the wireless power transfer application in the EVs. Furthermore, Figure 4.85, presents a clear comparison between the simulated and implemented Double D power pads of this work and similar power pads presented in the literature [36]. It can be noticed that the coupling factor versus lateral misalignment for simulated power pads (blue line graph) in this work showed a similar pattern of those of similar design specifications presented by authors in [36] by the purple line graph.

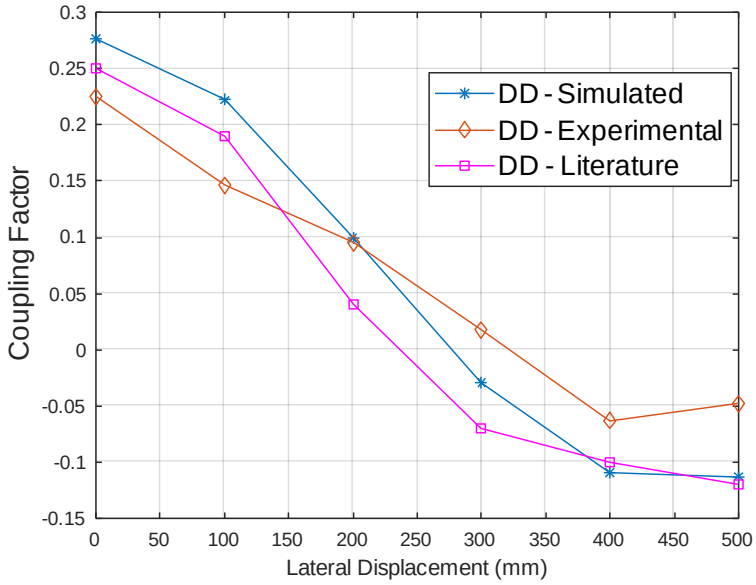

Figure 4.85: Comparison between simulated, experimental and literature DD power pad.

Figure 4.86 represents the impact of varying lateral and vertical misalignment on the mutual inductance behavior. At air gap of 10 cm and perfect lateral alignment, the mutual inductance is at the largest. However, at 400 mm misalignment it drops to the lowest negative value due to the magnetic null phenomena described earlier.

In [37], authors analyzed that asymmetrical pads with larger outer and inner diameter of transmitting coil, when compared to receiving coil, give larger tolerance to misalignment and gap variation [37]. The existence of magnetic null is due to flux cancelation in the pad at a horizontal offset of 38% pad diameter. The magnetic null

defines the limit of misalignment tolerance as power transfer in the vicinity of magnetic null is negligible. Magnetic null is independent of air gap, sensitive to lateral misalignment [37].

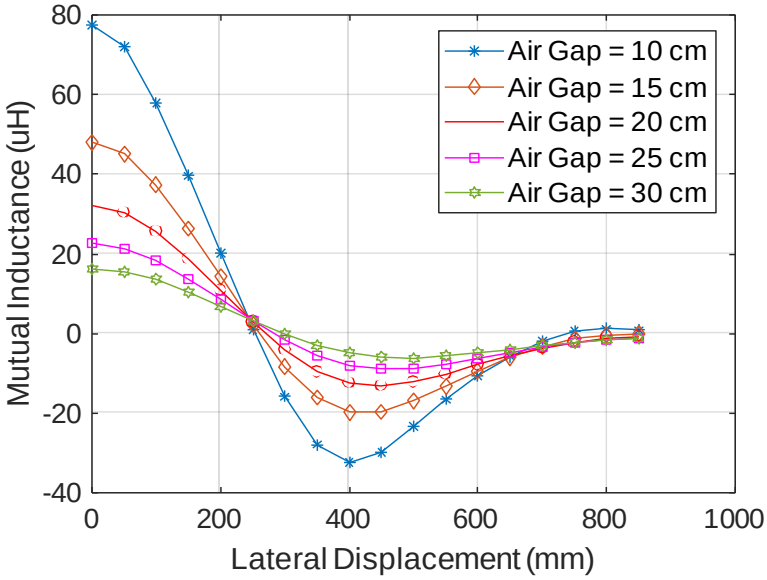

Figure 4.86: Mutual inductance under lateral and vertical misalignment variations.

In [38] authors compared between ferrite-less 4 turn power pads of different geometries such as rectangular, DD, and DDQ. Their results are shown in Table 4.22. These results can be compared to the previous results presented in this study.

Table 4.22: Ferrite-less four turns power pad geometries [38].

Parameter	D	DD	DDQ
M	42.59795	107.1174	90.30204
Lp	104.0497	235.4053	212.2261
Ls	102.9681	235.0381	210.1596
k	0.411545	0.455389	0.427586
Magnetic flux Tx	0.001466 Wb	0.003425	0.003025
Magnetic flux Rx	0.001456 Wb	0.003422	0.003005

4.9. Discussion

To highlight the comparative study contributions in this work, and after analyzing the results and outcomes of this research, it has been supported through the simulation and experimental findings of this thesis that the:

- Number of turns: increasing the number of turns shall increase the characteristics of the coil (L, ESR, M, k). A tradeoff has to be made to optimize the weight and the cost of the coil specifically the receiver side).
- Wire diameter: increasing wire diameter shall increase L, M, ESR, k. the wire diameter is chosen to be 4 mm for practicality.
- As the spacing between the turns increases to a certain limit (2-3*wire diameter), field losses decrease and hence increase quality factor.
- Spacing has the most dominant effect on the (Inner-to-outer area ratio) at fixed wire diameter 4 mm.
- Spacing affects k, Q, and kQ the most, in comparison to number of turns.
- DD_DD, and DD_DDQ are the best combinations that gives the best coupling performance for misalignment conditions. (dynamic charging systems).
- D or D_DD geometry are the proper geometries for static charging since it performs similar to Double-D in perfect alignment conditions
- Increasing Aluminum thickness does not affect the negative coupling happening at large lateral misalignment.
- Varying the Air gap affects the power pads parameters more when compared to varying the lateral misalignment.
- Non-polarized geometries such as rectangular are preferred to be identical for both transmitter and receiver coils.
- Non-polarized power pads such as circular and rectangular are preferred to be merged to form asymmetric transmitter and receiver inductive link. This shall improve the coupling performance of the WPT system.
- Increasing vertical misalignment shall push the magnetic null point further.
- Asymmetrical outer-to-inner dimension shall minimize the occurrence of magnetic null at low misalignment values.

Chapter 5. Conclusion and Future Work

5.1. Conclusion

This work aims at comparing the coupling performance and AC-AC power transfer efficiency of some of the most commonly adopted primary and secondary coil geometries, using accurate FEM simulations tools ANSYS Maxwell and analysis. At this stage of the work, only rectangular (D) and DD coil geometries are designed and simulated on both sides of the inductive link, and their coupling performance is compared. The physical models for both types of coils were built using ANSYS Maxwell 3D based on the recommended physical dimensions in SAE J2954. For each coil geometry, the variation of the mutual inductive coupling with respect to the separation between the coils pair, the Figure-of-Merit and the coil-to-coil and AC-to-AC efficiency versus air gap (vertical misalignment between transmitting and receiving sides varies between 10 cm to 30 cm), and the Figure-of-Merit and coil-to-coil AC-AC efficiency variation with respect lateral misalignment (Horizontal misalignments was applied from -800 mm to 800 mm) between primary and secondary coils ware analyzed and simulation results are presented. The initially obtained simulation results reveal that using DD coils provides the highest coupling factor and highest inductive link efficiency when the primary and secondary coils are perfectly identical, while having a better lateral misalignment tolerance. Hence, D coils may not be the most suitable option when it comes to maintain the maximum power transfer efficiency over a range of lateral misalignment, which thus opens the floor for further investigation. It can be concluded that DD_DD, and DD_DDQ are the best combinations that gives the best coupling performance for misalignment conditions for dynamic charging systems. Furthermore, the transmitter coil geometry is preferred to be polarized type to improve the coupling performance of the inductive link. Finally, lateral misalignment is a common issue that needs to be addressed where in fact, air gap variation has a drastic impact on the overall performance of the system.

5.2. Future Work

This section points out some flourishing ideas that seem to have potential and hopefully bright outcomes, as well as opportunities for improvement in the field of EVs wireless charging. Here are some points which can be considered for the future work:

- Additional pad parameter variations shall be explored to obtain the most optimum design for each geometry.
- More coupler (power pad) configurations with higher power transfer efficiency and better misalignment characteristics should be investigated.
    - Double-D Quadrature, Bipolar, and multi-thread rectangular coil geometries will be designed and simulated using ANSYS Maxwell.
- Experimental validation of the final power pad can be conducted in the future to validate its performance.
- Perhaps researching into the materials used in the coils manufacturing and comparing different materials with respect to the WPT performance and the coils prices, can lead to more optimization in terms of materials.

References

[1] C. C. Mi, G. Buja, S. Y. Choi and C. T. Rim, "Modern Advances in Wireless Power Transfer Systems for Roadway Powered Electric Vehicles," in *IEEE Transactions on Industrial Electronics*, vol. 63, no. 10, pp. 6533-6545, Oct. 2016.

[2] S. Kim, G. A. Covic and J. T. Boys, "Tripolar Pad for Inductive Power Transfer Systems for EV Charging," in *IEEE Transactions on Power Electronics*, vol. 32, no. 7, pp. 5045-5057, July 2017.

[3] V. Prasanth and P. Bauer, "Distributed IPT Systems for Dynamic Powering: Misalignment Analysis," in *IEEE Transactions on Industrial Electronics*, vol. 61, no. 11, pp. 6013-6021, Nov. 2014.

[4] D. Ongayo and M. Hanif, "Comparison of circular and rectangular coil transformer parameters for wireless Power Transfer based on Finite Element Analysis," *2015 IEEE 13th Brazilian Power Electronics Conference and 1st Southern Power Electronics Conference (COBEP/SPEC)*, Fortaleza, 2015, pp. 1-6.

[5] E. A. ElGhanam, M. S. Hassan and A. H. Osman, "Deployment Optimization of Dynamic Wireless Electric Vehicle Charging Systems: A Review," *2020 IEEE International IOT, Electronics and Mechatronics Conference (IEMTRONICS)*, Vancouver, BC, Canada, 2020, pp. 1-7.

[6] H. H. Kabalan, E. A. ElGhanam, M. S. Hassan and A. Osman, "The Impact of Coupling and Loading Conditions on the Performance of S-S EV Dynamic Wireless Charging Systems," *2019 International Conference on Electrical and Computing Technologies and Applications (ICECTA)*, Ras Al Khaimah, United Arab Emirates, 2019, pp. 1-5.

[7] E. A. ElGhanam, M. S. Hassan and A. Osman, "Design and Finite Element Modeling of The Inductive Link in Wireless Electric Vehicle Charging Systems," *2020 IEEE Transportation Electrification Conference & Expo (ITEC)*, Chicago, IL, USA, 2020, pp. 389-394.

[8] A. Ahmad, M. S. Alam and A. A. S. Mohamed, "Design and Interoperability Analysis of Quadruple Pad Structure for Electric Vehicle Wireless Charging Application," in *IEEE Transactions on Transportation Electrification*, vol. 5, no. 4, pp. 934-945, Dec. 2019.

[9] F. Y. Lin, G. A. Covic, and J. T. Boys, “Evaluation of magnetic pad sizes and topologies for electric vehicle charging,” *IEEE Transactions Power Electronics*, vol. 30, no. 11, pp. 6391–6407, Nov. 2015.

[10] R. Bosshard, U. Iruretagoyena, and J. W. Kolar, “Comprehensive evaluation of rectangular and double-D coil geometry for 50 kW/85 kHz IPT system,” *IEEE J. Emerg. Sel. Topics Power Electron*, vol. 4, no. 4, pp. 1406–1415, Dec. 2016.

[11] L. Strauch, M. Pavlin, and V. Bregar, “Optimization, design and modeling of ferrite core geometry for inductive wireless power transfer,” *International Journal of Applied Electromagnetics and Mechanics*, vol. 49, pp. 145–155, 2015.

[12] I. Ahmed, E. A. ElGhanam, M. S. Hassan and A. Osman, "Study of the Feasibility of Using Microwave Power Transfer for Dynamic Wireless Electric Vehicle Charging," *2020 IEEE Transportation Electrification Conference & Expo (ITEC)*, Chicago, IL, USA, 2020, pp. 365-370.

[13] J. P.-W. Chow, H. S.-H. Chung, and C.-S. Cheng, “Use of transmitter side electrical information to estimate mutual inductance and regulate receiver-side power in wireless inductive link,” *IEEE Transactions Power Electron*ics, vol. 31, no. 9, pp. 6079–6091, Sep. 2016

[14] T. Fujita, T. Yasuda, and H. Akagi, "A dynamic wireless power transfer system applicable to a stationary system," *IEEE Transactions Industry Applications,* Vol. 53, No. 4, pp. 3748-3757, 2017.

[15] C. Panchal, S. Stegen, J. Lu, "Review of static and dynamic wireless electric vehicle charging system," *Engineering Science and Technology, an International Journal,* vol. 21, no. 5, pp. 922-937, 2018.

[16] H. M. Sharf, E. A. ElGhanam, M. S. Hassan and A. H. Osman, "Assessing Efficiency and Aging of Lithium-Ion Battery in a Hybrid Energy Storage System," *2020 IEEE International IOT, Electronics and Mechatronics Conference (IEMTRONICS)*, Vancouver, BC, Canada, 2020, pp. 1-6.

[17] D.M. Vilathgamuwa, J.P.K. Sampath, Wireless Power Transfer (WPT) for Electric Vehicles (EVs)—Present and Future Trends, in: S.F. Rajakaruna, A. Ghosh (Eds.), Plug In Electric Vehicles in Smart Grids, Springer International Publishing AG, Part of Springer Science+Business Media, Springer Singapore, 2015, pp. 33–60.

[18] Plugless Power. Accessed: December 2, 2020. [Online]. Available: https://www.pluglesspower.com/shop/.

[19] J. G. Bolger, F. A. Kirsten and L. S. Ng, "Inductive power coupling for an electric highway system," *28th IEEE Vehicular Technology Conference*, Denver, Colorado, USA, 1978, pp. 137-144.

[20] Y. Liu, R. Mai, D. Liu, Y. Li and Z. He, "Efficiency Optimization for Wireless Dynamic Charging System With Overlapped DD Coil Arrays," *in IEEE Transactions on Power Electronics*, vol. 33, no. 4, pp. 2832-2846, April 2018.

[21] M. Budhia, J. T. Boys, G. A. Covic, and H. Chang-Yu, “Development of a single-sided flux magnetic coupler for electric vehicle IPT charging systems,” *IEEE Trans. Ind. Electron.*, vol. 60, no. 1, pp. 318–328,Jan. 2013.

[22] Soft ferrites and accessories: Data handbook, Ferroxcube, July 2013.

[23] Y. J. Jang, Y. D. Ko and S. Jeong, "Optimal design of the wireless charging electric vehicle," *2012 IEEE International Electric Vehicle Conference*, Greenville, SC, 2012, pp. 1-5.

[24] J. Shin et al., "Design and Implementation of Shaped Magnetic-Resonance-Based Wireless Power Transfer System for Roadway-Powered Moving Electric Vehicles," *in IEEE Transactions on Industrial Electronics*, vol. 61, no. 3, pp. 1179-1192, March 2014.

[25] Qualcomm Halo Wireless Electric Vehicle Charging. Accessed: December 2, 2020. [Online]. Available: http://www.qualcommhalo.com/index.php/media-centre.html?id=41#media-centre.

[26] T. M. Fisher, K. B. Farley, Y. Gao, H. Bai, and Z. T. H. Tse, “Electric vehicle wireless charging technology: A state-of-the-art review of magnetic coupling systems,” *Wireless Power Transf.*, vol. 1, no. 2, pp. 87–96, 2014.

[27] QualcommHalo. (2011). *First Electric Vehicle Wireless Charging Trial Announced for London*. Accessed: Jul. 2013. [Online]. Available: http://www.qualcomm.com/media/releases/2011/11/10/firstelectric- vehicle wireless-charging-trial-announced-london

[28] *DRIVE: Electric Vehicles*. Accessed: December 2, 2020. [Online]. Available: http://witricity.com/products/automotive/

[29] L. Sungwoo, H. Jin, P. Changbyung, C. Nam-Sup, C. Gyu-Hyeoung, and R. Chun-Taek, "On-line electric vehicle using inductive power transfer system," in *Proc. IEEE ECCE*, Sep. 2010, pp. 1598–1601.

[30] H. Jin, L. Wooyoung, C. Gyu-Hyeong, L. Byunghun, and R. Chun-Taek, "Characterization of novel inductive power transfer systems for on-line electric vehicles," in *Proc. 26th Annu. IEEE APEC Expo.*, Mar. 2011, pp. 1975–1979.

[31] (R. Bosshard, "Multi-objective optimization of inductive power transfer systems for ev charging," Ph.D. dissertation, ETH ZURICH, 2015.

[32] Marco, Davide & Dolara, Alberto & Longo, Michela & Yaïci, Wahiba. (2019). Design and Performance Analysis of Pads for Dynamic Wireless Charging of EVs using the Finite Element Method. Energies. 12. 4139. 10.3390/en12214139.

[33] G.A.Covic, M. L. Kissin, D. Kacprzak,N.Clausen, andH.Hao, "A bipolar primary pad topology for EV stationary charging and highway power by inductive coupling," in *Proc. IEEE Energy Convers. Congr. Expo.*, 2011, pp. 1832–1838.

[34] A. Zaheer, D. Kacprzak, and G. A. Covic, "A bipolar receiver pad in a lumped IPT system for electric vehicle charging applications," in *Proc. IEEE Energy Convers. Congr. Expo.*, 2012, pp. 283–290.

[35] S. Bandyopadhyay, P. Venugopal, J. Dong and P. Bauer, "Comparison of Magnetic Couplers for IPT-Based EV Charging Using Multi-Objective Optimization," *in IEEE Transactions on Vehicular Technology*, vol. 68, no. 6, pp. 5416-5429, June 2019.

[36] T. Nguyen, S. Li, W. Li and C. C. Mi, "Feasibility study on bipolar pads for efficient wireless power chargers," *2014 IEEE Applied Power Electronics Conference and Exposition - APEC 2014*, Fort Worth, TX, 2014, pp. 1676-1682.

[37] Vaka, R., Keshri, R.K. Design Considerations for Enhanced Coupling Coefficient and Misalignment tolerance Using Asymmetrical Circular Coils for WPT System. Arab J Sci Eng 44, 1949–1959 (2019).

[38] Ahmad, A., Alam, M., Chabaan, R., and Mohamed, A., "Comparative Analysis of Power Pad for Wireless Charging of Electric Vehicles," SAE Technical Paper 2019-01-0865, 2019.

[39] G. A. Covic and J. T. Boys, "Modern Trends in Inductive Power Transfer for Transportation Applications,"*in IEEE Journal of Emerging and Selected Topics in Power Electronics*, vol. 1, no. 1, pp. 28-41, March 2013.

[40] H.H. Wu, A. Gilchrist, K. D. Sealy and D. Bronson, "A High Efficiency 5 Kw Inductive Charger for EVs Using Dual Side Control, " in *IEEE Transactions on Industrial Informatics,* vol. 8, no. 3, pp. 585-595, Aug. 2012.

[41] R. Bosshard, J. W. Kolar and B. Wunsch, "Accurate finite-element modeling and experimental verification of inductive power transfer coil design, " *2014 IEEE Applied Power Electronics Conference and Exposition – APEC 2014, Fort Worth, TX, 2014*, pp. 1648-1653.

[42] T. Diekhans, and R. W. De Doncker, "A Dual-Side Controlled Inductive Power Transfer System Optimized for Large Coupling Factor Variations and Partial Load," in *IEEE Transactions on Power Electronics*, vol. 30, no. 11, pp. 6320-6328, Nov. 2015.

[43] C. Zheng, H. Ma, J. Lai and L. Zhang, “Design Considerations to Reduce Gap Variation and Misalignment Effects for the Inductive Power Transfer System,” in *IEEE Transactions on Power Electronics*, vol. 30, no. 11, pp. 6108-6119, Nov. 2015.

[44] N. Liu and T. G. Habetler, “Design of a Universal Inductive Charger for Multiple Electric Vehicle Models,” in *IEEE Transactions on Power Electronics*, vol. 30, no. 11, pp. 6378-6390, Nov. 2015.

[45] SAE J2954, “Wireless power transfer for light-duty plug-in/electric vehicles and alignment methodology,” 2019.

[46] General discussion on coupling coefficient and mutual inductance can be accesed at: https://www.electronicstutorials.ws/inductor/mutual-inductance.html [Janury 10, 2018].

[47] A. Zaheer, H. Hao, G. A. Covic, and D. Kacprzak, “Investigation of Multiple Decoupled Coil Primary Pad Topologies in Lumped IPT Systems for Interoperable Electric Vehicle Charging”, in: *IEEE Transactions on Power Electronics*, vol. 30, no. 4, pp. 1937-1955, April 2015.

[48] A. Marinescu, A. Vintila, D. G. Marinescu, V. Nicolae, Development of a Wireless Battery Charger for Dacia Electron EV, The 10th International Symposium ATEE, March 2017, Bucharest.

[49] Kalwar, K.A.; Aamir, M.; Mekhilef, S. A design method for developing a high misalignment tolerant wireless charging system for electric vehicles. Measurement 2018, 118, 237–245.

[50] X. Shi, C. Qi, M. Qu, S. Ye, G. Wang, L. Sun, et al., Effects of coil shapes on wireless power transfer via magnetic resonance coupling, J. Electr. Waves Appl., 28 (2014) 1316–1324.

[51] S. Ahn, and J. Kim. "Magnetic field design for high efficient and low EMF wireless power transfer in on-line electric vehicle." *Proceedings of the 5th European Conference on Antennas and Propagation (EUCAP),* pp. 3979 – 3982, 2011.

[52] F. Y. Lin, S. Kim, G. A. Covic, and J. T. Boys, “Effective coupling factors for series and parallel tuned secondaries in IPT systems using bipolar primary pads,” in *IEEE Transactions on Transportation Electrification*, vol. 3, no. 2, pp. 434–444, Jun. 2017.

[53] M. Budhia, G. A. Covic, and J. T. Boys, “Design and optimization of circular magnetic structures for lumped inductive power transfer systems,” *IEEE Trans. Power Electron.*, vol. 26, no. 11, pp. 3096–3108, Nov. 2011.

[54] G. Buja, M. Bertoluzzo, and K. N. Mude, “Design and experimentation of WPT charger for electric city car,” *IEEE Trans. Ind. Electron.*, vol. 62, no. 12, pp. 7436–7447, Dec. 2015.

[55] L. Xiang, X. Li, J. Tian and Y. Tian, "A Crossed DD Geometry and Its Double-Coil Excitation Method for Electric Vehicle Dynamic Wireless Charging Systems," in *IEEE Access*, vol. 6, pp. 45120-45128, 2018.

[56] E. A. Elghanam, M. S. Hassan, and A. Osman, “Modeling, simulation and comparison of different ferrite layer geometries for inductive wireless electric vehicle chargers,” in Goel N., Hasan S., Kalaichelvi V. (eds) *Modelling, Simulation and Intelligent Computing. MoSICom 2020. Lecture Notes in Electrical Engineering, vol 659.* Springer, Singapore.

[57] S. Bhattacharya, Y.K. Tan, ‘‘Design of static wireless charging coils for integration into electric vehicle, “*2012 IEEE Third International Conference on Sustainable Energy Technologies (ICSET)*, Kathmandu, 2012, pp. 146-151.

[58] C. Auvigne, P. Germano, Y. Perriard, and D. Ladas, “About tuning capacitors in inductive coupled power transfer systems,” in 2013 *15th European Conference on Power Electronics and Applications (EPE),* Sep. 2013, pp. 1–10.

[59] W. Li, H. Zhao, J. Deng, S. Li, and C. C. Mi, “Comparison study on SS and double-sided LCC compensation topologies for EV/PHEV wireless chargers,” *IEEE Transactions on Vehicular Technology*, vol. 65, no. 6, pp. 4429–4439, June 2016.

[60] S. Li and C. C. Mi, "Wireless Power Transfer for Electric Vehicle Applications," in *IEEE Journal of Emerging and Selected Topics in Power Electronics*, vol. 3, no. 1, pp. 4-17, March 2015.

[61] E.A. Elghanam, H. Kabalan, M.S. Hassan, A. Osman, “Design and modeling of ferrite core geometry for inductive wireless chargers of electric vehicles,” in *IEEE International Conference on Electrical and Computing Technologies and Applications,* Nov. 2019.

[62] Y. Li *et al*., "A New Coil Structure and Its Optimization Design with Constant Output Voltage and Constant Output Current for Electric Vehicle Dynamic Wireless Charging," in *IEEE Transactions on Industrial Informatics*, vol. 15, no. 9, pp. 5244-5256, Sept. 2019.

[63] I. Ahmed, E. A. ElGhanam, M. S. Hassan and A. Osman, " Design and Finite Element of Using Microwave Power Transfer for Dynamic Wireless Electric Vehicle Charging," *2020 IEEE Transportation Electrification Conference & Expo (ITEC)*, Chicago, IL, USA, 2020, pp. 365-370.

[64] H.H. Kabalan, E. A. Elghanam, M. S. Hassan, and A. Osman, “A Comparative Study of Rectangular and Double-D Coil Geometries for the Inductive Link Design of the IPT System,” in *6th International Conference on Electric Power and Energy Conversion Systems (EPECS’20)*.

[65] J. Deng, W. Li, T. D. Nguyen, S. Li and C. C. Mi, "Compact and Efficient Bipolar Coupler for Wireless Power Chargers: Design and Analysis," in *IEEE Transactions on Power Electronics*, vol. 30, no. 11, pp. 6130-6140, Nov. 2015.

[66] Hwang, & Jang,. (2020). Design and Analysis of a Novel Magnetic Coupler of an In-Wheel Wireless Power Transfer System for Electric Vehicles. Energies. 13. 332. 10.3390/en13020332.

[67] A. Mohamed, A. Shaier, H. Metwally, S. Selem, “ A comprehensive overview of inductive pad in electric vehicle stationary charging,, “*Applied Energy*,, vol 262, no. 0306-2619, 2020.

[68] Ahmad, A., Alam, M.S. Magnetic Analysis of Copper Coil Power Pad with Ferrite Core for Wireless Charging Application. *Trans. Electr. Electron. Mater.* **20,** 165–173 (2019).

[69] Dang, Zhigang and J. A. Qahouq. “Modeling and investigation of magnetic resonance coupled wireless power transfer system with lateral misalignment.” *2014 IEEE Applied Power Electronics Conference and Exposition - APEC 2014* (2014): 1317-1322.

[70] Samanta, Suvendu et al. “Analysis and Design of Current-Fed Half-Bridge (C)(LC)–(LC) Resonant Topology for Inductive Wireless Power Transfer Application.” *IEEE Transactions on Industry Applications* 53 (2017): 3917-3926.

Vita

Hanin Hassan Kabalan was born in 1993, in Dubai, United Arab Emirates. She received her primary and secondary education in Dubai, UAE. She received her B.Sc. degree in Electrical and Electronic Engineering from the United Arab Emirates University in 2016. From 2017 to 2020, she worked as a Creative Design and Innovation Teacher at the Ministry of Education.

In September 2018, she joined the Electrical Engineering master's program in the American University of Sharjah as a part time graduate teaching and research assistant. During her master's study, she co-authored 3 papers which were presented in international conferences. Her research interests are in (wireless communication, Electric Vehicle Charging systems, and mobile networks).